

Université MUSTAPHA Stambouli
Mascara



جامعة مصطفى أسطمبولي
معسكر

Faculté des Sciences et Technologies
Département de Génie des Procédés
Laboratoire des Sciences et Techniques de l'Eau

THESE de DOCTORAT de 3^{ème} cycle

Spécialité : Génie des Procèdes
Option : Chimie

Intitulée

Fonctionnalisation et caractérisation de matériaux hybrides
organique/inorganique élaborés par une simple oxydation chimique

Présentée par : BELARDJA Mohamed Sif Eddine

Le 10/03/2021

Devant le jury :

BENKOUIDER Ali Mustapha	Pr. Université M. S. de Mascara	Président
BOUSSALEM Ismail	Pr. Centre Universitaire d'Ain Temouchent	Examineur
MOUFFOK Benali	Pr. Université Djillali Liabès Sidi-Bel-Abbès	Examineur
BELMOKHTAR Abdelkader	Pr. Université M. S. de Mascara	Examineur
CHOULI Faiza	M.C.A. Université M. S. de Mascara	Invité
BENYOUCEF Abdelghani	Pr. Université M. S. de Mascara	Encadreur

Année Universitaire : 2020-2021.

MUSTAPHA STAMBOULI UNIVERSITY

Mascara



جامعة مصطفى أسطوبولي

معسكر

Faculty of Science and Technology

Departement of process engineering

Water Sciences and techniques laboratory

Doctoral Thesis of 3rd cycle

Specialty :Process Engineering

Option : Chemistry

Title

Fonctionnalization and characterization of organic/inorganic hybrid
materials produced by simple chemical oxidation

Presented by : BELARDJA Mohamed Sif Eddine

The 10/03/2021

The jury members :

BENKOUIDER Ali Mustapha	Pr. University M. S. de Mascara	President
BOUSSALEM Ismail	Pr. University center of Ain Temouchent	Examiner
MOUFFOK Benali	Pr. University Djillali Liabes Sidi-Bel-Abbes	Examiner
BELMOKHTAR Abdelkader	Pr. University M. S. de Mascara	Examiner
CHOULI Faiza	M.C.A. University M. S. de Mascara	Invited
BENYOUCEF Abdelghani	Pr. University M. S. de Mascara	Advisor

University year : 2020-2021.

Aknowledgement

Thanks ALLAH , the Merciful, the most Merciful.

I would like to express my thanks to Mr. BENYOUCEF Abdelghani for having agreed to frame me, offered me an attractive subject and the interest he brought to this modest work.

I warmly thank Mr. BENKOUIDER Ali Mustapha , Mr. BOUSSALEM Ismail , Mr MOUFFOK Benali and Mr. BELMOKHTAR Abdelkader for honouring me with their presence as a member of the jury.

I would like to express my gratitude to Mm. CHOULI Faiza who through his understanding and help I was able to do this work.

I am also grateful for my teacher and my colleague MA.Bekhti , and other colleagues H.Djelad , M.Lafjah

Finally, I thank all laboratory staff kenza and samir, khayr eddine.hayat and mohamed and all those who help me by a word, by a reflection or by a remark, have managed, with or without attention, to guid my attention to the rightway.

Dedicace

To

My dear mother and my dear father who helped me to get that point of study.

To my two dear brothers Dhiaa and Hadi

To my wife Messeguem Fatima Zohra and my dear little daughter Mariam Hind.

To my ancle Menouer Mohamed

For my whole family.

I dedicate this memory.

Summary

GENERAL INTRODUCTION.....	1
CHAPTER I Bibliographic Studies	5
I.1 HYBRID NANOCOMPOSITES.....	6
I.1.1 Introduction.....	6
I.1.2 Polymer matrix nanocomposites.....	7
I.1.3. The different types of polymer nanocomposites.....	7
I.1.3.1 Polymeric Nanocomposites based on inorganic materials.....	8
I.1.3.2 Polymeric Nanocomposites based on metallic materials	8
I.1.3.3 Polymeric carbon-based nanocomposites.....	9
I.1.4 SYNTHESIS OF HYBRID NANOCOMPOSITES	10
I.1.4.1 Direct mixing.....	11
I.1.4.2 Sol-Gel treatment.....	13
I.1.4.3 In-situ polymerization.....	14
I.1.5 APPLICATIONS OF HYBRID METAL OXIDE / POLYMER NANOCOMPOSITES	15
I.2. Nanocharges : Metal Oxides	15
I.2.1. Introduction.....	15
I. 2.2. TUNGSTEIN OXIDE (WO_3).....	16
I. 2.2.1. Production	16
I. 2.2.2. Structural study	17
I. 2.2.3. Phases of WO_3.....	18
I. 2.2.4. Monoclinic phase	19
I. 2.2.5. The chemistry of WO_3.....	19
I.2.2.6. Tungstein	20
I.2.3. Alumina (Al_2O_3)	20
I.2.3.1 Structural and chemical properties	21
I.2.3.2. Aluminium	22

I.2.3.3. Overall	23
I.2.4 General Information on prickly pear	24
I.2.4.1 advantages of opuntia ficus indica :	25
I.2.4.2 Chemical composition of barbarism snowshoes	26
I.3. Conductive polymers	27
I. 3.1. General information on conductive polymers	27
I. 3.2. Classification of conductive polymers	27
I. 3.3. Electronic structure of conductive polymers	30
I. 3.4. Doping of conductive polymers	32
I.3.5. Load carriers	33
I.3.6. Polyaniline	33
I.3.6. 1. Presentation	33
I.3.6. 2. Doping of polyaniline	35
I.3.6. 3. Synthesis of Polyaniline	37
I.3.6. 4. Polymerization mechanism	40
I.3.6. 5. Factors influencing the electrical conductivity of polyaniline	42
I.3.6. 6. Applications of polyaniline	43
I.4. Reference	46
CHAPTER II Materials and Methods	70
Materials and Methods	70
II.1. Introduction	71
II.2. The analysis techniques	71
II.2.1 Structural analysis techniques	71
II.2.2. Thermal characterization techniques	71
II.2.3. Electrochemical behavior was studied by cyclic voltammetry	72
II.2.4. Conductivity values are measured by the four-point method.	72
II.3. USED PRODUCTS	72
II.4. Synthesizing of differents nanocomposites	73
II.4.1. Synthesis of the aniline/tungstein oxide (WO ₃) nanocomposite	73
II.4.2. Synthesis of Aniline/Alumina (Al ₂ O ₃) nanocomposite	73
II.4.3. Synthesis of aniline/opuntia ficus indica OFI nanocomposite	74

II.5. Structural, morphological and chemical characterizations	74
II.5.1 X-ray diffraction	74
II.5.2 Fourier transform infrared spectroscopy (FTIR)	76
II.5.2.1 Transmission mounting	77
II.5.2.2 Qualitative and quantitative information	78
II.5.2.3 Measuring device	81
II.5.3 Scanning electron microscopy	81
II.5.4. X Photoelectron Spectroscopy (XPS).....	84
II.6. Optical and electrical characterizations.....	85
II.6.1. UV-Visible spectrophotometry	85
II.6.2. Measurement of electrical resistivity by the 4-point method	88
II.7. Electrochemical analysis techniques used.....	90
II.7.1. Oxidation-reduction reactions.....	90
II.7.2. Electrochemical analysis technique	91
II.7.2.1 The cyclic voltammetry (CV)	93
II.8. Thermal analysis	96
II.8.1 Thermogravimetric analysis.....	96
II.9. Conclusion.....	97
II.10. References	98

CHAPTER III The influence of the addition of tungsten trioxide nanoparticle size on structure, thermal and electroactivity properties of hybrid materials reinforced PANI	100
--	------------

III.1. Introduction	101
III.2 Results and discussion	102
III.2.1. XPS spectroscopy	102
III.2.2 XRD studies	107
III.2.3 FTIR spectroscopy	110
III.2.4. Optical properties	111
III.2.5. TGA analysis	113
III.2.6. Electrochemical Analysis.....	115
III.3. Conclusions.....	117
III.4. References.....	119

CHAPTER IV PANI/Al_2O_3	124
IV.1. Introduction	125
IV.2 Results and discussion	126
IV.2.1. X-ray photoelectron spectroscopy (XPS)	126
IV.2.2. X-ray diffraction	131
IV. 2.3. FT-IR spectroscopy	133
IV.2.4. Optical characterization	135
IV.2.5. Thermogravimetric analysis (TGA)	138
IV.2.6. Surface morphologies	139
IV.2.7. Electrochemical Analysis	140
IV.3. Conclusions	141
IV.4. References	143
CHAPTER V PANI/OPUNTIA Ficus indicat	147
V.1 Introduction	148
V.2 Results and discussion	149
V.2.1. FTIR	149
V.2.2 XRD analysis	151
V.2.3. SEM analysis	153
V.2.4. TGA analysis	155
V.3. Conclusion	156
V.4. References	158

CHAPTER I

Figure I.1. Methods for synthesizing polymer / metal nanocomposites	11
Figure I.2. Synthesis of PANI nanocomposite by in situ polymerisation.....	14
Figure I.3. Elementary form of WO_6 , (b) Crystal lattice of monoclinic WO_3 obtained at room temperature].	17
Figure I.4. Projection of the hexagonal structure on the base plane of the structure. Small black circles represent cations, large circles and small circles without colors represent anions and vacant octahedral sites respectively	22
Figure I.5. General appearance of <i>Opuntia ficus-indica</i>	25
Figure I. 6. Electrical conductivity of intrinsic conductive polymers.....	30
Figure I. 7. Theoretical diagram established according to the theory of energy bands	31
Figure I. 8. Conductivity of various conductive polymers and conventional materials.....	32
Figure I. 9. Generic structure of Polyaniline.....	34
Figure I. 10. Different oxidation states of Polyaniline.....	35
Figure I. 11. Doping of the different states of Polyaniline.....	36
Figure I. 12. Proton doping of emeraldine base and redox doping of leucoemeraldine base (HA: acid, A^- : against ion).....	37
Figure 1.13. First steps in the oxidation of aniline and anilinium cations by APS in acidic HCL	42

CHAPTER II

Figure II.1. Schematic representation of Bragg's diffraction law. The black spheres represent the atoms of a crystal structure.....	76
Figure II.2. Schematic diagram of the infrared spectrometer.	78
Figure II.3. FTIR device used	81
Figure II.4. Electron interaction pair in scanning electron microscopy inspired by	83
Figure II.5. Representation of the photoelectron emission mechanism by a photon with an energy h in the X-ray domain	85
Figure II.6. Schematic of the dual beam and optical path configuration of the Varian Cary 500 spectrophotometer	86
Figure II.7. Example of an optical transmittance curve of an example metal : Al film with a thickness of 110 nm.....	86
Figure II.8. Example of measurement of the indirect gap of a tungsten oxide film WO_3	88
Figure II.9. Diagram showing the operation of the "4 points" method.....	89
Figure II.10. Diagram of the 3-electrode cell used for electrochemical analyzes	92
Figures II.11. Photographs of the "open" (a) and "closed" (b) cells	93
Figure II.12. Cyclic voltammetry: (a) shape of the electrode potential (b) Shape of the resulting voltammogram	94
Figure II. 13. Diagram of the principle of thermogravimetric analysis	96

CHAPTER III

Figure III. 1. Survey (a) and high-resolution WO_3 nanoparticle; (b) X-ray photoelectron spectra of three PANI/ WO_3 samples.	102
Figure III. 2. XPS spectra C1s of three PANI/ WO_3 nanocomposites synthesized.	104
Figure III. 3. XPS spectra N1s of three PANI/ WO_3 nanocomposites synthesized.	106
Figure III. 4. XRD patterns of pure PANI, WO_3 nanoparticle and three PANI/ WO_3 nanocomposites synthesized.	108
Figure III. 5. FT-IR adsorption spectra of pure PANI, WO_3 nanoparticle and three PANI/ WO_3 nanocomposites synthesized.	111
Figure III. 6. UV-vis spectra of pure PANI and three PANI/ WO_3 samples dispersed in DMSO.	112
Figure III. 7. Thermogravimetric analysis of pure PANI, WO_3 nanoparticle and three PANI/ WO_3 nanocomposites obtained in N_2 atmosphere at $10^\circ\text{C}\cdot\text{min}^{-1}$	114
Figure III. 8. SEM image of nanocomposites prepared for (a) PANI/ WO_3 (0.5) ; (b) PANI/ WO_3 (1.0) ; (c) PANI/ WO_3 (1.5).	115
Figure III. 9. Stabilized cyclic voltammograms recorded for a graphite carbon electrode covered by pure PANI.	116

CHAPTER VI

Figure IV. 1. XPS spectra (survey scan) of Al_2O_3 and PANI/ Al_2O_3 samples.	128
Figure IV. 2. XPS spectra C1s of three PANI/ Al_2O_3 nanocomposites synthesized.	129

Figure IV. 3. XPS spectra N1s of three PANI/Al ₂ O ₃ nanocomposites synthesized.	130
Figure IV. 4. XRD patterns of pure PANI, Al ₂ O ₃ nanoparticle and PANI/ Al ₂ O ₃ nanocomposites synthesized.	132
Figure IV. 5. FTIR spectra of pure PANI, Al ₂ O ₃ nanoparticle and three PANI/Al ₂ O ₃ nanocomposites synthesized.	134
Figure IV. 6. UV-vis spectrum (a)	136
Figure IV.7. Tauc plots (b) corresponding to pure PANI and PANI/Al ₂ O ₃ nanocomposites dissolved in DMSO.	137
Figure IV .8. TGA of pure PANI, Al ₂ O ₃ nanoparticle and PANI/Al ₂ O ₃ nanocomposites. .	139
Figure IV. 9. SEM images of nanocomposites prepared for (a) PANI/Al ₂ O ₃ (2%) ; (b) PANI/Al ₂ O ₃ (4%) ; (c) PANI/Al ₂ O ₃ (6%).....	139
Figure IV. 10. Stabilized CV recorded at 50 mV.s ⁻¹ in a 1 M HClO ₄ solution for a GC electrode covered by pure PANI and PANI/Al ₂ O ₃ nanocomposites.	140

CHAPTER V

Figure.V.1 OFI cladodes	148
Figure V. 2. FTIR spectra of pure PANI, OFI and three PANI/OFI nanocomposites synthesized.....	150
Figure V. 3. XRD patterns of pure PANI, OFI and PANI/OFI composites synthesized.....	152
Figure V.4. SEM images of nanocomposites prepared for (a) OFI ; (b) PANI; (c) PANI/OFI.....	154
Figure V.5. TGA of pure PANI, OFI and PANI/OFI nanocomposites.....	156

CHAPTER I

Table I.1 The different types of nanoparticles used in polymer nanocomposites.....	7
Table I.2. The different crystallographic phases of WO ₃	18
Table I.3. Lattice parameters of crystallographic phases of WO ₃	18
Table I.4. Chemical composition of <i>Opuntia</i> snowshoes	26
Table I. 5. The main families of conductive polymers.....	29
Table I.6. Gap of the main families of conjugated polymers	31
Table I.7. Main applications of polyaniline and associated specific properties.....	44

CHAPTER II

Table II.1. Vibration frequencies of some functions encountered in organic compounds.	79
---	-----------

CHAPTER III

Table III.1. XPS Binding Energy/eV results for nanocomposites: (A) WO ₃ nanoparticles, (B) PANI/WO ₃ (0.5), (C) PANI/WO ₃ (1.0) and (D) PANI/WO ₃ (1.5).....	105
Table III.2. Doping degree and defect density in different PANI nanostructures	107
Table III.3. X-ray diffraction data with Bragg angle, <i>d</i> -spacing, FWHM and crystallite size of the main principal peak for WO ₃ nanoparticles and nanocomposites.....	109
Table III.4. UV-vis absorption spectra properties (λ_1 , λ_2 and λ_{onset}) optical band gap energy (E_g) of PANI/WO ₃ nanocomposites.....	112
Table III.5. Electrochemical parameters obtained from CVs of pure PANI and PANI/WO ₃ nanocomposites on glassy carbon electrode in 1M HCl solution at scan rate 50 mV.s ⁻¹	117

CHAPTER VI

Table IV.1. the conditions and yeild of our synthesis.....	126
Table IV.2. Summary of the XPS binding energy values (eV) obtained for nanocomposites: (A) Al ₂ O ₃ nanoparticles, (B) PANI/Al ₂ O ₃ (2%) and (C) PANI/Al ₂ O ₃ (4%).....	127
Table IV.3. Doping degree and defect density in different PANI nanostructures.....	131
Table IV.4. XRD data and calculated particle sizes for Al ₂ O ₃ nanoparticles and nanocomposites.	133
Table IV. 5. Characteristics of UV-Vis absorption spectra of PANI/Al ₂ O ₃ nanocomposites.	136
Table IV.6. Parameters of the peaks of electrochemical saturation of pure PANI and PANI/Al ₂ O ₃ nanocomposites in 1M HCl solution on the GC electrode according to the CV data.	141

CHAPTER V

Table V.1. X-ray diffraction data with Bragg angle, <i>d</i> -spacing, FWHM and crystallite size of the main principal peak for PANI, OFI-A and OFI-A samples.	153
Table V. 2. The electrical conductivity values of PANI, OFI-A and OFI-A samples.	155

GENERAL INTRODUCTION

In the recent years, the intensive use of polymeric materials is attributed to their extraordinary combination of several properties, fairly light weight, low cost and ease of processing. However, for the improvement of certain properties such as thermal and mechanical stability, a large number of additives have been added to the host polymer matrix to develop hybrid composites (organic-inorganic) [1].

Polymers usually melt or degrade before 200 °C. Although there is a class of thermally stable polymers that are able to withstand temperature of at least 300 °C. In our study we have been tried to support our polymer with another materials which can improving their characteristics, thermal stability and conductivity...etc. This can augment its approach of application.

A polymer matrix composite is a material consisting of a polymer matrix combined with one or more other dispersed phases. These phases can have significantly different physical and chemical properties. Through the controlled combination of components, new materials are obtained with distinct properties of the individual components [2].

If at least one of the components has nanometric dimensions, these materials are called nanocomposites. Compared to composites of micrometric size and due to the dimensions of the particles of the nanometric phase, nanocomposites exhibit new and improved properties such as for example dispersion homogeneity, thermal stability and flame resistance, properties more efficient mechanics, more interesting electrical and optical properties [3-5]. The diversity of properties is attracting more and more attention from researchers and manufacturers. Currently their field of application continues to widen [6].

Incorporation of inorganic nanoparticles into suitable polymer matrices can impart improved optical, mechanical, magnetic and optoelectronic properties to the resulting

nanocomposites . Therefore, these nanocomposites have been widely used in different fields such as military equipment, security, protective clothing, automotive, aerospace, electronics and optical devices. However, these fields of application continually demand higher performance properties and additional functions such as high mechanical properties, flame retardance, chemical resistance, UV resistance, electrical conductivity, environmental stability, water repellency, resistance to magnetic field, radar absorption. So considerable effort is needed to answer this requirement.

Among inorganic nanoparticles, nanoparticles based on metal oxides can exhibit interesting physical and chemical properties due to their very small size and the resulting large surface / volume ratio. Nanoparticles and or nanocrystals of metal oxide semiconductor materials have been widely studied over the past decade due to their unique properties and application in various fields. Many research groups have focused on the dispersion of metal oxide nanoparticles in polymer matrices, as hybrid nanocomposites not only inherit the functionality of semiconductor nanoparticles but also polymer advantages such as flexibility and conformance.

Nanocomposite materials based on metal oxides / polymers are used in the manufacture of LEDs, photo-detectors and displays due to their very interesting electroluminescence (EL) and photoluminescence (PL) properties. To optimize their properties, the chemical nature, the microstructure and the dispersion (dimensions and spatial distribution) of the nanoparticles as well as the production process must be well defined to obtain the desired characteristics [7].

Much research has focused on the development of metaloxide/polymer nanocomposites using different polymer matrices. Among the most used polymers, polystyrene (PS) and the polyaniline (PANI) occupy a privileged spot. Those are thermoplastic materials; this particularity makes it possible to combine them with

nanoparticles of inorganic semiconductors such as WO_3 and Al_2O_3 , OFI opuntia ficus indica, the optical activity of which is in the visible range. The goal of this work is to enhance the optoelectronic properties of the resulting nanocomposites.

The work to be carried out consists in synthesizing nanoparticles of WO_3 and Al_2O_3 and OFI to develop thin films of nanocomposites PANI/ WO_3 , PANI/ Al_2O_3 , PANI/OFI and to proceed to their structural and optical characterization. The work carried out includes the following stages:

- Synthesis of the composites of WO_3 and Al_2O_3 and OFI semiconductors.
- The structural and optical characterization of the nanopowders of the metallic oxide and inorganic semiconductors (WO_3 and Al_2O_3 and OFI) synthesized.
- The structural characterization of the nanocomposites produced.
- The morphological study of the nanocomposite films produced.
- The optical characterization of the nanocomposites produced.
- The electrical characterization of nanocomposites.

The results of the work are reported in this manuscript which includes an introduction, five chapters and a general conclusion.

The first chapter presents the synthesis of a bibliographic research on polymer composites in general and more particularly on metal oxide/polymer nanocomposites and inorganic materials and the methods of development of the hybrid composite materials based on metal oxides/polymers , while highlighting evidence of their physical properties and applications.

In the second chapter were exposed to the method of synthesis of the particules (WO_3 and Al_2O_3 and OFI) with the experimental techniques used in the preparation of our samples (PANI/ WO_3 , PANI/ Al_2O_3 , PANI/OFI). Also the different techniques used for their structural, optical and electrical characterization have been described.

The third and fourth chapter presents the results of the structural characterization by X diffraction, IR spectroscopy and X Photoelectron Spectroscopy (XPS) of the synthesized nanocrystals (WO_3 , Al_2O_3) as well as the results of their optical characterization by UV-Visible-near spectrophotometry, infrared spectroscopy, electric and electrochemical proprieties by cyclic voltammetry (CV). This chapter also presents the results of the morphological study of surface nanocomposite made by scanning microscopy electronics has (SEM).

The fifth chapter presents the results of the structural, electrochemical, electrical characterization and the morphological study of OFI / polymer composites.

Finally, the manuscript ends with a general conclusion in which an assessment of the work carried out is established.

CHAPTER I
Bibliographic Studies

I.1 HYBRID NANOCOMPOSITES

I.1.1 Introduction

A composite is defined as a combination of two or more materials with different physical and chemical properties and a distinct interface. Composite materials have a very wide range of applications. The important advantages of composites over many metal compounds are high specific stiffness, high toughness, better corrosion resistance, low density and some thermal insulation [8].

In most composite materials, one phase is generally continuous and referred to as the matrix, while the other phase is referred to as the dispersed phase. Based on the nature of the matrices, composites can be classified into four broad categories:

- 1- Polymer matrix composites;
- 2- Metal matrix composites;
- 3- Ceramic matrix composites;
- 4- Carbon matrix composites [9].

Polymer matrix composites can be processed at a much lower temperature, compared to other composites. Depending on the type of polymer matrix, the composite polymer matrix are divided into thermoset composites and thermoplastic composites [9].

Hybrid materials most often result from the assembly of two materials: an inorganic part and an organic part. The association of such different materials generally gives the composite new properties that each component cannot have on its own (mechanical properties, density, permeability, color, hydrophobic properties, etc.).

I.1.2 Polymer matrix nanocomposites

To improve the properties of composite materials, scientists have resorted to low-charge containing composites with smaller grain sizes, leading to the development of microcomposites and the recent trend in composite research is dominated by nanocomposites.

Nanocomposites are composites in which a phase has nanometric morphology such as nanoparticles, nanotubes or lamellar nanostructure [10]. The improvement of the properties by the addition of particles can be obtained by a good interaction between the nanoparticles and the matrix and a good dispersion of the nanoparticles in the matrix.

In nanocomposites, covalent bonds, ionic bonds, Vander Waals forces, hydrogen bonding can exist between the matrix and the components of the charge [9].

I.1.3. The different types of polymer nanocomposites

Many nanocomposites are made from a polymer in which nanoparticles have been dispersed. Indeed, the incorporation of nanofillers within polymer materials makes it possible to modify their mechanical [11], thermal [13], [14], electrical [15] or magnetic [16] properties and thus widen their domain of application. Table I.1 lists the nanocomposites according to their nature and the form of the nanofillers used as reinforcements in the polymers.

Table I.1 The different types of nanoparticles used in polymer nanocomposites

Nature of the nanocharge	Form	Examples
Inorganic	Spheres	Preformed silica [12], [17] [18], metal oxides [19], carbonate calcium [20]
	Fibers	Sepiolite [21], potassium titanate [22]
	Platelets	Lamellar silicates [23]
Metallic	Spheres	Magnetite [16], Gold particles [24]
Carbon-based compound	Spheres	Carbon black [25]
	Fibers	Nanotubes [26], Cellulose [27] graphene [28]
	Platelets	Graphite [29]

I.1.3.1 Polymeric Nanocomposites based on inorganic materials.

Polymer composites made up of inorganic nanoparticles and organic polymers represent a new class of materials that have more performance properties compared to their microparticle counterparts [30]. Inorganic particles provide mechanical and thermal stability and new functionalities which depend on the chemical nature, structure, size and crystallinity of inorganic nanoparticles (silica, oxides of transition metals, nanocells, metal phosphates, metal chalcogenides and nanometallic). Inorganic particles provide better mechanical, thermal, magnetic, electronic and optical properties [31]. Various processes are used for the preparation of inorganic nanocomposites based on polymers. The most important are:.

- i. Molten intercalation.
- ii. Direct mixing of polymers and particles.
- iii. Chemical synthesis.
- iv. In situ polymerization.
- v. Sol-gel process.

I.1.3.2 Polymeric Nanocomposites based on metallic materials

Metal/polymer nanocomposite materials combine properties of several components. Nowadays, they are regarded as promising systems for advanced functional applications [32]. Therefore, the incorporation of nanoparticles metal in the polymer has paved the way for a new generation of materials having electrical, optical or mechanical unique that make them attractive for applications in areas such as optics, [33] the a photoimaging and modeling [34] , sensor design [35], catalysis [36] and antimicrobial coatings [37]. The search for new methods of preparing metallic nanocomposite materials has been greatly stimulated due to their attractive properties and promising applications. One of the main interests of metallic

nanoparticles is their unique physical properties which can be adapted by chemical control of their shape and size [38]. Among these, nanoscale gold and silver play a primary role because these nanoparticles exhibit a very intense absorption band in the visible region due to their surface plasmon resonance. Metal / polymer nanocomposites can be prepared by two approaches:

i) The first involves a dispersion of metallic nanoparticles in a polymerizable formulation, or in a polymer matrix. In this case, the reduction of the metal ions and the polymerization occur successively, hence the aggregation of the nanoparticles which makes this synthesis procedure often problematic.

ii) In the second approach, the nanoparticles are generated in situ during polymerization to avoid agglomeration. The polymerization reaction and the synthesis of nanoparticles which take place simultaneously have been the subject of in-depth studies. Another technique consists of polymerizing the matrix around a metallic nanocore using chemically compatible ligands [39] or polymeric structures [40].

I.1.3.3 Polymeric carbon-based nanocomposites

Carbon nanofillers such as nanotubes and graphene exhibit excellent properties due to their high mechanical strength and high aspect ratio. Graphene and its polymer nanocomposite derivatives have demonstrated immense potential applications in electronics, aerospace, automotive, defense industries and green energy thanks to their exceptional reinforcement in composites . To take full advantage of its properties, the integration of individual graphene into polymer matrices is essential. Compared to carbon nanotubes, graphene has a higher surface area to volume ratio which makes it potentially more favorable for improving mechanical, electrical, thermal, gas permeability and microwave absorption properties [41]. The nanotubes of carbon (CNT) are considered unique elements promoting

the development of various polymer composites because of their unique properties such as high electrical conductivity ($\sim 10^6 \text{ m.s}^{-1}$), the has improved resistance to traction (50 GPa) and low density. These characteristics make them useful in a wide range of industrial applications [42].

There are three main mechanisms of interaction of the polymer matrix with carbon:

- (a) Micro-mechanical interconnection.
- (b) Chemical bond between the nanotubes and the matrix.
- (c) Poor van der Waals adhesion between filler and matrix.

I.1.4 SYNTHESIS OF HYBRID NANOCOMPOSITES

To endow polymer nanocomposites with new properties, synthetic methods that have an effect on the control of particle size distribution, dispersion and interfacial interactions are essential . Synthesis techniques for nanocomposites are different from those for conventional composites. The development of nanocomposites polymers is difficult because of the physicochemical differences between systems. Each polymer system may require a set of processing conditions and different synthetic techniques which in general give non-equivalent results; considerable research has been done to develop suitable synthetic techniques for making good polymer nanocomposites [43].

The methods for producing polymer nanocomposites are all based on a first step of dispersing the nanoparticles in a liquid, however they differ by the type of organic phase [44] and by the subsequent treatment to be carried out: heat treatment, elimination of any solvent. .

The nanopowders are mainly metals, semiconductors, or metal oxides. This section mainly studies how to form nanocomposites with metal oxides and polymers. Generally, there are three preparation methods for synthesizing polymer / metal oxide nanocomposites (Figure II.4). The first is the direct mixing of a polymer and metal oxide nanoparticles, either as

discrete phases (called melt mixing) or in solution (solution mixing). The second is a sol-gel process, which begins with the association of molecular precursors at room temperature, then the formation of a metal oxide by hydrolysis and condensation. The third is the in-situ polymerization of monomers in the presence of metal oxide nanoparticles.

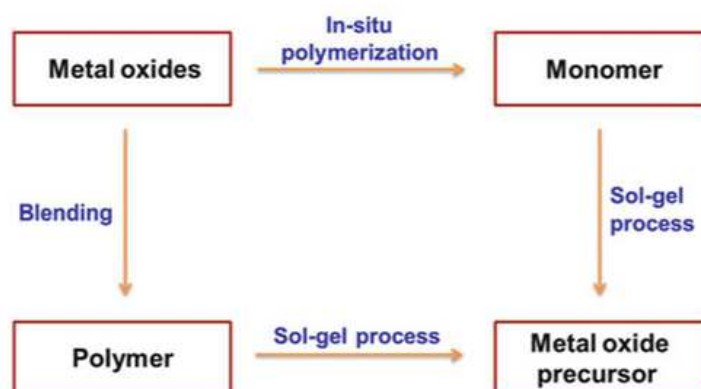


Figure I.1. Methods for synthesizing polymer/metal nanocomposites

I.1.4.1 Direct mixing

Direct mixing is the simplest method of preparing polymer / metal oxide nanocomposites. This ex-situ method is popular because it does not limit the nature of the nanoparticles and host polymers used. Depending on the conditions, the mixture can normally be divided into molten mixture and solution mixture. The main difficulty in the direct mixing process is always the efficient dispersion of the nanoparticles in the polymer matrix because the latter tend to agglomerate.

I.1.4.1 .1 Molten mixtures

One of the conventional techniques for preparing polymer composites is to disperse particles in a polymer, generally a thermoplastic, in the molten state. The dispersion of the particles is improved if they are functionalized by organic molecules whose chemical nature is compatible with that of the polymer. Currently, this process is used for a wide range of materials such as metal oxides and carbon nanotubes.

Molten blending is the fastest method to introduce new nanocomposites to the market since it can take full advantage of well-constructed polymer processing equipment, including extruders or injectors.

Although the processing conditions of the polymers are optimized to obtain a good uniform dispersion of the metal oxide nanoparticles in the polymer matrix, the surface characterization indicates the clustering of the nanoparticles. Agglomeration has been attributed to particle interactions mediated by steric forces in the polymer matrix. On the other hand, mixing polymers and nanoparticles of metal oxides to produce nanoparticles that are homogeneous and well dispersed in the polymer poses significant challenges.

Despite the aforementioned advantages of melt blending, polymer degradation could be a significant problem that should not be overlooked. Since a certain elevated temperature is normally required during melt mixing, the polymer matrix and the compatibilizer can degrade the organic surfactant, which can lead to a significant decrease in the mechanical properties of the final products.

I.1.4.1.2 Mixing of solutions

This method consists in dispersing nanoparticles in a polymer solution using a suitable solvent, then in evaporating this solvent to form nanocomposite films or sheets.

The advantages of solution mixing include the thorough mixing of the inorganic filler with the polymer in a solvent, which facilitates the disintegration and dispersion of nanoparticles from the filler.

This method consists of three steps: dispersion of the nanoparticles in an appropriate solvent, mixing with the polymer (at room temperature or high temperature), and recovery of the nanocomposite by precipitation or casting of a film.

In this process, the dispersion of the nanoparticles can be obtained by magnetic stirring, mixing by shearing, reflux or, most often, by ultrasonication .

Solution mixing can overcome some of the limitations of melt mixing if the polymer and nanoparticles are both dissolved or dispersed in solution. On the other hand, for industrial applications, melt processing is the preferred choice due to its low cost and simplicity for large scale production for commercial applications.

I.1.4.2 Sol-Gel treatment

Several approaches have been developed to improve the compatibility between organic and inorganic components. Among the many methods under development, the sol-gel route has been widely applied due to its ability to control miscibility between organic and inorganic components at the molecular level. The term sol-gel is associated with two reaction steps: sol and gel. A sol is a colloidal suspension of solid particles in the liquid phase and a gel is the interconnected network formed between the phases.

The nanocomposites organo -inorganiques are normally prepared by the sol-gel method in the solvent containing precursors and organic polymers. The most direct route is to hydrolyze and condense the precursors in the presence of a polymer in a solvent system. Materials prepared by sol-gel treatment have uniformity, high purity, and low sintering temperatures compared to those prepared by conventional solid state reactions. Sol-gel materials are classified by the mode of formation and the types of bonds between the components: organic, organometallic and inorganic.

The most important problem associated with the sol-gel process is that the gelation process leads to a considerable decrease in internal stress, which can lead to contraction of fragile materials due to the evaporation of solvents, small molecules and water. In addition, the precursors are expensive and sometimes toxic, preventing further improvement and application.

I.1.4.3 In-situ polymerization

The nanometric particles are dispersed in the solution of the monomers and the resulting mixture is polymerized by simple polymerization methods. The advantage of this method is the possibility of grafting the polymer onto the surface of the particles. The key to in situ polymerization is proper dispersion of the particles in the monomer. This often requires modification of the particle surface, because although dispersing is easier in a liquid than in a viscous molten bath, the settling process is also faster.

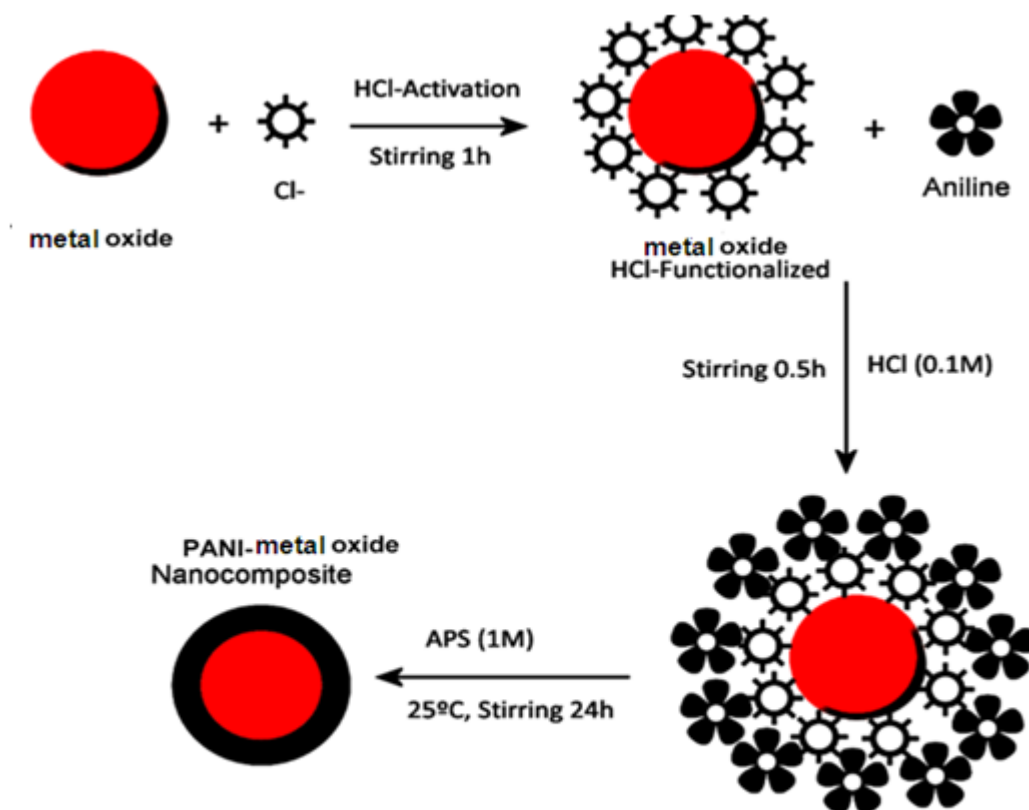


Figure I.2. Synthesis of PANI nanocomposite by in situ polymerisation

I.1.5 APPLICATIONS OF HYBRID METAL OXIDE / POLYMER NANOCOMPOSITES

The applications of metal oxide / polymer nanocomposites have experienced rapid growth. The advantages of incorporating metal oxide nanoparticles into polymer matrices can lead to significant potential applications. These areas include photocatalysts, membranes for gas separation, sensors, and environmental and biomedical applications. These areas include photocatalysts, membranes for gas separation, sensors, and environmental and biomedical applications, aerospace industries, automobile sectors, oil and gas pipeline [45] , bone repair , batteries[46]

I.2. Nanocharges : Metal Oxides

I.2.1. Introduction

The nanocrystals of metal oxides are of great interest because their properties differ from those of the bulk material. They have a large surface area to volume ratio, increased chemical reactivity, special electronic properties and exceptional optical properties [47].

Metal oxide nanoparticles are scientifically and technologically interesting functional materials with a variety of structures and properties spanning nearly all aspects of materials science and physics. They are present in many technological fields such as gas detection, medical science, electronics, ceramics, energy conversion and storage as well as surface coatings [48].

Metal oxide semiconductor nanostructures are very important for " nanosensor " research because of their theoretical and practical importance in applications in biology, environment and analytical chemistry [49].

The most popular areas of research for these nanostructures are optoelectronics [50], sensors [51] and actuators [52]. Metal oxide nanostructures have in addition to the high surface area / volume ratio, low toxicity, are environmentally friendly, have chemical stability and biocompatibility. Metal oxide nanostructures also exhibit fast electron transfer properties required to improve the performance of nanomaterials when used as a biomimetic membrane to for example detect proteins and retain their activity [50, 51].

Among these metal oxides, WO_3 and Al_2O_3 may have different and interesting morphologies such as the nanowires, nanorods (NRs), nanotubes, nanoleaves, nanoflowers etc. which make them useful for fabricating nanodevices for optoelectronic and sensing applications.

I. 2.2. TUNGSTEIN OXIDE (WO_3)

Tungsten oxides With the chemical symbol WO_3 , it is also called wolframic acid or tungsten oxide (HSDB, 2002d). They have numerous applications, in particular in the fields of catalysis [53, 54], electrochromic systems [55] and chemical sensors for the detection of polluting gases. Depending on the oxidation state of the W atom, the conductivity of tungsten oxides changes from a semiconductor or even insulating behavior, for WO_3 , to that of a conductor, for WO_2 and even to that of a superconductor for certain sub-oxides and complexes between WO_3 and WO_2 . All these oxides do not differ only in their composition but also in their crystallographic structure. These two parameters have a great influence on the sensitivity, selectivity and stability of chemical sensors and catalysts.

I. 2.2.1. Production

Tungsten trioxide (WO_3) is prepared from sodium tungstate. It can also be produced by treating scheelite ore with sulfuric acid.

Reaction of concentrated tungsten ore with sodium carbonate yields para ammonium tungstate, which is used to produce tungsten trioxide (HSDB, 2002d).

I. 2.2.2. Structural study

The conductivity of tungsten trioxide, like most other semiconductor metal oxides, depends on its crystallographic structure. This is derived from the face-centered cubic structure of rhenium oxide (ReO_3) [56] in which the tungsten atoms are located at the vertices of a cube, while the oxygen atoms are located at the middle of the ridges. Each tungsten atom is surrounded by six oxygen atoms (figure 1.9) [57]. At room temperature, the monoclinic phase is observed. Its structure can then be described as a three-dimensional network of octahedra (WO_6) linked together by the oxygen atoms forming their vertices. From a crystallographic point of view, the derived structure is slightly distorted because the tungsten atom is shifted from the center of the octahedron.

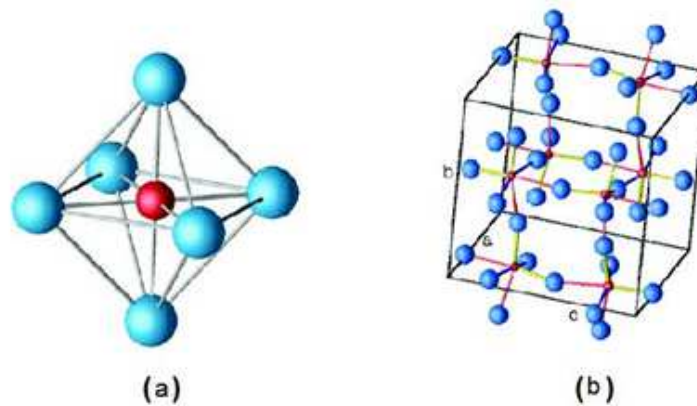


Figure I.3. (a) Elementary form of WO_6 , (b) Crystal lattice of monoclinic WO_3 obtained at room temperature.

This distortion is not local but is repeated in the three directions of the network. The displacement of atoms in the structure is temperature dependent and induces the change in symmetry of WO_3 .

I. 2.2.3. Phases of WO₃

Tungsten trioxide exists in different crystallographic phases in which the tungsten network is always irregular. The nature of the distortion is a function of the temperature (Table 1.2). The authors have defined several crystallographic forms of WO₃ [58]. According to their study, it was possible to construct a table (Table 1.3) which recapitulates the various data concerning the structure of this oxide. These different phases of WO₃ exist in well-defined temperature ranges. This results in different crystallographic forms, the experimental parameters of which are given in the table below [58, 59]:

Table I.2. The different crystallographic phases of WO₃

Phases	Symmetry	Stability domain
α -WO ₃	Tetragonal	1010 -1170 K
β -WO ₃	Orthorhombic	600-1170 K
γ -WO ₃	Monoclinic	290 -600 K
δ -WO ₃	Triclinic	230 -290 K
ε -WO ₃	Monoclinic	0 -230 K
h-WO ₃	Hexagonal	Special conditions of synthesis
c-WO ₃	Cubic	<280 K

Tungsten trioxide can also lose oxygen atoms to form a multitude of suboxides. When certain oxygen atoms are removed from the lattice formed by the octahedra of WO₆, the other atoms rearrange themselves, which creates shear planes in the basic structure.

According to Table 1.2, the dominant phase between 290 and 600 K is monoclinic. So, in our study, we will be working with the monoclinic phase detailed below

Table I.3. Lattice parameters of crystallographic phases of WO₃

Structure	a (Å)	b (Å)	it	α	β	γ
α -WO ₃	5.25	5.25	3.92	90	90	90
β -WO ₃	7.34	7.57	7.75	90	90	90
γ -WO ₃	7.30	7.54	7.69	90	90.9	90
δ -WO ₃	7.31	7.52	7.69	88.8	90.9	90.9

I. 2.2.4. Monoclinic phase

The monoclinic structure is the stable structure of WO_3 at room temperature and up to 600K. Widely studied by X-ray diffraction [60], its lattice parameters ($a = 0.730 \text{ nm}$, $b = 0.754 \text{ nm}$ $c = 0.769 \text{ nm}$ and $\beta = 90.9^\circ$) and its space group $P2_1/n$ [61, 62] are very well known.

Like all phases of tungsten trioxide, the monoclinic phase differs from the ideal cubic structure by a slight shift of the tungsten atoms which is repeated periodically in the three directions of space. The structure of the octahedra has thus been deduced by infrared and Raman spectroscopy and by X-ray absorption spectroscopy (XAS) [63, 64].

Taking into account these experimental data, Lambert-Mauriat and Oi-son [57] of the microsensors team carried out studies by numerical computation on the monoclinic phase, and in particular obtained $a = 7.24 \text{ \AA}$ ($a = 7.48 \text{ \AA}$), $b = 7.45 \text{ \AA}$ ($b = 7.66 \text{ \AA}$), $c = 7.61 \text{ \AA}$ ($c = 7.85 \text{ \AA}$) and $\beta = 90.5^\circ$ ($\beta = 90.4^\circ$).

I. 2.2.5. The chemistry of WO_3

WO_3 is an oxide whose transition metal is in a +6 oxidation state, although due to the strong covalent bonds between atoms, tungsten (VI) ions cannot be considered fully charged. +6. Without taking into account the crystallographic structure and at room temperature, tungsten trioxide is a semiconductor with a gap between 2.62 eV [65, 66] and 2.7 eV [67]. Its electrical properties strongly depend on the defects which appear in its volume and on its surface. These defects are mainly oxygen vacancies [68, 69]. Thus, surfaces with oxygen vacancies present active sites for the adsorption process, which determines its properties for gas detection [70]. From an electronic point of view, an oxygen deficiency causes an increase in the electron density on the tungsten cations leading to the formation of electron donor states, which makes WO_3 an n-type semiconductor.

I.2.2.6. Tungstein

The free element is remarkable for its robustness, especially the fact that it has the highest melting point of all the elements discovered, melting at 3,422 °C (6,192 °F; 3,695 K). It also has the highest boiling point, at 5,555 °C (10,031 °F; 5,828 K) [71]. Its density is 19.25 grams per cubic centimetre [72], comparable with that of uranium and gold, and much higher (about 1.7 times) than that of lead [73]. Polycrystalline tungsten is an intrinsically brittle [249] [74][75] and hard material (under standard conditions, when uncombined), making it difficult to work. However, pure single-crystalline tungsten is more ductile and can be cut with a hard-steel hacksaw [76].

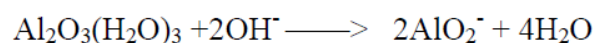
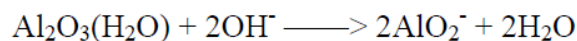
I.2.3. Alumina (Al₂O₃)

Alumina is the generic term given to aluminum oxides of chemical formula Al₂O₃ whether they are anhydrous or hydrated, crystallized or amorphous, without distinction of the phases present. In addition to power electronics applications, alumina is used in many other fields for a wide variety of applications (heat shield, nuclear protection, medical prostheses, etc.)

In the Natural state, alumina is found in bauxite in the form of a hydrate: monohydrate (Al₂O₃ (H₂O)) and trihydrate (Al₂O₃ (H₂O)₃). It is also found as an ore, corundum also known as α-alumina.

The most widely used process for extracting alumina from bauxite is the Bayer process, which is based on dissolving alumina from bauxite.

When hot, soda (NaOH → Na⁺ + OH⁻) dissolves the alumina according to the reactions below, while the impurities (iron oxides and various oxides apart from silica) remain insoluble:



The impurities are separated from the alumina liquor by decantation and filtration. By cooling and diluting the liquor, the reaction is reversed. There is precipitation of an alumina hydrate. After calcination, the alumina powder is obtained which is used in the manufacture of ceramics.

I.2.3.1 Structural and chemical properties

Aluminas exist in seven different crystallographic forms (polymorphs), six of which are metastable forms, also called transition aluminas: Al_2O_3 - θ , - χ , - η , - κ , - δ , - γ . They are all thermally unstable. Above about 1000 °C, they are transformed, by an irreversible exothermic reaction, into α alumina [77]. The latter, also called corundum is the only stable form of aluminum oxide Al_2O_3 .

α -alumina or corundum of trigonal symmetry belonging to the space group R-3c has a rhombohedral structure with ten atoms per unit cell. However, for the convenience of calculations or drawings, the structure of α -alumina is often considered to be a compact hexagonal stack of O^{2-} oxygen anions with Al^{+3} cations occupying two-thirds of the interstices (Figure I.5). This simplified model describes the general nature of the ion arrangement, but not the actual crystal structure of alumina, as it does not reflect the true trigonal symmetry of the crystal.

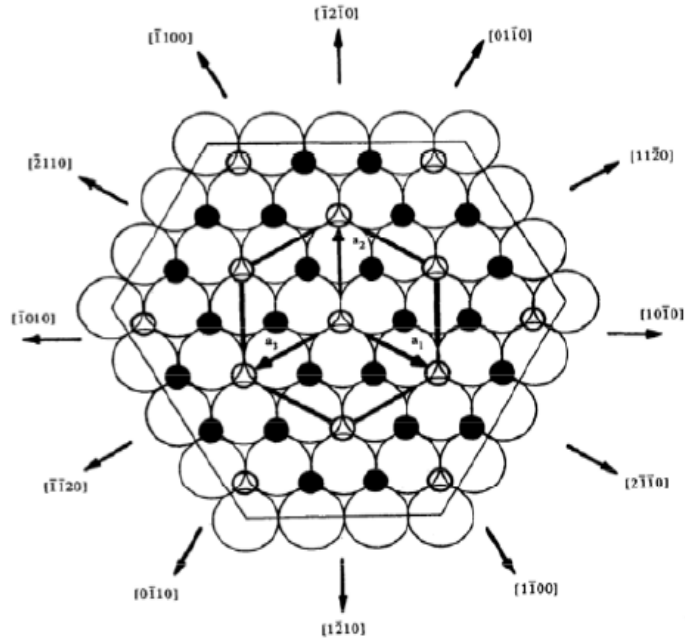


Figure I.4. Projection of the hexagonal structure on the base plane of the structure. Small black circles represent cations, large circles and small circles without colors represent anions and vacant octahedral sites respectively[77].

Alumina is distinguished by ionic and covalent hybrid bonds. Its great ability to resist degradation due to external agents is explained by the strength and stability of these two types of connections. At room temperature, it is unaffected by common chemical compounds, it melts at more than 2000 °C. In addition, the chemical inertia of ceramics is due to their energy state unfavorable to chemical combinations. In particular, the inexistence reactivity of alumina with respect to air.

I.2.3.2. Aluminium

Aluminum is a soft, light, but strong metal with a matte silver-gray appearance, due to a thin five to ten nanometer oxidation layer that forms quickly when exposed to air and prevents corrosion to progress under normal chemical exposure conditions. This film composed of alumina forms spontaneously very quickly when the aluminum comes into contact with an oxidizing medium such as oxygen in the air. Unlike most metals, it is usable

even if it is oxidized on the surface. We can even say that without this oxide layer, it would be unsuitable for most of its applications. It is possible to artificially increase the thickness of this oxidation layer by anodizing, which increases the protection and decorates the rooms by coloring the oxide layer. Unlike aluminum, which is a very good conductor, aluminum oxide is an excellent insulator. Aluminum has a density (2.7) about three times lower than that of steel or copper; it is malleable, ductile and easily machined and molded. It is the second most malleable metal and the sixth most ductile. It is paramagnetic and does not cause sparks.

I.2.3.3. Overall

Alumina is used in various fields for high voltage applications in power electronics due to its good electrical resistance [78], thermal conductivity [79] and mechanical resistance [79, 80]. Its choice as a substrate for providing electrical insulation in power modules results from a good compromise between its dielectric properties and its economic cost.

The correct functioning of the modules strongly depends on the reliability of the materials integrated in the module, in particular the insulating substrate. However, in a high voltage environment, the alumina substrate is subjected to various stresses mainly of an electrical nature which can lead to dielectric breakdown. The advent of new technologies such as SiC semiconductor chips which can allow even better performance in terms of voltage withstand could lead to the appearance of even more intense stresses at the level of insulation in a power module. . A preliminary study of the structure and of the various physical characteristics of the material used for the electrical insulation is therefore necessary. The electrical, thermal and mechanical characteristics of alumina make it a good candidate for applications in a high voltage environment. In addition to these insulating properties, its high thermal conductivity allows it to dissipate heat easily, its thermal expansion coefficient close to the thermal expansion coefficients of the surrounding

materials, makes it possible to minimize the stresses generated under the effect of heating and finally, its high mechanical strength makes it suitable for coping with the mechanical stresses generated by the high voltage environment.

I.2.4 General Information on prickly pear

Nopal is the Mexican name, of Aztec origin, for the prickly pear. It is a succulent, original and very useful plant, characterized by stems in the shape of thick, elliptical rackets, surmounted in spring by beautiful flowers of bright yellow color, followed by yellowish green ovoid fruits, sometimes tinged with red. They contain a sweet, reddish, greenish or yellowish pulp dotted with many small seeds. Its fruit is picked from late July to September, is eaten peeled, and its pulp, coral or red in color, appears full of small dark seeds (figure 1).

Its sobriety and its incredible vitality allow this Cactus to thrive even in often inhospitable desert regions, where it offers man and domestic animals its nourishing and therapeutic virtues. There are more than 400 species and countless varieties.

Among the American Indians, Nopal has always belonged to the most widely used medicinal plants. For pre-Columbian populations, modern medical research is rediscovering with growing interest the plant and its properties. She studies the active molecules that compose it and allow it to fight effectively against some of the most serious ailments of our time: anxiety, arteriosclerosis, cholesterol, diabetes, obesity, spasmophilia, stress

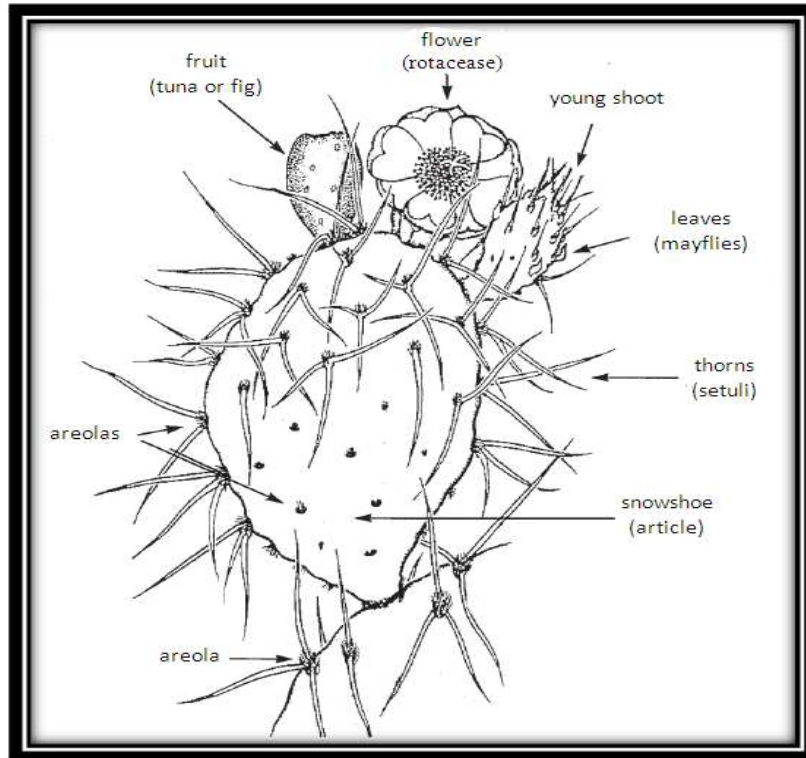


Figure I.5. General appearance of *Opuntia ficus-indica*. [81]

I.2.4.1 advantages of opuntia ficus indica :

Scientifically , biomass is defined as the total mass of all organisms , plant , animal . or otherwise in a given area . it can be any naturally occuring materials that are in our surroundings . technically , it constitutes organic and inorganic matters from the animal and plants sources ; however, the majority of folks are using this term for plant-based materials , which are in debate , these unused plant or plant-based materials are specifically known as opuntia ficus indica .today it is well known that biomass is a rich source of energy and other daily useful products . biomass emerged as a potential alternative . this is attributed to their green nature , low cost . and easy and large availability .

Environmental activities . natural resource conservation , and strict laws passed by developing countries compel researchers to develop materials having renewable characteristics [82].

in this regard *Opuntia ficus indica* emerged as a suitable candidate as they are derived from renewable resources and are environmental –friendly . Furthermore , other features like amazingly low weight and high strength make them further attractive for future use

I.2.4.2 Chemical composition of barbarism snowshoes

The prickly pear snowshoes are characterized by a nutritional imbalance although they are a source of energy and water. The water content of fresh snowshoes varies from 80 to 90%. Snowshoes are known to be rich in minerals, mainly calcium and oxalates, and in mucilage, polysaccharides with a sometimes very complex chemical structure found in several higher plants

The majority fraction of the mucilage of prickly pear consists of a neutral polysaccharide and analyzes of sugars show a predominance of D-galactose, D-xylose, L-arabinose, L-rhamnose and D- acid. galacturonic.

It has the ability to absorb large amounts of water or solvents and disperses forming viscous or gelatinous colloids. [83]

Researchers have reported in the composition of Nopal the presence of tannin, traces of berberine and another indeterminate alkaloid. The mucilaginous substance which makes the richness of *Opuntia* is pectin (1 kg of fresh stems provides 7.5 grams of calcium pectate). Its ashes are rich in iron. [81]

Table I.4. Chemical composition of *Opuntia* snowshoes [84].

Feature	Value in % dry matter
Cellulose	15
Starch	12
Total nitrogenous matter	5-7
Fat	2
Ashes	16-18
Oxalates	13
Calcium	2-4
Phosphorus	0.2

I.3. Conductive polymers

I. 3.1. General information on conductive polymers

Studies of the first conductive polymers began with the work of Heeger, MacDiarmid and Shirakawa in 1977 [85] on the conductivity of polyacetylene by doping with iodine. Indeed, they have demonstrated that it is possible to vary the conductivity of this polymer by means of doping making it possible to go from an insulating state to a conductive state. The electrical conductivity of this material could reach values up to 10^5 S.cm^{-1} .

The discovery of Heeger, MacDiarmid and Shirakawa was an upheaval in the perception of organic polymers; this discovery earned them the Nobel Prize for chemistry in 2000.

Therefore, different families of conductive polymers have been synthesized. Among others, mention may be made of polyacetylene [86], polyparaphenylene [87-89], polyphenylene [90], polythiophene [91], polypyrrole [92, 93], as well as polyaniline [94-97].


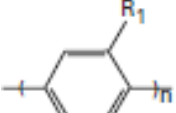
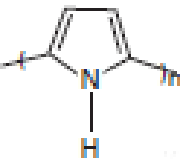
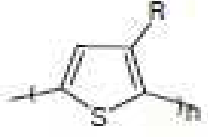
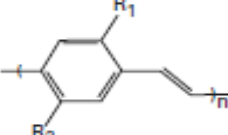
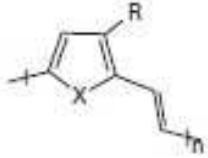
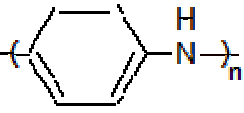
Among the existing conductive polymers, Polyaniline (Pani) is widely used because of its optical and electrochemical properties, its good chemical stability and above all its electronic conduction properties, making it possible to achieve conductivities greater than 10^4 S.cm^{-1} .

I. 3.2. Classification of conductive polymers

Conductive polymers belong to the family of π -conjugated polymers. These polymers are characterized by an alternating structure of single bonds (σ type) and double bonds (π type) in their carbon chains, allowing the delocalization of π electrons along the macromolecule. Conductive polymers can be classified according to the structure of their carbon chain into different families [98].

- Polyene polymers whose carbon chain is linear, such as polyacetylene (PA).
- Heterocyclic aromatic polymers whose chain contains aromatic heterocycles such as polyparaphenylene (PPP) and its derivatives, polypyrrole (PPy), polythiophene (PT) and its derivatives or polyethylene dioxythiophene (PEDOT).
- Mixed polymers whose chains alternate heterocycles and double bonds, such as polyphenylene vinylene and its derivatives (PPV) and polyheteroarylene vinylene and its derivatives (PTV).
- Aromatic polymers with heteroatoms whose chain is formed of aromatic rings containing heteroatoms such as polyparaphenylene sulfide (PPS) and Polyaniline (PANI) (Table I. 2).

Table I. 5. The main families of conductive polymers

Family	Example of polymer
The polymers polyene	Polyacetylene 
The polymers aromatic heterocyclic	<p>polyparaphenylene </p> <p>Polypyrrole </p> <p>Polythiophene </p>
The polymers mixed	<p>Polyphenylene vinylene </p> <p>Polyheteroarylene vinylene </p>
The polymers aromatic with heteroatoms	Polyaniline 

The conductivity of a material generally depends on the density of charge carriers and their mobility. In the case of metals, the charge carriers are electrons, while in conductive polymers, electrons as well as holes are able to move freely generating a current. Conductivity also varies with temperature; she decreases with increasing temperature for metals [99], while it increases for conductive polymers [100]. The conductivity of the latter can be controlled by doping (Figure I. 14). It can evolve from an insulating state $\sigma < 10^{-10}$ S.cm⁻¹, to that of a semiconductor $\sigma \sim 10^{-5}$ S.cm⁻¹, to that of a conductor $\sigma > 10^5$ S.cm⁻¹ [101].

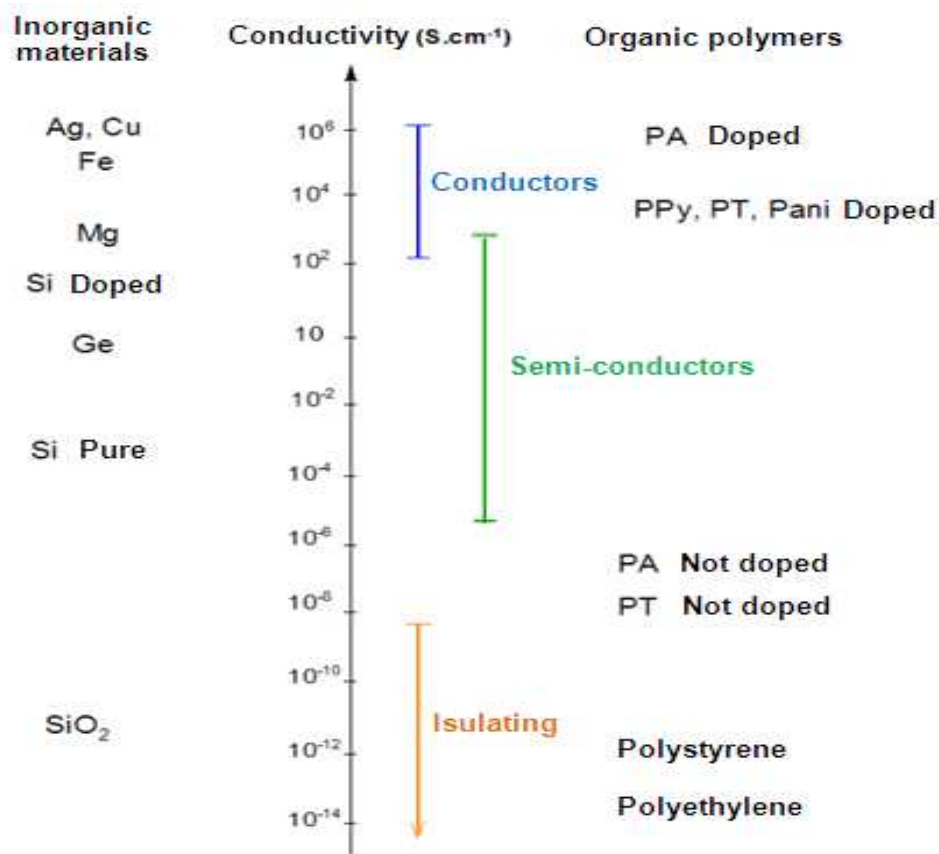


Figure I. 6. Electrical conductivity of intrinsic conductive polymers

I. 3.3. Electronic structure of conductive polymers.

In the case of conductive polymers, electronic conduction and the transport of charges cause the creation of free charge carriers along the polymer chain. Their electronic structure depends on band theory, originally designed to interpret conduction in semiconductors.

In a semiconductor, the energy bands correspond to the energy levels that are allowed, or prohibited, for the electrons of the elements or compounds that make up the material. The last band filled is called the BV valence band or HOMO (High Occupied Molecular Orbitals) and the next higher band is the BC or LUMO (Lowest Unoccupied Molecular Orbitals)

conduction band. The energy band between these two levels corresponds to the forbidden band or the Fermi energy or more simply "gap".

The energy difference E_g between these two levels ($E_g = E_{BC} - E_{BV}$), of the order of an electronvolt (eV), constitutes the width of the gap which determines the intrinsic electrical properties of the material [102]. The position of the energy bands for a metal, a semiconductor and an insulator, is shown schematically in figure I. 15.

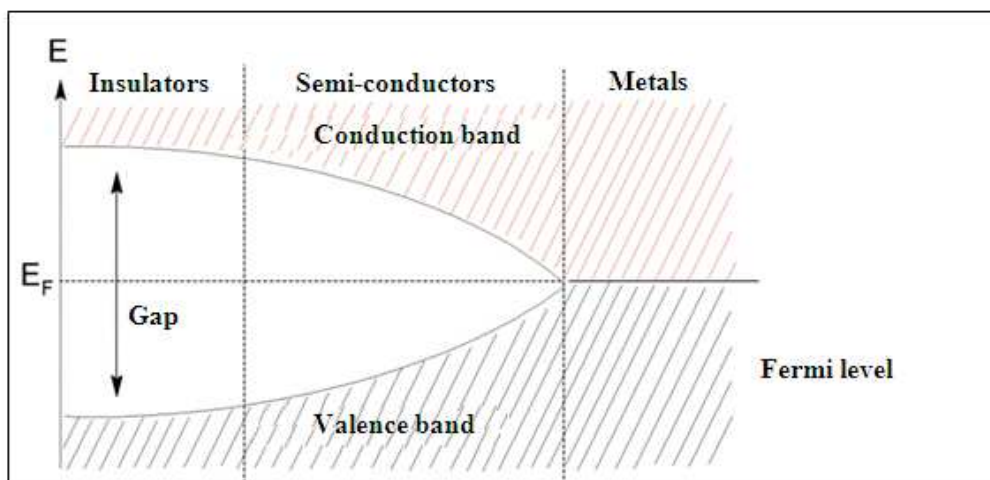


Figure I. 7. Theoretical diagram established according to the theory of energy bands

The undoped π -conjugated polymers are semiconductors or even insulators in the neutral state. Their electronic conductivity σ_{dc} is of the order of $10^2 - 10^8 \text{ S.cm}^{-1}$. Table I. 3 groups together the gaps of the most studied conjugated polymers.

Table I.6. Gap of the main families of conjugated polymers

Conjugated polymer	Gap (eV)	Conjugated polymer	Gap (eV)
PPP	2.7 [103]	Trans-PA	1.4 - 1.5 [106]
PPV	2.5 - 2.7 [104]	Pani -EB	1.4 [107]
PPY	3.2 [105]	Pani -PNGP	1.8 - 2.0 [107]
PT	2.0 - 2.1 [105]	Pani -LEB	3.8 [107]

I. 3.4. Doping of conductive polymers

Conductive polymers in the neutral or reduced state are insulators. Through a process called doping, they are transformed into conductive materials by the introduction of mobile charge carriers. The term doping is adopted from solid-state physics by analogy to the doping of inorganic semiconductors. However, the doping of conductive polymers is totally different from that of inorganic semiconductors.

In fact, the doping of polymers is a chemical reaction to increase the conductivity of the polymer to reach values close to that of metals (Figure I. 16).

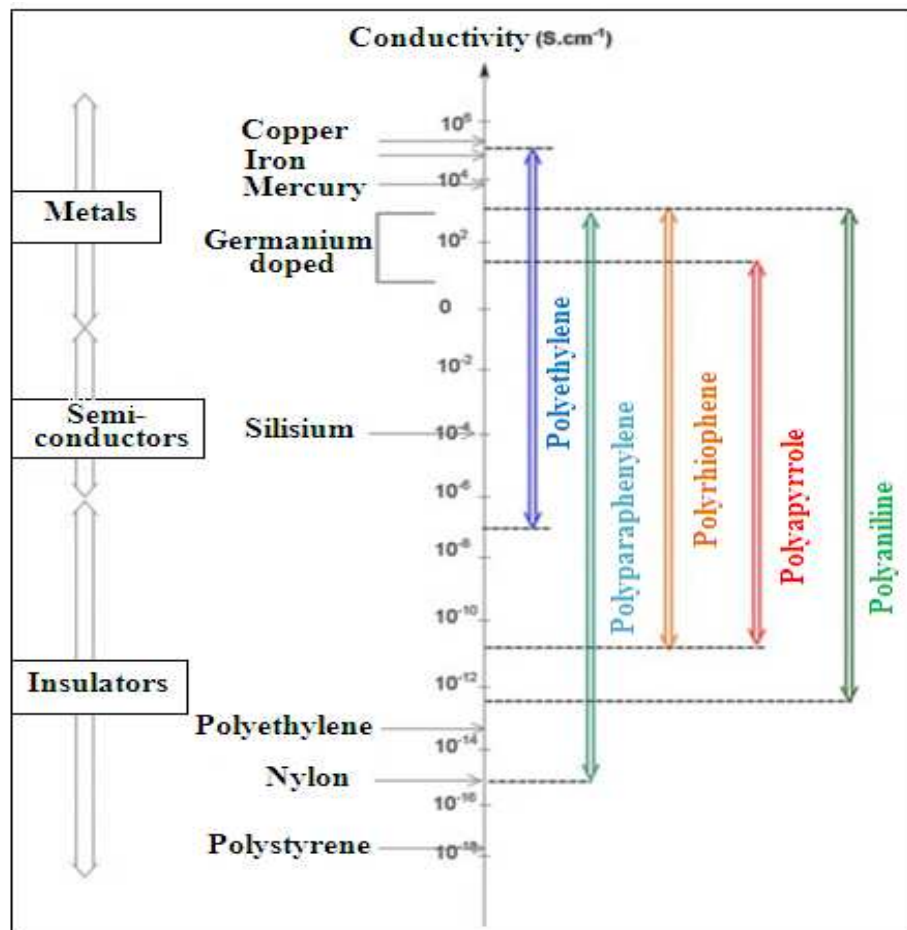


Figure I. 8. Conductivity of various conductive polymers and conventional materials

Generally, this doping is carried out by an oxidation-reduction reaction which consists in introducing donor species: n-type doping (reduction of the polymer) or acceptors of

electrons : p-type doping (polymer oxidation). These species are called dopants or counter ions which ensure the electroneutrality of the material. Electric charges are then created on the polymer chains. The increase in the doping rate makes it possible to witness an insulator-conductor transition [108].

I.3.5. Load carriers

Electronic conduction in the case of conductive polymers and the transport of charges in general first require the possibility of creating free charge carriers. Indeed, during the injection of a charge into a polymeric backbone, a charge defect is created, accompanied by a local modification of the geometry of the chain. As seen previously, energy states are then created in the gap due to the shift of the valence band and the conduction band [109].

Conjugated polymers are classified into two categories according to the symmetry of their ground state. The degenerate ground state where several different forms of the same polymer have the same energy (case of polyacetylene). The non-degenerate ground state where the permutation leads to a different energy structure, possibly several forms associated with local energy minima, but only one form is associated with the general minimum (case of polythiophene).

The introduction of charges by doping these polymers leads to the formation of charge carriers on the macromolecular chain. These charges formed are called solitons for polymers in the degenerate ground state and polaron or bipolaron for polymers in the non-degenerate ground state [109].

I.3.6. Polyaniline

I.3.6. 1. Presentation

The polyaniline , better known under the name "aniline black," has been studied since the XIXth century [110,111]. In 1862, Letheby obtained Polyaniline for the first time by

electrochemical synthesis. [112] Following Letheby's work, many studies were devoted to the preparation of aniline black, as well as to the understanding of the reaction mechanism [113, 114].

It was in 1910 that Green and Woodhead succeeded in defining the current terminology of Polyaniline and its different degrees of oxidation [115]. They have contributed to the explanation of the different redox and protonated states of this polymer.

Two decades later, Shirakawa et al. have discovered the conduction properties of the polyaniline, thus opening a new perspective to conductive polymers [116].

After this discovery, MacDiarmid et al. [117, 118] and Travers et al. [119] reported the detailed mechanism of polyaniline formation. This mechanism is accompanied by a remarkable increase in conductivity of more than 10 orders of magnitude (up to $1-5 \cdot 10^2 \text{ S.cm}^{-1}$) highlighting the conduction properties of Polyaniline, recognized as one of the intrinsically conductive polymers.

The generic structure of the different forms of the Pani is shown in Figure I.17.

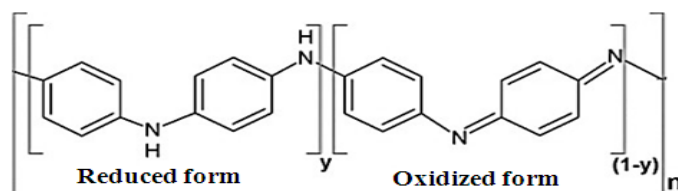


Figure I. 9. Generic structure of Polyaniline

where y accounts for the fraction of reduced units associated with amines and $(1-y)$ corresponds to the fraction of oxidized units containing imines. MacDiarmid [120-123] defined three discrete values of the quantity $(1-y)$:

- $(1-y) = 0$: the polymer is totally reduced, it is **leucoemeraldine base**.
- $(1-y) = 0.5$: the polymer is semi-oxidized, it is known under the name of **emeraldine base**.

- $(1-y) = 1$: the polymer is totally oxidized, it is the **pernigraniline base**.

These three forms of Polyaniline are insulating compounds (Figure I. 18). In an acidic medium, these polymers are protonated at their amine or imine sites. So, in addition to these different oxidation states, there is the effect of protonation to become conductive material. This

This phenomenon will be further developed in the following paragraph devoted to the doping of Polyaniline

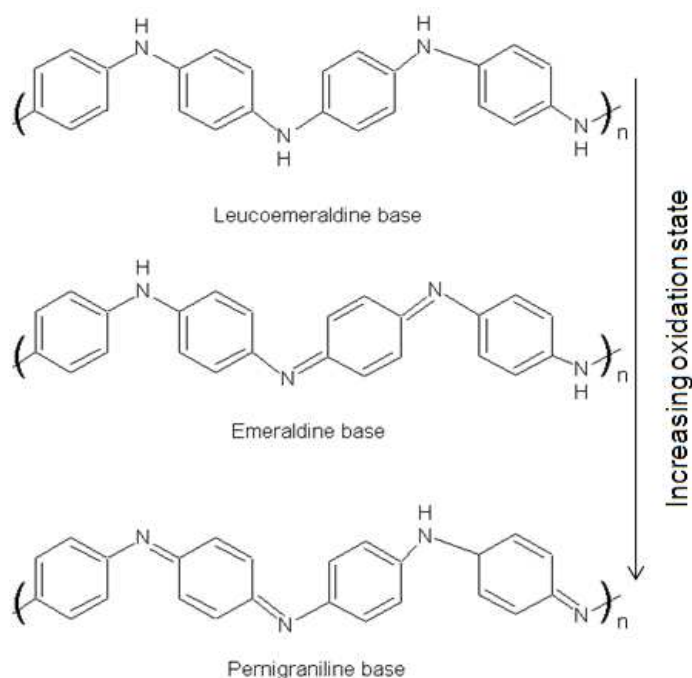


Figure I. 10. Different oxidation states of Polyaniline

I.3.6. 2. Doping of polyaniline

As for the other conductive polymers, the doping of Polyaniline can be carried out thanks to an oxidation-reduction reaction which corresponds to a modification of the number of electrons of the π system. In the case of Polyaniline, a p-type doping is observed. This

process creates a delocalized positive charge, accompanied by the insertion of a doping counterion to balance the charge on the polymer chain [124, 125].

The doping of the Pani can also be carried out without modifying the number of electrons of the π system, following an acid-base doping or protonation. Unlike redox doping, only the number of electrons in p orbitals in imine sites are involved [126]. This process is made possible by the acid-base properties of Polyaniline. Indeed, Pani has two pKa equal to 2.5 and 5.5 attributed to the quinone diimines and benzene diamines functions, respectively [127, 128].

Consequently, this polymer has the particularity of passing from the insulating state to the conductive state either by oxidation or by protonation as indicated in Figure. I. 18 below.

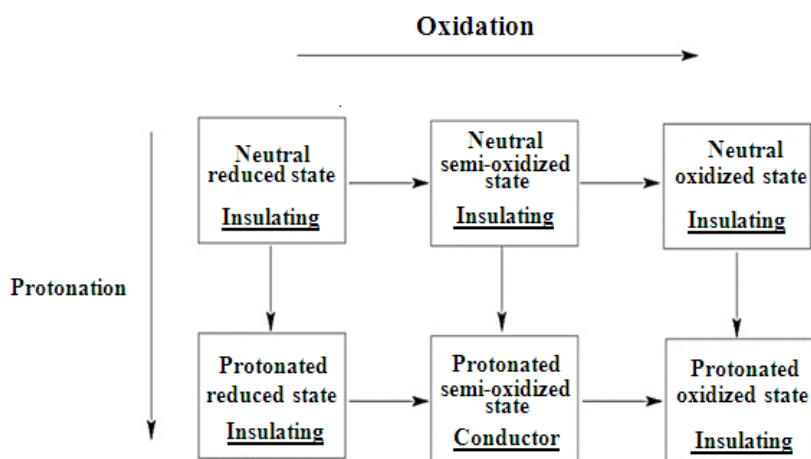


Figure I. 11. Doping of the different states of Polyaniline

Each base state of Polyaniline can be protonated by an acid to give the corresponding Polyaniline salt. Only the proton doping of the semi-oxidized state (Pani-Émelaldine Base) makes it possible to lead to a conductive emeraldine salt (Figure I. 20).

The protonated polymer chain performs an internal redox rearrangement to leave room only for benzene rings (energetically equivalent) accompanied by the insertion of the counterion, thus ensuring the electroneutrality of the system to form the emeraldine salt. A

protonation rate is then defined by the ratio of the number of counterions inserted to that of nitrogen atoms which can reach a maximum of 50 mol% (protonation of the imine sites of emeraldine base).

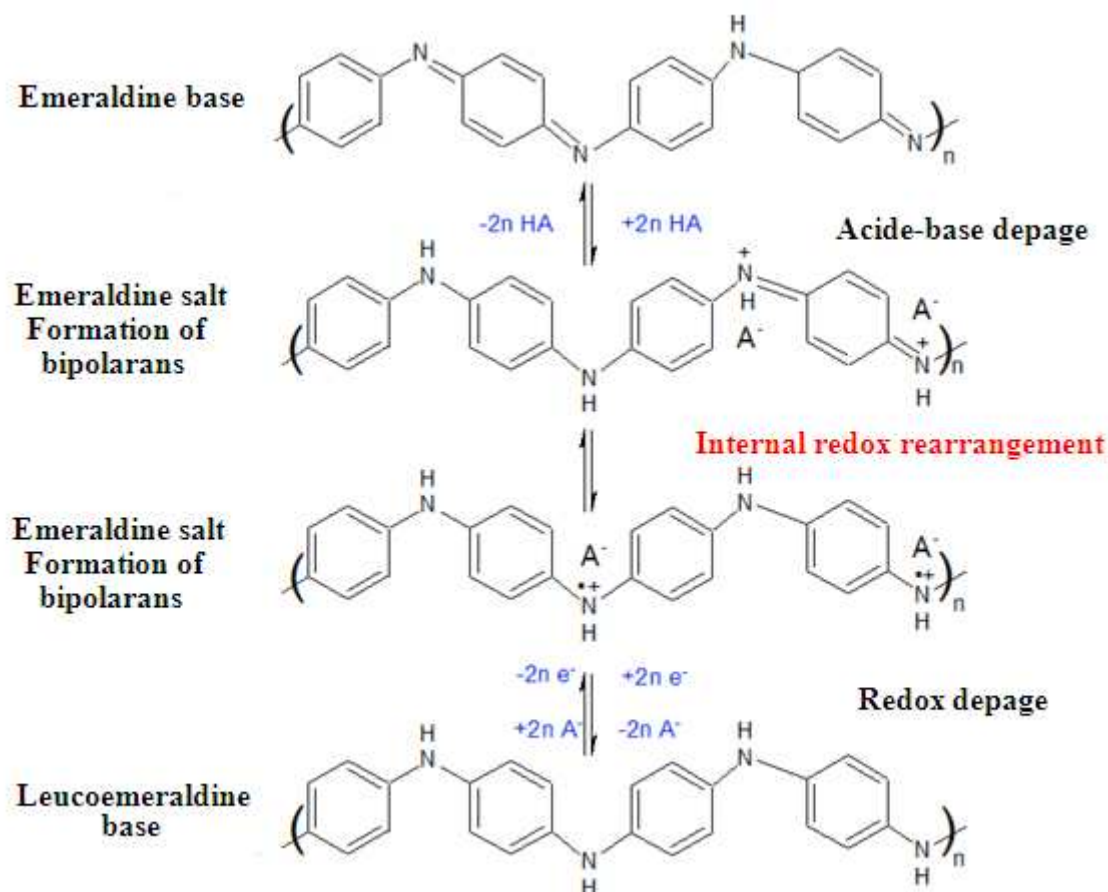


Figure I. 12. Proton doping of emeraldine base and redox doping of leucoemeraldine base (HA: acid, A⁻ : against ion)

I.3.6. 3. Synthesis of Polyaniline

Various synthetic methods have been developed for the production of Polyaniline. There are physical methods such as electrospinning [129], lithography [130], spincoating [131] and pulsed plasma irradiation [132], but also chemical methods using a template or "template", with hard templates called "hard template" [133-135] or with flexible templates called "soft template" [136-140], or also without the use of a template (template -free

method); for example polymerization without stirring [141], mechanochemical synthesis [142] and electrochemical synthesis (cyclic voltammetry [143], potentiostatic [144] and galvanostatic [145] mode).

As part of our work, we have chosen to synthesize Polyaniline by the oxidative chemical polymerization of aniline ($C_6H_5NH_2$) by an oxidizing agent. This synthetic route was developed by MacDiarmid et al in 1985 [92]. It has the advantage of being simple and often used to synthesize Pani.

Several studies have shown that various experimental parameters influence the properties of the polymer obtained. These parameters can be classified in a hierarchical order according to their importance: the nature of the oxidant, the oxidant / monomer molar ratio, the polymerization time and the nature of the dopant:

- The nature of the oxidant

The standard synthesis procedure is carried out with ammonium persulfate $(NH_4)_2S_2O_8$ (APS) as an oxidant. However, the choice of the oxidizing must satisfy two criteria: its ability to oxidize aniline ($E_{oxidant} > E_{aniline}$) and its stability in the reaction medium. MacDiarmid et al [92] synthesized Pani in an acidic aqueous medium (HCl) in the presence of aniline by adding a solution of $(NH_4)_2S_2O_8$ ($E^\circ (SO_4^{2-}/SO_5^{2-}) = 1760$ mV/ECS). Many oxidizing agents were then used such as KIO_3 , $KMnO_4$, $FeCl_3$, K_2CrO_4 , $KBrO_3$, etc. The only condition is to avoid any chemical degradation (iodination, chlorination, decomposition following crosslinking reactions chemicals...) caused by the oxidant during its reaction with the monomer, such as the example of hydrogen peroxide H_2O_2 ($E^\circ (H_2O_2/H_2O) = 1530$ mV/ECS) [146].

- The oxidant / monomer molar ratio

Another parameter of the synthesis which influences the properties of the polymer obtained is the oxidant / aniline ratio. Pron et al [147] suggested using a normalized ratio which is defined by

$$K_N = 2.5 \frac{n_{\text{aniline}}}{n_{\text{oxydant}} n_e} \quad (\text{I. 1})$$

n_{aniline} = mole's number of aniline

n_{oxydant} = number of moles of oxidant oxidizing e

n_e = number of electrons needed to reduce an oxidant molecule

For a polymerization reaction where Pani is obtained in its emeraldine form, each monomer must remove on average 2.5 electrons. In the case of ammonium peroxodisulphate, the K_N ratio is equal to 1.25 due to the electronic nature of the couple ($\text{S}_2\text{O}_8^{2-}/\text{SO}_4^{2-}$).

- The time of polymerization

The time of the synthesis reaction plays an important role in the formation of polyaniline. Studies by Cao et al. [148] and Gospodinova et al. [149] demonstrated the existence of two competitive mechanisms during the preparation of the polymer: polymerization and degradation of the molecular chain at quinone diimines sites. The latter was found to increase with increasing synthesis time (greater than 4 hours for the standard procedure).

- The nature of the dopant

The standard procedure uses hydrochloric acid (HCl) as a dopant [150, 151]. The conductive powder Pani (HCl), once compacted in the form of a pellet reveals an electrical conductivity of the order of 1 to 20 $\text{S}\cdot\text{cm}^{-1}$. Many dopants were then used by various researchers:

- Mineral acids: sulfuric acid (H_2SO_4) [152], hydrofluoric acid (HF) [153], perchloric acid (HClO_4) [154]
- Organic acids: formic acid, acetic acid, acrylic acid [155]

- Sulfonic acids: camphor sulfonic acid (CSA) [156-158], methanesulfonic acid (MeSA) [159], p-toluenesulfonic acid (PTSA) [160], dodecyl benzenesulfonic acid (DBSA) [161]
- Les acides phtaliques [162]

I.3.6. 4. Polymerization mechanism

Even if many teams have been interested in the polymerization mechanism of aniline [163-171], these mechanisms still remain to this poorly known day. The acidity of the reaction medium increases during the polymerization of the aniline because protons are produced during the reaction. Even when the reaction is carried out under alkaline or weakly acidic conditions, i.e. under conditions where the aniline is essentially unprotonated ($\text{pH} > \text{pK}_a$ of aniline = 4.6), the proportion of anilinium cation can increase sharply during the reaction. Aniline oxidizes more easily than the anilinium cation. Thus, the oxidation of anilinium sulfate occurs slowly in the first moments. The oxidation of aniline is rapid and generates a significant exotherm in the first moments when the polymerization starts in a weakly acidic, neutral or alkaline medium, then, when the pH reaches the value of 3.5, the reaction slows down considerably because the aniline is then essentially protonated. The reaction remains slow in the pH range 2.5-3.5. In this pH range, chain growth occurs by oxidation of $\text{C}_6\text{H}_5\text{NH}^{+3}/\text{C}_6\text{H}_5\text{NH}_2$ by non-protonated oligoaniline pernigraniline chains. At around pH 2-2.5, the reaction accelerates due to the protonation of pernigraniline. This is because the oxidizing power of protonated pernigraniline is much stronger than that of non-protonated pernigraniline. Stejskal's team recently proposed a mechanism for the oxidation of anilinium sulfate and aniline by ammonium persulfate (APS) in aqueous solution [172, 173] (Figure 1.10). Polymerization of anilinium sulfate and aniline leads to para-linked trimers and tetramers by N-C bonds. The nitrenium cation of aniline is the main electrophile formed

during the priming step. It should be emphasized that the dimer formed is predominantly 4-aminodiphenylamine (4-ADPA). In an acidic medium, the electrophilic substitution of the anilinium cation with the nitrenium cation should preferably take place in the meta position and lead to 3-aminodiphenylamine. Thus, despite the low proportion of aniline in an acidic medium, the markedly higher reactivity of aniline compared to the anilinium cation leads to the predominant 4-ADPA dimer. 4-ADPA is rapidly oxidized by peroxydisulfate to give N-phenyl-1,4-benzoquinonediimine (PBQI). Another reaction path for the oxidation of aniline results in the formation of substituted phenazines such as pseudomauvein, by ortho N-C coupling. The formation of these substituted phenazines is limited in an acidic medium (pH < 2.5). The self-assembly of these phenazine units leads to the formation of particular morphologies for the polyaniline such as nanofibers, nanotubes, or nanospheres.

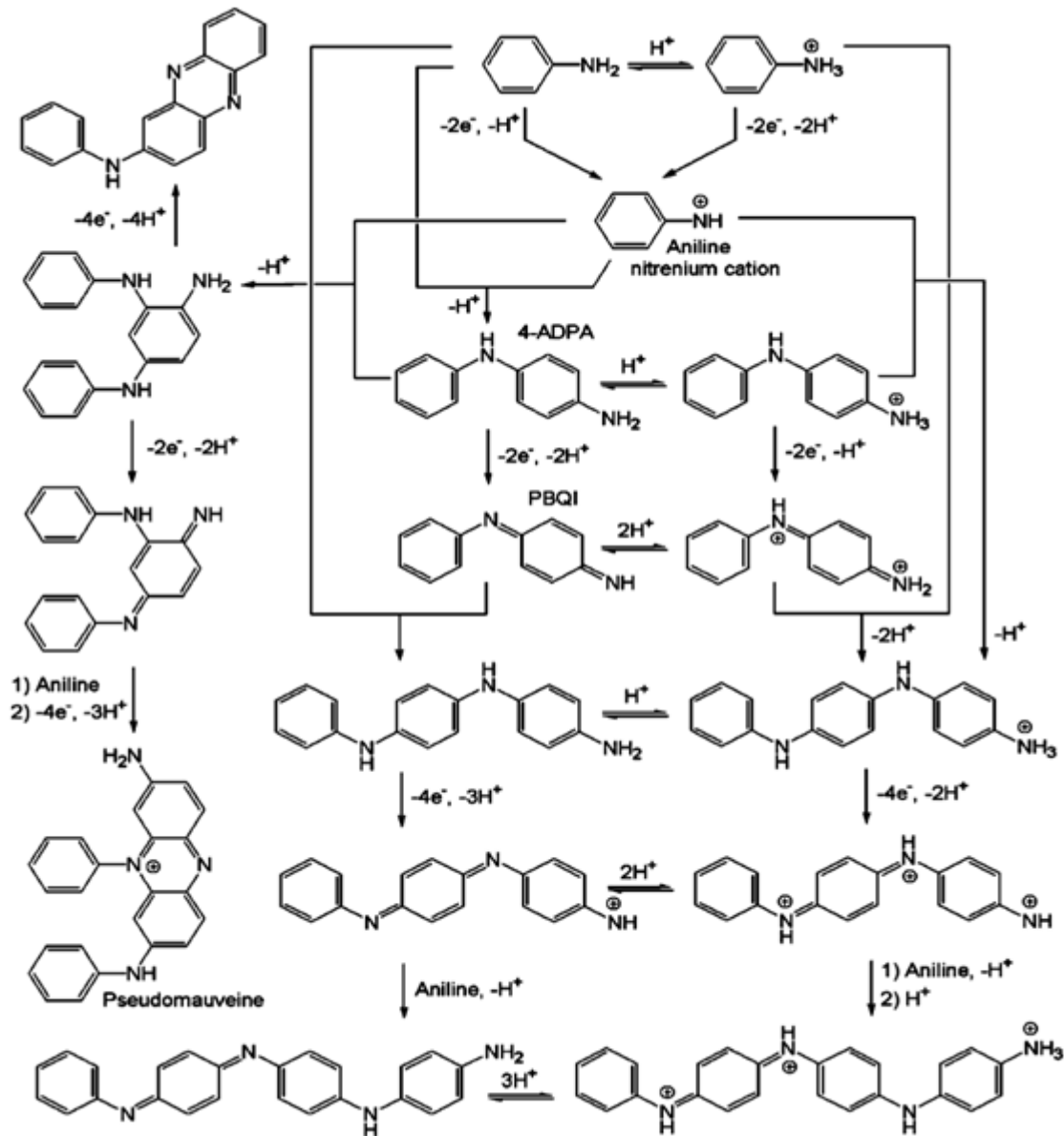


Figure 1.13. First steps in the oxidation of aniline and anilinium cations by APS in acidic HCl [171]

I.3.6. 5. Factors influencing the electrical conductivity of polyaniline

The overall conductivity (σ) of PANI is the sum of the intra-molecular (intra), inter-molecular (inter) and inter-domain (domain) conductivities (Equation 1.1).

$$\sigma = \sigma_{\text{intra}} + \sigma_{\text{inter}} + \sigma_{\text{domain}} \quad (\text{Equation 1.1})$$

Intra-molecular charge transfer depends on the well-defined band structure specific to the polymer. Any defect in the structure can lead to a decrease in intramolecular (intra)

conductivity. Inter-domain (domain) conductivity is associated with clusters of organized polymer chains trapped in an insulating matrix, the movement of charge carriers from one crystalline region to another crystalline region or between a crystalline region and an amorphous region. The four main factors that influence the conductivity of PANI are: (i) molecular mass, (ii) rate of crystallinity and inter-chain distance, (iii) level of oxidation and molecular arrangement, and (iv) the doping rate and the type of dopant [174-178]. Thus, a chain distortion observed at high molar masses leads to a decrease in electrical conductivity [175-181]. It is generally accepted that the intra-molecular mobility of charged species along the chain, and to some extent the inter-molecular jump of charge carriers, increases with increasing rate of crystallinity. This leads to an increase in conductivity. Moreover, a decrease in the inter-chain distance increases the possibility of inter-chain jump of the charge carriers and therefore leads to an increase in conductivity [182-185]. A 50% doping rate of the emeraldine base form leads to maximum conductivity because it leads to an ideal polaron structure. On the other hand, the formation of bipolaron at higher doping rates (> 50%) causes a decrease in conductivity [186-188].

I.3.6. 6. Applications of polyaniline

Polyaniline is particularly interesting because of its possibilities of chemical or electrochemical polymerization from inexpensive reagents, easy doping and processing combined with high electronic conductivity and finally good stability to water. environment and during operation. Its use, alone or in mixtures [189,190] makes it possible to achieve a wide range of conductivity ranging from 10^{-12} to 10^3 S.cm⁻¹. Also, the existence of three degrees of oxidation and an easy to control doping allows to consider the use of PANI in multiple applications. Polyaniline has properties analogous to inorganic semiconductors and can therefore potentially replace them in conventional electronic and optoelectronic devices,

such as photovoltaic cells, field effect transistors (FET), organic light-emitting diodes (OLED), capacitors, etc. PANI has also entered the formulation of paints, inks and conductive adhesives for various applications as conductive coating, anticorrosion treatment, or as electromagnetic or antistatic shielding.

The main applications of polyaniline are summarized in Table 1.3. The aspect associated with the protection of metals against corrosion will be described in the next paragraph

Table I.7. Main applications of polyaniline and associated specific properties

Specific properties	Applications	Ref
Electrical conductor	Paints, inks, conductive adhesives	[191-195]
	Antistatic textile	[196]
	Electrostatic discharge materials	[197-198]
Viscosity increases under electric field	Electro-rheological (ER) material	[200-204]
Conductivity electric or change of color after exposure to liquids or vapors acid , basic or neutra	Gas sensor: NH ₃ , CO ₂ , NO ₂ , CO, Cl ₂ , O ₃	[205-210]
	Toxic gas sensor, compounds volatile organic	[211], [212]
	Chemical sensor, humidity, petroleum	[213]-[214]
	PH sensor, mercury, biosensor	[215-216]
	Vitamin C detector, bacteria	[218], [219]
Change of color in depending on the medium PH	"Acid-Base" indicator	[220]
Change of morphology of the process of protonation-deprotonation and oxidation-reduction	Gas separation membranes	[221], [222]
	Solution separation membranes neutral	[223], [224]
Change in oxidation state loading and unloading at both of the ion diffusion.	Ion exchange material	[225], [226]
Values of capacity very high	Capacitor	[227], [228]
	Energy storage devices	[229], [230]
Absorptivity and reflectivity of radiation electromagnetic	Shielding against the interference electromagnetic	[231-233]
Modulation possible of the conductivity	Digital memory device conductivity	[234]
Varriations of constraint under pulsed current.	Artificial muscle	[235], [236]

Capacity at accumulate and transform energy (understood of the frequencies optical) and by therefore, to memorize (to erase) of information	Electrode for rechargeable batteries	[237-240]
	Microbial fuel cell anode (MFC)	[241]
	Electrochromic screen and smart window	[242-245]
Possibility of edit his electro-donor properties or electro-acceptor in function oxidation state	p-n heterojunctions	[246], [247]
	Solar cell	[248], [249]
	Diode	[250], [251]
Program of color under electrical stress	Polymer light emitting diode	[252], [253]

I.4. Reference

- [1] Mouritz AP, Gibson AG. Fire Properties of Polymer Composite Materials Pub Springer (2006).
- [2] Iona Plesa, Petru V. No tingher, Sandra Schlögl, Christof Sumereder and Michael Muhr. *Polymers*, 8, 173 (2016).
- [3] Jeong S.H, Song H.C, Lee W.W, Choi Y.M, Lee S.S, Hwan-Ryu B.Y, *J. Phys. Chem. C*, 114, 22277-22283 (2010).
- [4] Zhang Y.H, Lv F.Z, Ke S.J, Yu L, Huang H.T, Chan H.L.W, *Mater. Chem. Phys*, 129, 77- 82 (2011).
- [5] Bokern S, Getze J, Agarwal S, Greiner A, *Polymer*, 52, 912-920 (2011).
- [6] FAN Fangqiang, XIA Zhengbin, LI Qingying, LI Zhong and CHEN Huanqin. *Chinese Journal of Chemical Engineering*, 21(2) 113—120 (2013).
- [7] Wyckoff, R.W.G. *Crystal Structures*, 2nd ed; Wiley: New York, (1964).
- [8] Mouritz AP, Gibson AG. Fire Properties of Polymer Composite Materials Pub Springer, (2006).
- [9] Ratna D Rapra Review Reports Volume 16, Number 5, (2005).
- [10] Friedrich K Fakirov S Zhang Z. Springer (2005)
- [11] A. Okada, A. Usuki, *Materials Science and Engineering C*, Vol. 3, p. 109-115 (1995).
- [12] E. Reynaud, T. jouen, C. Gauthier, G. Virgier, J. Varlet, *polymer*, Vol. 42, p. 8759-8768 (2001).
- [13] J. W. Gilman, *Applied Clay Science*, Vol. 15, p.31-49 (1999).
- [14] S. Wang, Y. Hu, R. Zong, Y. tang, Z. Chen, W. fan, *Applied clay Science*, Vol. 25, p. 49-55 (2004).
- [15] M. Knite, V. Teteris, B. Polyakov, D. Erts, *Materials Science and Engineering C*, Vol. 19, p. 15-19 (2002).

- [16] Yu A. Barnakov, B.L. Scott, V. Golub, L. Kelly, V. Reddy, K.L. Stokes, *Journal of Physics and Chemistry of Solids*, Vol.65, p.1005-1010 (2004).
- [17] V.A. Soloukhin, W. Posthumus, J.C.M. Brokken-Zijp, J. Loos, G. de With, *Polymer*, Vol. 43, p. 6169-6181 (2002).
- [18] L. Matejka, K. Dusek, J. Plestil, J. kriz, F. Lednický, *Polymer*, Vol. 40, p. 171-181 (1998).
- [19] Yuvaraj Haldorai and Jae-Jin Shim, *Adv Polym Sci* DOI: 10.1007/12-285 (2014).
- [20] C-M. Chan, J. Wu, J-x. Li, Ying-Kit Cheung, *polymer*, Vol. 43, p. 2982-2992 (2002).
- [21] Y. Zheng, Y. Zheng, *journal of applied polymer science*, Vol.99, N°5,p. 2163-2166 (2006).
- [22] W. Jiang, S.C. Tjong, *Polymer Degradation and Stability*, Vol. 66, p. 241-246 (1999).
- [23] P.J. yoon, D.L. Hunter, D.R. Paula, *Polymer*, Vol. 44, p. 5323-5339 (2003).
- [24] F.-K. Liu, S.-Y. Hsieh, F.-H. Ko, T-C. Chu, *Colloids and Surfaces a Physicochem.Eng. Aspects*, Vol. 231, p. 31-38 (2003)
- [25] M. Knite, V. Teteris, al. Kiploka, J. Kaupuzs, *Sensors and Actuators A*, Vol. 110, p. 142-149 (2004).
- [26] J. Zeng, B. Saltysiak, W.S. Johnson, D. A. Schiraldi, S. Kumar, *Composites : Part B*, Vol. 35, p.173-178 (2004).
- [27] L. Chazeau, J.Y. Cavaille, P. Terech, *Polymer*, Vol. 40, p. 5333-5244 (1999).
- [28] Dilini Galpaya, Mingchao Wang, Meinan Liu, Nunzio Motta, Eric Waclawik, Cheng Yan, *Graphene*, 1, 30-49 (2012).
- [29] W. Zheng, S.-C Wong, H.-J. Sue *Transport behavior of PMMA/expanded graphite nanocomposites* *Polymer*, 2002, Vol.73, p. 6767-6773.
- [30] Min Zhi Rong, Ming Qiu Zhang, Guang Shi, Qiu Long Ji, Bernd Wetzel, Klaus Friedrich *Graft Tribology International* 36 697– 707 (2003).

- [31] In-Yup Jeon and Jong-Beom Baek, 3, 3654-3674 doi: 10. 3390/ma3063654 (2010).
- [32] Armelao L, Barreca D, Bottaro G, Gasparotto A, Gross S, Maragno C, Tondello E
Coord. Chem. Rev., 250, 1294-1314 (2006).
- [33] Jin R.C, Cao Y. W, Mirkin C. A, Kelley K. L, Schatz G. C, Zheng J. G, Science 294,
1901-1903 (2001).
- [34] Tizazu G, Adawi A. M, Leggett G. J, Lidzey D. G, Langmuir 25 (18), 10746–
10753 (2009).
- [35] Shenhar R, Rotello V. M, Acc. Chem. Res. 36, 549-561(2003).
- [36] Vriezema D.M, Comellas-Aragones M, Elemans J.A.A.W, Cornelissen J.J.L.M,
Rowan A.E. and Nolte R.J.M, Self-Assembled Nanoreactors. Chem. Rev. 105,1445-
1490 (2005).
- [37] Humberto Palza, International Journal of Molecular Sciences, Int. J. Mol. Sci, 16,
2099- 2116 (2015).
- [38] El-Sayed M. A, Acc. Chem. Res, 34, 257-264 (2001).
- [39] Mandal T.K, Fleming M. S, Walt. D.R, Nano Lett., 2, 3-7 (2002).
- [40] Corbierre M. K, Cameron N. S, Sutton M, Mochrie S. G. J, Lurio L. B, Ruhm A,
Lennox R. B, J. Am.Chem. Soc, 123, 10411-10412 (2001).
- [41] Dilini Galpaya, Mingchao Wang, Meinan Liu, Nunzio Motta, Eric Waclawik, Cheng
Yan. Graphene, 1 30-49 (2012).
- [42] T. Filleter, A.M. Beese, M.R. Roenbeck, X. Wei, H.D. Espinosa, Nanotub. Superfib.
Mater. 61–85 (2014)
- [43] Park C. I, Park, O. O, Kim, H. J, Polymer 42, 7465 (2001).
- [44] H. Althues, J. Henle, and S. Kaskel. Chemical Society Reviews, 36(9):1454–1465,
(2007).
- [45] Okpala (2014) , the benefits and applications of nanocomposites , international journal

of advanced engenering technology , Vol.V issue IV , pg 12-18

- [46] <http://www.understandingnano.com/nanocomposites-applications.html>
- [47] H. Zhu, J. Njuguna, Heal. Environ. Saf. Nanomater, 133–146 (2014).
- [48] Tarek Ahmed Al Ammar, thèse Ruhr-Universität Bochum Anorganische Chemie I, Festkörperchemie und Materialien (2011).
- [49] G. Malandrino, S. T. Finocchiaro, R. T. Nigro, Chem. Mater, 16, 5559 (2004).
- [50] N. Chopra, V.G. Gavalas, L.G. Bachas, B.J. Hinds, L.G. Bachas, Anal. Lett. 40 2067 (2007).
- [51] K. Kerman, M. Saito, S. Yamamura, Y. Takamura, E. Tamiya, Trends Anal. Chem. 27 585 (2008).
- [52] D.C. Chow, M.S. Johannes, W.K. Lee, R.L. Clark, S. Zauscher, A. Chilkoti, Materials Today, 8 30 (2005).
- [53] M. A. Gondal, M. A. Dastageer and A. Khalil. Synthesis of nano-WO₃ and its catalytic activity for enhanced antimicrobial process for water purification using laser induced photocatalysis. Catalysis communication, 11 (3) : 214-219, 2009. 17
- [54] J. R. Darwent. Photo-oxydation of water sensitized by WO₃ powder. Journal of chemical society, 78 (2) : 359-367, 1982. 17
- [55] C. G. Granqvist. Electrochromic tungsten oxide films : Review of progress 1993-1998. Solar Energy Materials and Solar Cells, 60 (3) : 201-262, 2000. 17
- [56] G. Aka. Chimie du solide partie b : défauts ponctuels dans les solides, modèle du cristal réel. École Nationale Supérieure de Chimie de Paris : Paris, 12-24, 2006. 18
C Lambert-Mauriat and V. Oison. Density-functional study of oxygen vacancies in monoclinic tungsten oxide. J. Phys. : Condesn. Matter, 18 : 7361–7371, 2006. vii, 18, 20

- [57] T. Hirose. Structural phase transitions and semiconductor metal transition in WO₃.
Journal of the Physical society of Japan, 49 (2) : 562-568, 1980. 19
- [58] L. J. LeGore, R. J. Lad, S.C. Moulzolf, J. F. Vetelino, B. G. Frederick, E. A. Kenik.
Defects and morphology of tungsten trioxide thin films. Thin solid films, 406 (1-2) :
79-86, 2002. 19
- [59] P. M. Woodward, A. W. Sleight, T. Vogt. Structure refinement of triclinic tungsten
trioxide. Journal of Physics and Chemistry of Solids, 56 (10) : 1305–1315, 1995. 20
- [60] B. O. Loopstra, P. Boldrini. Neutron diffraction investigation of WO₃. Acta.
Cristallagr. B, 21, 1996. 20, 68, 69
- [61] I. P. Swainson, K. R. Locherer and E. K. H. Sajle. Transition to a new tetragonal
phase of WO₃ : crystal structure and distortion parameters. Journal Phys. : Cond.
Mat., 11 (21) : 4143–4156, 1999. 20
- [62] S. Yamazoe, Y. Hitomi, T. Shishido, T. Tanaka. XAFS study of tungsten L-1- and L-
3-edges : Structural analysis of WO₃ species loaded on TiO₂ as a catalyst for
photooxidation of NH₃. Journal of Physical Chemistry C, 112 (17) : 6869–6879,
2008. 20
- [63] G. Poirier, F. C. Cassanjes, Y. Messaddeq, S. J. L. Ribeiro, A. Michalowicz, M.
Poulain. Local order around tungsten atoms in tungstate fluorophosphate glasses by
X-ray absorption spectroscopy. Journal of NonCrystalline Solids, 351 (46-48) : 3644-
3648, 2005. 20
- [64] R. A. Dixon, J. J. Williams, D. Morris, J. Rebane, F. H. Jones, R. G. Egdell, S.
W.Downes. Electronic states at oxygen deficient WO₃(001) surfaces : a study by
resonant photoemission. Surface Science, 399 (2-3) : 199-211, 1998. 20

- [65] K. Miyake, H. Kaneko, M. Sano, N. Suedomi. Physical and electrochromic properties of the amorphous and crystalline tungsten oxide thick films prepared under reducing atmosphere . *J. Appl. Phys.*, 55 (7) : 2747, 1984. 20
- [66] E. Washizu, A. Yamamoto, Y. Abe, M. Kawamura, K. Sasaki. Optical and electrochromic properties of RF reactively sputtered WO₃ films. *Solid State Ionics*, 165 (1-4) : 175–180, 2003. 20, 73
- [67] A. M. T. Stoneham, A. M. T., P.W. Theory of Ceramic Surfaces. Elsevier Science Ltd : Kidlington, UK., 351 (46-48) : 1-22, 1988. 20
- [68] C. Lambert-Mauriat, V. Oison, L. Saadi, and K. Aguir. Ab initio study of oxygen point defects on tungsten trioxide surface. *Surface Science*, 606 : 40–45, 2012. 20
- [69] L. Ottaviano, E. Maccallini, S. Santucci. Visualisation of the preferential adsorption sites of oxygen onto WO₃ nano-particles. *Surface Science*, 492 (1-2) : L700–L704, 2001. 20
- [70] I. Levin and D. Brandon, Metastable alumina polymorphs : Crystal structures and transition sequences, *J. Am. Ceram. Soc*, 81, 1998. microwave dielectric properties of sintered alumina, *J. of the American Ceramic Society*, 1997.
- [71] Zhang Y; Evans JRG and Zhang S (2011). "Corrected Values for Boiling Points and Enthalpies of Vaporization of Elements in Handbooks". *J. Chem. Eng. Data*. 56 (2): 328–337. doi:10.1021/je1011086.
- [72] "This Chinese Company Proudly Sells Tungsten-Filled Gold Bars". 2012.
- [73] Daintith, John (2005). *Facts on File Dictionary of Chemistry* (4th ed.). New York: Checkmark Books. ISBN 978-0-8160-5649-1.
- [74] Lassner, Erik; Schubert, Wolf-Dieter (1999). "low temperature brittleness". *Tungsten: properties, chemistry, technology of the element, alloys, and chemical compounds*. Springer.

pp. 20–21. ISBN 978-0-306-45053-2.

- [75] Gludovatz, B.; Wurster, S.; Weingärtner, T.; Hoffmann, A.; Pippan, R. (2011). "Influence of impurities on the fracture behavior of tungsten". *Philosophical Magazine* (Submitted manuscript). 91 (22): 3006–3020. Bibcode:2011PMag...91.3006G. doi:10.1080/14786435.2011.558861. S2CID 137145004.
- [76] Stwertka, Albert (2002). *A Guide to the elements* (2nd ed.). New York: Oxford University Press. ISBN 978-0-19-515026-1.
- [77] D. D. Avrov and al. Electrical conductivity of ceramics of SiC-AlN, SiC-BeO and Al₂O₃ in the temperature range 300-1800 K, IEEE, 1998.
- [78] FM Clark, *Insulating materials for design and engineering materials*, John Wiley and Sons, Inc. New-York, 1962.
- [79] N. J Simon, *Cryogenic properties of inorganic insulating materials for ITER Magnets, A Review*, 1994.
- [80] Schweizer M. *Docteur nopal le médecin du bon dieu*. APB Edition, Paris, 1997, 81pp.
- [81] Briha O. *Potentialité thérapeutiques d'Opuntia ficus-indica au Maroc et Tunisie*. Thèse de doctorat en pharmacie. Université Mohamed V Rabat. Maroc. 2012, 171 pp.
- [82] Lamghari El Kossori R, Villaume C, El Boustani E, Sauvaire Y, Méjean L. Composition of pulp, skin and seeds of prickly pear fruit (*Opuntia ficus-indica* sp.). *Plant. Foods. Hum.Nutr.*, 1998, 52 : 263-270.
- [83] Nouveaux aliments pour les ruminants à base de fruits de cactus, ministère de l'agriculture et de la pêche maritime, royaume du Maroc, N°176 Mai, 2009
- [84] C.K. Chiang, C.R. Fincher, Y.W. Park, A.J. Heeger, H. Shirakawa, E.J. Louis, S.C.Gau , A.G. MacDiarmid, *Phys. Rev. Lett.* 39 (1977) p 1098

- [85] M. Leclerc, R. Prud'homme, *Macromolecules* 20 (1987) p 2153
- [86] D.M. Ivory, G.G. Miller, J.M. Sowa, L.W. Shacklette, R.R. Chance, R.H. Baughman, *J. Chem. Phys.*,71(1979) p 1506
- [87] M. Rehahn, A.D. Schluter, G. Wegner, *Makromol. Chem.* 191 (1990) p 1991
- [88] C.L. Gettinger, A.J. Heeger, J.M. Drake, D.J. Pine, *J. Chem. Phys.* 101 (1994) p 1673
J. Roncali, *Chem. Rev.* 92 (1992) p 711
- [89] A.F. Diaz, K.K. Kanazawa, G.P.J. Gardini, *Chem. Soc., Chem. Commun.* (1979) p 635
- [90] D.K. Moon, A.B., Padias, H.K. Hall, T. Huntoon, P.D. Clavert, *Macromolecules* 28 (1995) p 6205
- [91] A.G. MacDiarmid, J.E. Chiang, M. Halpern, W.S. Huang, S.L. Mu, N.L. Somarisi, W. Wu, S.I. Yaniger, *Molec. Cryst. Liq. Cryst.* 121 (1985) p 173
- [92] C. Yong, P. Smith, A.J. Heeger, *Synth. Met.* 57 (1993) p 3514
- [93] X.G. Li, M. R, Huang, Y. Yang, *J. Polym.* 32 (2000) p 348
- [94] B. Zhao, K.G. Neoh, E.T. Kang, *Chem. Mater.* 12 (2000) p 1800
- [95] G.G. Wallace, P.R. Teasdale, G.M. Spinks, L.A.P. Kane-Maguire, *Conductive electroactive polymers-intelligent materials systems*, 2nd Edition, CRC Press (2003) p 237
- [96] R.S. Kohlman, and A.J., Epstein, *Handbook of Conducting Polymers*. Marcel Dekker, inc. 2nd Edition, New York, (1998)
- [97] C.C. Bidwell, *Phys. Rev.* 58 (1940) p 561
- [98] C.L. Choy, *Polymer* 18 (1977) p 984
- [99] A.J. Attias, *Polymères conjugués et polymères conducteurs électroniques*, Techniques

de l'ingénieur, traité d'électronique, E1 862-1 (2002) p 1

[100] O. Solomeshch, Y.J. Yu, V. Medvedev, A. Razin, B. Synth. Met. 157 (2007) p 841

[101] G. Grem, G. Leditzky, B. Ulrich, Synth. Met. 51 (1992) p383

[102] J. Obrzut, F. E. Karasz, J. Chem. Phys. 87 (1987) p 2349

[103] P. Reiss, A. pron, Encyclopedia of Nanoscience and nanotechnology, H. S.

Nalwa ,American Scientific Publishers, Stevenson Ranch, Californy, 6 (2004) p 587

[104] A.J. Heeger, Handbook of conducting polymers, M. Dekker, New York, 2 (1986) p 279

[105] J. L. Bredas, Conjugated polymers and related materials: the interconnection of chemical and electronic structure, B. Randy (1993) p 187

[106] A.J. Heeger, Synth. Met. 125 (2002) p 23

[107] J L. Bredas, G. B. Street, Acc. Chem. Res. 18 (1985) p 309

[108] F.F. Runge, Annalen der Physik und Chemie 107 (1834) p 65

[109] J. Fritzsche, Journal fur praktische Chemie,20 (1840) p 453

[110] H. Letheby, J. Chem. Soc. 15 (1862) p 161

[111] E. Noelting, Scientific and Industrial History of Aniline Black, WM. J. Matheson & Co (1889)

[112] J.J. Coquillon, Compt. Rend. 81 (1985) p 408

[113] A.G. Green, A.E. Woodhead, J. Chem. Soc. Trans. 97 (1910) p 2388

[114] O.W. Brown, W.C. Friche, J. Phys. Chem. 51 (1947) p 1394

[115] H.Shirakawa, E.J. Louis, A.G. MacDiarmid, C.K. Chiang, A. J. Heeger , J. Chem. Soc.Chem. Commun. 16 (1977) p 578

- [116] A.G. MacDiarmid, J.C. Chiang, M. Halpern, W.S Huang., S.L. Mu, N.L.D. Somasiri,
W. Wu, S.I. Yaniger, *Molecular Crystals and Liquid Crystals*, 121 (1985) p 173
- [117] J.P. Travers, J. Chroboczek, F. Devreux, F. Genoud, M. Nechtschein, A. Syed, E.M.Genies, C. Tsintavis, *Mol. Cryst. Liq. Cryst.* 121 (1985) p 195
- [118] A.G. Mac Diarmid,. *Conjugated Polymers and Related Materials, The polyanilines : a novel class of conducting polymers*, W. R. Salaneck, I. Lundström et B. Ranby, Oxford University Press, part 2 (1993) p 73
- [119] M. Dioromedof, F.H. Cristofini, R. DeSurville, M. Jozefowicz, L.T. Yu, R. Buvet, *J.Chem. Phys* 68 (1971) p 1005
- [120] A. G. MacDiarmid, J. C. Chiang, M. Halppern, W. S. Huang, S. L. Mu, N. L. Somasiri,*Mol. Cryst. Liq. Cryst. Sci. Technol. A* 121 (1985) p 173
- [121] M. Ginder, A.F. Richter, A.G. MacDiarmid, A.J. Epstein, *Bull. Am. Phys. Soc.* 31 (1986) p 582
- [122] A.G. Macdiarmid, A.J. Epstein, *Lower-dim pentional system and Molecular Electronic*,Plenum Press, New-York, (A991) p 303
- [123] A.G. Macdiarmid, *Conjugated polymers and Related Materials : the interconnection of chemical and electronic structure*, Eds, W.R. Salaneck, I. Lundstrom, R. Ranby, Oxford Universiy Press, Oxford, Part 2, p (1993) 73
- [124] A. Pron, P. Rannou, *Prog. Polym. Sci.* 27 (2002) p 135
- [125] M. Dioromedof, F. Hautier-Cristofini, R. de Surville, M. Jozefowicz, L.T. Yu, R, Buvet. *J. Chim. Phys.* 68 (1971) p 1005
- [126] F. Genoud, C. Menardo, M. Nechtshein, J.P. Tavers, P. Hany, *springer series in solid-*

- state, Eds. H. Kuzmany, M Mehring, S. Roth, Springer-verlag, Heidelberg 76 (1987)
p 244
- [127] E.T. Kang, K.G. Neoh, K.L. Tan. B.T.G Tan, Synth. Met. 46 (192) p 227
- [128] A.G. MacDiarmid, W.E. Jones Jr., I.D. Norris, J. Gao, A.T. Johnson Jr., N.J. Pinto, J. Hone, B. Han, F.K. Ko, H. Okuzaki, M. L laguno Synth. Met. 119 (2001) p 27
- [129] C.D. Liu, S.Y. Wu, J.L.Han, K.H. Hsieh, J. Appl. Poly. Sci. 115 (2010) p 2271
- [130] D. Chaudhuri, S. Datar, R. Viswanatha, D.D. Sarma, H. Amenitsch Appl. Phys. Letter. 87 (2005) p 093117
- [131] S.R. Mohanty, N.K. Neog, R.S. Rawat, P. Lee, B.B. Nayak, B.S. Acharya, Phys. Letter.A 373 (2009) p 1962
- [132] S.P. Surwade, N. Manohar, S.K. Manohar, Macromolecules 42 (2009) p 1792
- [133] S.M. Yang, K.H. Chen, Y.F. Yang, Synth. Met. 152 (2005) p 65
- [134] X. Zhang, W.J. Goux, S.K. Manohar, J. Am.Chem. Soc. 126 (2004) p 4502
- [135] L.J. Pan, L. Pu, Y. Shi, S.Y. Song, Z. Xu, R. Zhang, Y.D. Zheng Adv. Mater. 19 (2007) p 461
- [136] W. Li, H.L. Wang, J. Am.Chem. Soc. 126 (2004) p 2278
- [137] S. Xing, C. Zhao, S. Jing, Z. Wang, Polymer 47 (2006) p 2305
- [138] P. Nickels, W.U. Dittmer, S. Beyer, J.P. Kotthaus, F.C. Simmel, Nanotechnology 15 (2004) p 1524
- [139] T. Jeevananda, J.H. Lee, Siddaramaiah, Mater. Letter. 62 (2008) p 3995
- [140] X. Jing, Y. Wang, D. Wu, L. She, Y. Guo, J. Polym. Sci. A: Polym. Chem. 44 (2006) p 1014
- [141] X. Lu, H. Mao, D. Chao, W. Zhang, Y. Wei, Macro.Chem. Phy. 207 (2006) p 2142

- [142] W. Huang, B.D. Humphrey, A.G. MacDiarmid, J. Am.Chem. Soc., Faraday Transactions 1: Physical Chemistry in Condensed Phases 82 (1986) p 2385
- [143] A.G. MacDiarmid, J.C. Chiang, A.F. Richter, A.J. Epstein, Synth. Met. 18 (1987) p 285
- [144] A.G. MacDiarmid, J.C. Chiang, A.F. Richter, N.L.D. Somarisi, Conducting Polymers :Special applications, Ed. L. Alcacer, Reidel, Dordrecht, (1984) p 105
- [145] A.Pron, F. Genoud, C. Mnerdo, M. Nechtschein, Synth. Met. 24 (1988) p 193
- [146] A. Pron, P. Rannou, Prog. Polym. Sci. 27 (2002) p 135
- [147] Y. Cao, A. Andreatta, A. J. Heeger, P. Smith, Polymer 30 (1989) p 2305
- [148] N. Gopodinova and L. Terlemzyan. Prog. Polym. Sci. 23 (1998) p 1443
- [149] J. Stejskal, I. Spurina, Pure Appl. Chem. 77 (2005) p 815
- [150] J. Stejskal, R. G. Gilbert, Pure Appl. Chem. 74 (2002) p 857
- [151] A. Andreatta, Y. Cao, J. C. Chiang, A. J Heeger, P. Smith, Synth. Met. 26 (1988) p 383
- [152] M. Lapkowski, Synth. Met. 35 (1990) p 169
- [153] J. Yano, T. Ohnishi, A. Kitani, Synth. Met. 101 (1999) p 752
- [154] M.V. Kulkarni, A.K. Viswanath, U.P. Mulik, Mater. Chem. Phys. 89 (2005) p 1
- [155] Y.Z. Wang, J. Joo, C.H. Hsu, A.J. Epstein, Synth. Met. 68 (1995) p 207
- [156] E.R. Holland, S.J. Pomfret, P.N. Adams, L. Abell, A.P. Monkman, Synth. Met. 84 (1997) p 777
- [157] Y.F. Nicolau, P.M. Beadle, E. Banka, Synth. Met. 84 (1997) p 585
- [158] S.K. Jeong, J.S. Suh, E.J. Oh, Y.W. Park, C.Y. Kim, A.G. MacDiarmid, Synth. Met.

69 (1995) p 171

[159] V.I. Krinichnyi, S.V. Tokarev, H.K. Roth, M. Schrödner, B. Wessling, *Synth. Met.*

156 (2006) p 1368

[160] Y. Cao, A. J. Heeger, *Synth. Met.* 52 (1992) p 193

[161] I. Kulszewicz-Bajer, M. Zagórska, J. Nizioł, A. Pron, W. Luzny, *Synth. Met.* 114

(2000) p 125

[162] G. G. Wallace, G. M. Spinks, and L. A. P. Kane-Maguire, *Conductive Electroactive Polymers: Intelligent Materials Systems*, CRC Press. 2002.

[163] D. Nicolas-Debarnot and F. Poncin-Epaillard, —Polyaniline as a new sensitive layer for gas sensors,|| *Anal. Chim. Acta*, vol. 475, no. 1–2, pp. 1–15, Jan. 2003.

[164] G. Zotti, S. Cattarin, and N. Comisso, —Cyclic potential sweep electropolymerization of aniline: The role of anions in the polymerization mechanism,|| *J. Electroanal. Chem. Interfacial Electrochem.*, vol. 239, no. 1–2, pp. 387–396, Jan. 1988.

[165] M. Takakubo, —Molecular orbital study of the initial reaction paths in the electrochemical polymerization of aniline,|| *Synth. Met.*, vol. 33, no. 1, pp. 19–26, Nov. 1989.

[166] F. Lux, —Properties of electronically conductive polyaniline: a comparison between well-known literature data and some recent experimental findings,|| *Polymer*, vol. 35, no. 14, pp. 2915–2936, Jul. 1994.

[167] Y. Wei, X. Tang, Y. Sun, and W. W. Focke, —A study of the mechanism of aniline polymerization,|| *J. Polym. Sci. Part Polym. Chem.*, vol. 27, no. 7, pp. 2385–2396, Jun. 1989.

[168] N. Gospodinova, L. Terlemezyan, P. Mokreva, and K. Kossev, —On the mechanism of oxidative polymerization of aniline,|| *Polymer*, vol. 34, no. 11, pp. 2434–2437, 1993.

[169] N. Gospodinova, P. Mokreva, and L. Terlemezyan, —Chemical oxidative polymerization of aniline in aqueous medium without added acids,|| *Polymer*, vol. 34, no. 11, pp. 2438–2439, 1993.

- [170] G. Ćirić-Marjanović, E. N. Konyushenko, M. Trchová, and J. Stejskal, —Chemical oxidative polymerization of anilinium sulfate versus aniline: Theory and experiment,|| *Synth. Met.*, vol. 158, no. 5, pp. 200–211, Mar. 2008.
- [171] G. Ćirić-Marjanović, M. Trchová, and J. Stejskal, —Theoretical study of the oxidative polymerization of aniline with peroxydisulfate: Tetramer formation,|| *Int. J. Quantum Chem.*, vol. 108, no. 2, pp. 318–333, 2008.
- [172] J. Stejskal, I. Sapurina, and M. Trchová, —Polyaniline nanostructures and the role of aniline oligomers in their formation,|| *Prog. Polym. Sci.*, Jul. 2010
- [173] J. K i , L. Starovoytova, M. Trchová, E. N. Konyushenko, and J. Stejskal, —NMR Investigation of Aniline Oligomers Produced in the Early Stages of Oxidative Polymerization of Aniline,|| *J. Phys. Chem. B*, vol. 113, no. 19, pp. 6666–6673, May 2009
- [174] S. Bhadra, S. Chattopadhyay, N. K. Singha, and D. Khastgir, —Improvement of conductivity of electrochemically synthesized polyaniline,|| *J. Appl. Polym. Sci.*, vol. 108, no. 1, pp. 57–64, 2008.
- [175] S. Bhadra, N. K. Singha, and D. Khastgir, —Polyaniline by new miniemulsion polymerization and the effect of reducing agent on conductivity,|| *Synth. Met.*, vol. 156, no. 16–17, pp. 1148–1154, Aug. 2006.
- [176] S. Bhadra, N. K. Singha, S. Chattopadhyay, and D. Khastgir, —Effect of different reaction parameters on the conductivity and dielectric properties of polyaniline synthesized electrochemically and modeling of conductivity against reaction parameters through regression analysis,|| *J. Polym. Sci. Part B Polym. Phys.*, vol. 45, no. 15, pp. 2046–2059, 2007.
- [177] S. Bhadra, N. K. Singha, and D. Khastgir, —Dual functionality of PTSA as electrolyte and dopant in the electrochemical synthesis of polyaniline, and its effect on electrical properties,|| *Polym. Int.*, vol. 56, no. 7, pp. 919–927, 2007.

- [178] S. Bhadra and D. Khastgir, —Degradation and stability of polyaniline on exposure to electron beam irradiation (structure–property relationship),|| *Polym. Degrad. Stab.*, vol. 92, no. 10, pp. 1824–1832, Oct. 2007.
- [179] A. G. MacDiarmid, —Polyaniline and polypyrrole: Where are we headed?,|| *Synth. Met.*, vol. 84, no. 1–3, pp. 27–34, Jan. 1997.
- [180] S. Bhadra, N. K. Singha, and D. Khastgir, —Electrochemical synthesis of polyaniline and its comparison with chemically synthesized polyaniline,|| *J. Appl. Polym. Sci.*, vol. 104, no. 3, pp. 1900–1904, 2007.
- [181]
- [182] S. Kobayashi, H. Uyama, and S. Kimura, —Enzymatic Polymerization,|| *Chem. Rev.*, vol. 101, no. 12, pp. 3793–3818, Dec. 2001.
- [183] R. Cruz-Silva, C. Ruiz-Flores, L. Arizmendi, J. Romero-García, E. Arias-Marin, I. Moggio, F. F. Castillon, and M. H. Farias, —Enzymatic synthesis of colloidal polyaniline particles,|| *Polymer*, vol. 47, no. 5, pp. 1563–1568, Feb. 2006.
- [184] E. Arias-Marín, J. Romero, A. Ledezma-Pérez, and S. Kniajansky, —Enzymatic mediated polymerization of functional aniline derivatives in nonaqueous media,|| *Polym. Bull.*, vol. 37, no. 5, pp. 581–587, Nov. 1996
- [185] I. Y. Sakharov, A. C. Vorobiev, and J. J. C. Leon, —Synthesis of polyelectrolyte complexes of polyaniline and sulfonated polystyrene by palm tree peroxidase,|| *Enzyme Microb. Technol.*, vol. 33, no. 5, pp. 661–667, Oct. 2003.
- [186] S. Bhadra, N. K. Singha, and D. Khastgir, —Polyaniline by new miniemulsion polymerization and the effect of reducing agent on conductivity,|| *Synth. Met.*, vol. 156, no. 16–17, pp. 1148–1154, Aug. 2006.

- [187] E. R. Holland, S. J. Pomfret, P. N. Adams, L. Abell, and A. P. Monkman, —Doping dependent transport properties of polyaniline-CSA films,|| *Synth. Met.*, vol. 84, no. 1–3, pp. 777–778, Jan. 1997.
- [188] P. Kiattibutr, L. Tarachiwin, L. Ruangchuay, A. Sirivat, and J. Schwank, —Electrical conductivity responses of polyaniline films to SO₂–N₂ mixtures: effect of dopant type and doping level,|| *React. Funct. Polym.*, vol. 53, no. 1, pp. 29–37, Oct. 2002.
- [189] S. Roth and W. Graupner, —Conductive polymers: Evaluation of industrial applications,|| *Synth. Met.*, vol. 57, no. 1, pp. 3623–3631, Apr. 1993.
- [190] B. Wessling, —Dispersion as the link between basic research and commercial applications of conductive polymers (polyaniline),|| *Synth. Met.*, vol. 93, no. 2, pp. 143–154, Mar. 1998.
- [191] M. S. Cho, S. Y. Park, J. Y. Hwang, and H. J. Choi, —Synthesis and electrical properties of polymer composites with polyaniline nanoparticles,|| *Mater. Sci. Eng. C*, vol. 24, no. 1–2, pp. 15–18, Jan. 2004
- [192] T. Hino, S. Taniguchi, and N. Kuramoto, —Syntheses of conductive adhesives based on epoxy resin and polyanilines by using N-tert-butyl-5-methylisoxazolium perchlorate as a thermally latent curing reagent,|| *J. Polym. Sci. Part Polym. Chem.*, vol. 44, no. 2, pp. 718–726, 2006.
- [193] M. Hosoda, T. Hino, and N. Kuramoto, —Facile preparation of conductive paint made with polyaniline/dodecylbenzenesulfonic acid dispersion and poly(methyl methacrylate),|| *Polym. Int.*, vol. 56, no. 11, pp. 1448–1455, 2007.
- [194] R. A. de Barros, C. R. Martins, and W. M. de Azevedo, —Writing with conducting polymer,|| *Synth. Met.*, vol. 155, no. 1, pp. 35–38, Oct. 2005.
- [195] Y. Yoshioka and G. E. Jabbour, —Desktop inkjet printer as a tool to print conducting polymers,|| *Synth. Met.*, vol. 156, no. 11–13, pp. 779–783, Jun. 2006.

- [196] D. Bowman and B. R. Mattes, —Conductive Fibre Prepared From Ultra-High Molecular Weight Polyaniline for Smart Fabric and Interactive Textile Applications,|| *Synth. Met.*, vol. 154, no. 1–3, pp. 29–32, Sep. 2005.
- [197] A. Ohtani, M. Abe, M. Ezoe, T. Doi, T. Miyata, and A. Miyake, —Synthesis and properties of high-molecular-weight soluble polyaniline and its application to the 4MB-capacity barium ferrite floppy disk's antistatic coating,|| *Synth. Met.*, vol. 57, no. 1, pp. 3696–3701, Apr. 1993.
- [198] K. F. Schoch Jr., W. A. Byers, and L. J. Buckley, —Deposition and characterization of conducting polymer thin films on insulating substrates,|| *Synth. Met.*, vol. 72, no. 1, pp. 13–23, Apr. 1995.
- [199] V. G. Kulkarni, J. C. Campbell, and W. R. Mathew, —Transparent conductive coatings,|| *Synth. Met.*, vol. 57, no. 1, pp. 3780–3785, Apr. 1993.
- [200] M. S. Cho, Y. H. Cho, H. J. Choi, and M. S. Jhon, —Synthesis and Electrorheological Characteristics of Polyaniline-Coated Poly(methyl methacrylate) Microsphere: Size Effect,|| *Langmuir*, vol. 19, no. 14, pp. 5875–5881, Jul. 2003.
- [201] I. S. Lee, M. S. Cho, and H. J. Choi, —Preparation of polyaniline coated poly(methyl methacrylate) microsphere by graft polymerization and its electrorheology,|| *Polymer*, vol. 46, no. 4, pp. 1317–1321, Feb. 2005.
- [202] I. S. Lee, J. Y. Lee, J. H. Sung, and H. J. Choi, —Synthesis and electrorheological characteristics of polyaniline-titanium dioxide hybrid suspension,|| *Synth. Met.*, vol. 152, no. 1–3, pp. 173–176, Sep. 2005.
- [203] M. S. Cho, H. J. Choi, and W.-S. Ahn, —Enhanced Electrorheology of Conducting Polyaniline Confined in MCM-41 Channels,|| *Langmuir*, vol. 20, no. 1, pp. 202–207, Jan. 2004.

- [204] H. J. Choi, T. W. Kim, M. S. Cho, S. G. Kim, and M. S. Jhon, —Electrorheological characterization of polyaniline dispersions,|| *Eur. Polym. J.*, vol. 33, no. 5, pp. 699–703, May 1997.
- [205] H. Bai, Q. Chen, C. Li, C. Lu, and G. Shi, —Electrosynthesis of polypyrrole/sulfonated polyaniline composite films and their applications for ammonia gas sensing,|| *Polymer*, vol. 48, no. 14, pp. 4015–4020, Jun. 2007.
- [206] M. Irimia-Vladu and J. W. Fergus, —Suitability of emeraldine base polyaniline-PVA composite film for carbon dioxide sensing,|| *Synth. Met.*, vol. 156, no. 21–24, pp. 1401–1407, Dec. 2006.
- [207] X. B. Yan, Z. J. Han, Y. Yang, and B. K. Tay, —NO₂ gas sensing with polyaniline nanofibers synthesized by a facile aqueous/organic interfacial polymerization,|| *Sens. Actuators B Chem.*, vol. 123, no. 1, pp. 107–113, Apr. 2007.
- [208] V. Dixit, S. C. K. Misra, and B. S. Sharma, —Carbon monoxide sensitivity of vacuum deposited polyaniline semiconducting thin films,|| *Sens. Actuators B Chem.*, vol. 104, no. 1, pp. 90–93, Jan. 2005.
- [209] S. Jain, A. B. Samui, M. Patri, V. R. Hande, and S. V. Bhoraskar, —FEP/polyaniline based multilayered chlorine sensor,|| *Sens. Actuators B Chem.*, vol. 106, no. 2, pp. 609–613, May 2005.
- [210] M. Ando, C. Swart, E. Pringsheim, V. M. Mirsky, and O. S. Wolfbeis, —Optical ozone-sensing properties of poly(2-chloroaniline), poly(N-methylaniline) and polyaniline films,|| *Sens. Actuators B Chem.*, vol. 108, no. 1–2, pp. 528–534, Jul. 2005.
- [211] J.-S. Kim, S.-O. Sohn, and J.-S. Huh, —Fabrication and sensing behavior of PVF₂ coated-polyaniline sensor for volatile organic compounds,|| *Sens. Actuators B Chem.*, vol. 108, no. 1–2, pp. 409–413, Jul. 2005.

- [212] S. H. Hosseini and A. A. Entezami, —Preparation and characterization of polyaniline blends with polyvinyl acetate, polystyrene and polyvinyl chloride for toxic gas sensors,|| *Polym. Adv. Technol.*, vol. 12, no. 8, pp. 482–493, 2001.
- [213] S. S. Joshi, C. D. Lokhande, and S.-H. Han, —A room temperature liquefied petroleum gas sensor based on all-electrodeposited n-CdSe/p-polyaniline junction,|| *Sens. Actuators B Chem.*, vol. 123, no. 1, pp. 240–245, Apr. 2007.
- [214] R. Nohria, R. K. Khillan, Y. Su, R. Dikshit, Y. Lvov, and K. Varahramyan, —Humidity sensor based on ultrathin polyaniline film deposited using layer-by-layer nano-assembly,|| *Sens. Actuators B Chem.*, vol. 114, no. 1, pp. 218–222, Mar. 2006.
- [215] C. Muthukumar, S. D. Kesarkar, and D. N. Srivastava, —Conductometric mercury [III] sensor based on polyaniline–cryptand-222 hybrid,|| *J. Electroanal. Chem.*, vol. 602, no. 2, pp. 172–180, Apr. 2007.
- [216] A. Talaie, J. Y. Lee, Y. K. Lee, J. Jang, J. A. Romagnoli, T. Taguchi, and E. Maeder, —Dynamic sensing using intelligent composite: an investigation to development of new pH sensors and electrochromic devices,|| *Thin Solid Films*, vol. 363, no. 1–2, pp. 163–166, Mar. 2000.
- [217] K. Arora, G. Sumana, V. Saxena, R. K. Gupta, S. K. Gupta, J. V. Yakhmi, M. K. Pandey, S. Chand, and B. D. Malhotra, —Improved performance of polyaniline-uricase biosensor,|| *Anal. Chim. Acta*, vol. 594, no. 1, pp. 17–23, Jun. 2007.
- [218] J. Ren, F. He, L. Zhang, C. Su, and Z. Liu, —A new B-PAn-P system for the detection of bacteria population,|| *Sens. Actuators B Chem.*, vol. 125, no. 2, pp. 510–516, Aug. 2007.
- [219] Y. Andreu, S. de Marcos, J. R. Castillo, and J. Galbán, —Sensor film for Vitamin C determination based on absorption properties of polyaniline,|| *Talanta*, vol. 65, no. 4, pp. 1045–1051, Feb. 2005.

- [220] A. A. Syed and M. K. Dinesan, —Polyaniline: Reaction stoichiometry and use as an ion-exchange polymer and acid/base indicator,|| *Synth. Met.*, vol. 36, no. 2, pp. 209–215, Jun. 1990.
- [221] M. R. Anderson, B. R. Mattes, H. Reiss, and R. B. Kaner, —Conjugated polymer films for gas separations,|| *Science*, vol. 252, no. 5011, pp. 1412–1415, Jun. 1991.
- [222] S. Kuwabata and C. R. Martin, —Investigation of the gas-transport properties of polyaniline,|| *J. Membr. Sci.*, vol. 91, no. 1–2, pp. 1–12, May 1994.
- [223] D. L. Pile and A. C. Hillier, —Electrochemically modulated transport through a conducting polymer membrane,|| *J. Membr. Sci.*, vol. 208, no. 1–2, pp. 119–131, Oct. 2002.
- [224] V. M. Schmidt, D. Tegtmeier, and J. Heitbaum, —Conducting polymers as membranes with variable permeabilities for neutral compounds: Polypyrrole and polyaniline in aqueous electrolytes,|| *Adv. Mater.*, vol. 4, no. 6, pp. 428–431, 1992.
- [225] G. Bidan and B. Ehui, —One-step electrosynthesis and characterization of poly(aniline)–Nafion and poly(3-methylthiophene)–Nafion composite films,|| *J. Chem. Soc. Chem. Commun.*, no. 20, pp. 1568–1570, Jan. 1989.
- [226] K. Doblhofer and R. D. Armstrong, —Membrane-type coatings on electrodes,|| *Electrochimica Acta*, vol. 33, no. 4, pp. 453–460, Apr. 1988.
- [227] J. Lu, K.-S. Moon, B.-K. Kim, and C. P. Wong, —High dielectric constant polyaniline/epoxy composites via in situ polymerization for embedded capacitor applications,|| *Polymer*, vol. 48, no. 6, pp. 1510–1516, Mar. 2007.
- [228] V. Gupta and N. Miura, —Polyaniline/single-wall carbon nanotube (PANI/SWCNT) composites for high performance supercapacitors,|| *Electrochimica Acta*, vol. 52, no. 4, pp. 1721–1726, Dec. 2006.

- [229] J.-H. Sung, S.-J. Kim, and K.-H. Lee, —Preparation of compact polyaniline films: electrochemical synthesis using agar gel template and charge-storage applications,|| *J. Power Sources*, vol. 126, no. 1–2, pp. 258–267, Feb. 2004.
- [230] C. Meng, C. Liu, and S. Fan, —Flexible carbon nanotube/polyaniline paper-like films and their enhanced electrochemical properties,|| *Electrochem. Commun.*, vol. 11, no. 1, 186–189, Jan. 2009.
- [231] S. Bhadra, N. K. Singha, and D. Khastgir, —Dielectric properties and EMI shielding efficiency of polyaniline and ethylene 1-octene based semi-conducting composites,|| *Curr. Appl. Phys.*, vol. 9, no. 2, pp. 396–403, Mar. 2009.
- [232] A. J. Epstein, J. Joo, R. S. Kohlman, G. Du, A. G. MacDiarmid, E. J. Oh, Y. Min, J. Tsukamoto, H. Kaneko, and J. P. Pouget, —Inhomogeneous disorder and the modified Drude metallic state of conducting polymers,|| *Synth. Met.*, vol. 65, no. 2–3, pp. 149–157, Aug. 1994.
- [233] J. Joo, E. J. Oh, G. Min, A. G. MacDiarmid, and A. J. Epstein, —Evolution of the conducting state of polyaniline from localized to mesoscopic metallic to intrinsic metallic regimes,|| *Synth. Met.*, vol. 69, no. 1–3, pp. 251–254, Mar. 1995.
- [234] R. J. Tseng, J. Huang, J. Ouyang, R. B. Kaner, and Yang, —Polyaniline Nanofiber/Gold Nanoparticle Nonvolatile Memory,|| *Nano Lett.*, vol. 5, no. 6, pp. 1077–1080, Jun. 2005.
- [235] T. E. Herod and J. B. Schlenoff, —Doping-induced strain in polyaniline: stretchoelectrochemistry,|| *Chem. Mater.*, vol. 5, no. 7, pp. 951–955, Jul. 1993.
- [236] K. Kaneto, M. Kaneko, Y. Min, and A. G. MacDiarmid, —‘Artificial muscle’: Electromechanical actuators using polyaniline films,|| *Synth. Met.*, vol. 71, no. 1–3, pp. 2211–2212, Apr. 1995.

- [237] A. . MacDiarmid, L. . Yang, W. . Huang, and B. . Humphrey, —Polyaniline: Electrochemistry and application to rechargeable batteries,|| *Synth. Met.*, vol. 18, no. 1–3, pp. 393–398, Feb. 1987.
- [238] N. L. D. Somasiri and A. G. Macdiarmid, —Polyaniline: characterization as a cathode active material in rechargeable batteries in aqueous electrolytes,|| *J. Appl. Electrochem.*, vol. 18, no. 1, pp. 92–95, Jan. 1988.
- [239] K. Koga, S. Yamasaki, K. Narimatsu, and M. Takayanagi, —Electrically conductive composite of polyaniline—aramid and its application as a cathode material for secondary battery,|| *Polym. J.*, vol. 21, no. 9, pp. 733–738.
- [240] J. Desilvestro, W. Scheifele, and O. Haas, —In Situ Determination of Gravimetric and Volumetric Charge Densities of Battery Electrodes Polyaniline in Aqueous and Nonaqueous Electrolytes,|| *J. Electrochem. Soc.*, vol. 139, no. 10, pp. 2727–2736, Oct. 1992.
- [241] Y. Qiao, C. M. Li, S.-J. Bao, and Q.-L. Bao, —Carbon nanotube/polyaniline composite as anode material for microbial fuel cells,|| *J. Power Sources*, vol. 170, no. 1, pp. 79–84, Jun. 2007.
- [242] A. Watanabe, K. Mori, Y. Iwasaki, Y. Nakamura, and S. Niizuma, —Electrochromism of polyaniline film prepared by electrochemical polymerization,|| *Macromolecules*, vol. 20, no. 8, pp. 1793–1796, Aug. 1987.
- [243] M. A. Rodrigues, M.-A. De Paoli, and M. Mastragostino, —Electrochromic properties of chemically prepared polyaniline,|| *Electrochimica Acta*, vol. 36, no. 14, pp. 2143–2146, 1991.
- [244] B. P. Jelle, G. Hagen, S. M. Hesjevik, and R. Ødegård, —Transmission through an electrochromic window based on polyaniline, tungsten oxide and a solid polymer electrolyte,|| *Mater. Sci. Eng. B*, vol. 13, no. 3, pp. 239–241, Apr. 1992.

- [245] B. P. Jelle, G. Hagen, S. Sunde, and R. Ødegård, —Dynamic light modulation in an electrochromic window consisting of polyaniline, tungsten oxide and a solid polymer electrolyte,|| *Synth. Met.*, vol. 54, no. 1–3, pp. 315–320, Mar. 1993.
- [246] Y. Renkuan, L. Yuxue, Y. Hong, W. Yongbin, Z. Xiangqin, X. Jian, and S. Xuechu, —Study of photoelectric characteristics of p-PAn/n-Si junction,|| *Synth. Met.*, vol. 57, no. 1, pp. 4087–4092, Apr. 1993.
- [247] E. Dalas, S. Sakkopoulos, E. Vitoratos, G. Maroulis, and L. Kobotiatis, —Aqueous precipitation and electrical properties of In₂S₃: characterization of the In₂S₃/polyaniline and In₂S₃/polypyrrole heterojunctions,|| *J. Mater. Sci.*, vol. 28, no. 20, pp. 5456–5460, Jan. 1993.
- [248] P. Y. Stakhira, Y. I. Vertsimaha, O. I. Aksimentyeva, B. R. Cizh, and V. . Cherpak, —Hybrid solar cells based on dispersed InSe- polyaniline composites,|| *Phys. Chem. Solid State*, vol. 6, no. 1, pp. 96–98, 2005.
- [249] Z. Liu, J. Zhou, H. Xue, L. Shen, H. Zang, and W. Chen, —Polyaniline/TiO₂ solar cells,|| *Synth. Met.*, vol. 156, no. 9–10, pp. 721–723, May 2006.
- [250] S. Xing, C. Zhao, L. Niu, Y. Wu, J. Wang, and Z. Wang, —Diode-like behavior based on polyaniline and Pt,|| *Solid-State Electron.*, vol. 50, no. 9–10, pp. 1629–1633, Sep. 2006.
- [251] C. Zhao, S. Xing, Y. Yu, W. Zhang, and C. Wang, —A novel all-plastic diode based upon pure polyaniline material,|| *Microelectron. J.*, vol. 38, no. 3, pp. 316–320, Mar. 2007.
- [252] S.-A. Chen, K.-R. Chuang, C.-I. Chao, and H.-T. Lee, —White-light emission from electroluminescence diode with polyaniline as the emitting layer,|| *Synth. Met.*, vol. 82, no. 3, pp. 207–210, Sep. 1996.
- [253] N. P. Gaponik, D. V. Talapin, and A. L. Rogach, —A light-emitting device based on a CdTe nanocrystal/polyaniline composite,|| *Phys. Chem. Chem. Phys.*, vol. 1, no. 8, pp. 1787–1789, Jan. 1999.

CHAPTER II
Materials and Methods

II.1. Introduction

This chapter is dedicated to the presentation and description of experimental techniques used to determine the structural, microstructural, thermal, morphological and electrical, magnetic and electromagnetic measurements of Polyaniline/metal composites after their development.

II.2. The analysis techniques

II.2.1 Structural analysis techniques

For the eventual practical use of a newly manufactured material it is necessary to properly determine all its structural parameters. For the structural characterization of elaborate materials (polymers and nanocomposites) and nanoparticles, several analytical techniques such as X-ray diffraction (DRX) for phase identification, Infrared Spectroscopy (FTIR) were used to give vibration modes, Scanning Electron Microscopy SEM to realize their surface topography and composition and Photoelectron X spectroscopy (XPS) to detect their surface chemical composition

The specific study of their structural characteristics will also optimize their mode of elaboration according to the optical properties (obtained by UV-visible) and spectroscopic sought

II.2.2. Thermal characterization techniques

Thermal characterization is done by ATG thermogravimetric analysis to determine the mass losses of our materials throughout a temperature cycle

II.2.3. Electrochemical behavior was studied by cyclic voltammetry

II.2.4. Conductivity values are measured by the four-point method.

All these techniques have been used whose purpose is to highlight the incorporation of nanoparticles into the polymer matrix, to verify their chemical nature, to study their distribution in the dies, to assess the crystal quality of the synthesized materials, to estimate their size, to establish their morphology and to define their orientation.

II.3. USED PRODUCTS

In all the studies conducted during these experiments, the products used are:

- Aniline's monomer ($C_6H_5NH_2$) is of analytical grade obtained from Aldrich (99%)
(The aniline monomer was vacuum distilled before using)
- Hydrochloric acid (HCl) is analytical grade obtained from Merck (37%, d -1.18)
is used as a doping agent.
- A solution of Ammonium Hydroxyde (NH_4OH) is obtained from (Haene Reidel)
is used as a dedopiant.
- Ammonium persulfate ($(NH_4)_2S_2O_8$) is obtained from (Haene's Riedel; 98%) is
used as an oxidizer.
- The distilled water used to prepare solutions is obtained from a Gesellschaft fur
labortechnikmbH (D-309 38 Burgwedel).
- The demineralized water used for the purification of the resulting materials is
obtained from an ultra Elga Labwater Purelab system
- Metal oxides that are used as reinforcement (Al_2O_3 , WO_3) (99%) purchased near
Sigma-Aldrich.

- OFI (*Opuntia ficus indica*) from Mascara with our preparation in laboratory of Stambouli Mustapha
- N-Methylpyrrolidone (NMP) and Methylsulfinylmethane (DMSO) were obtained from supplied by the company Sigma Aldrich located in Madrid Spain was used as solvent of the nanocomposite. Deionized water was used for all purposes.

II.4. Synthesizing of different nanocomposites

II.4.1. Synthesis of the aniline/tungsten oxide (WO_3) nanocomposite

Hybrid material was fabricated by in-situ oxidative polymerization method. In a typical experiment, 0.22 mol of ANI monomer and stoichiometric amounts of WO_3 nanoparticles ($\text{WO}_3/\text{ANI monomer} = 0.01, 0.02$ and 0.03) were added in 25 ml of HClO_4 0.1M solution obtained under vigorous stirring for half an hour. Then, 220 mmol of APS was added dropwise to above solution and stirred for 24 hours at ambient temperature. After, the black powder was then washed with ethanol and distilled water several times, and then dried overnight at 60°C [1-3]. The resulting samples were named as PANI@WO_3 (0.5), PANI@WO_3 (1.0) and PANI@WO_3 (1.5), respectively. Pure PANI were synthesized in the same manner as the nanocomposite mentioned above, without of WO_3 nanoparticle.

II.4.2. Synthesis of Aniline/Alumina (Al_2O_3) nanocomposite

$\text{PANI/Al}_2\text{O}_3$ nanocomposites were synthesized by in situ oxidative polymerization method. In a typical synthesis, 0.22 mol of aniline monomer was dissolved in 25 ml of HClO_4 0.1M aqueous solution, then, an stoichiometric amount of Al_2O_3 nanoparticles ($\text{Al}_2\text{O}_3/\text{ANI monomer} = 0.02, 0.04$) were added to the solution, then, the solution was stirred for 1 hour at 15°C , the final product was collected by filtration and washed with methanol and distilled water, then dried at 60° overnight [1-3], the resulting samples were named as $\text{PANI/Al}_2\text{O}_3$

2% , PANI/Al₂O₃ 4% respectively, pure PANI was prepared in the same maner as the nanocomposite mentioned above, without of Al₂O₃ nanoparticle

II.4.3. Synthesis of aniline/opuntia ficus indica OFI nanocomposite

Preparation of Opuntia ficus indica (OFI) : the cactus cladodes are cut, washed in the laboratory with distilled water, dried in an oven (110 °C) for 72 h then crushed and sieved at 0.125 µm . after sieving, put 10g of biomass in 100 ml of distilled water with stirring for 24 hours. Repeat this operation until water is clear. for activation of the hybrides particles (OFI) ,a quantity of OFI was put in 10ml of H₂SO₄ 1M , the mixture remain stirring for 6 hours then filtred and washed with destiled water , then dried at 105 °C.

Preparation of polymer composite/OFI, 0.6g of dried OFI a 1M HClO₄ solution and stirred for 1 hour then add a quantity of the monomer (the concentration of the monomers is 0.22 M) ; after 10 minutes of magnetic stirring , the oxidizing solution which is prepared separately was slowly poured in by adding 2.5g of ammonium persulfate (NH₄)₂S₂O₈ to 15 ml of a solution of HClO₄ 1M (using the 1:1 monomer/oxidant molar ratio). And the mixture was left under magnetic stirring at room temperature for 24 hours. The final products were washed with NH₄OH 0.5M at room temperature for 3h. The product was collected by filtration and washing the precipitate with ethanol and deionized water and dried at 60°overnight [1-3].

II.5. Structural, morphological and chemical characterizations

II.5.1 X-ray diffraction

The X-ray diffraction technique is a widely used technique in materials science. This can in particular be attributed to the wealth of information which derives from it as well as to its non-destructive nature, more particularly when one is interested to the characterization of

thin films which often have a flat surface. X-rays are emitted when a metal target (usually copper or cobalt), called an anticathode or anode, is bombarded by an electron beam. The radiation emitted is composed of a polychromatic spectrum from which it is necessary to isolate intense monochromatic. This method of analysis allows, among other things, the identification of crystalline phases, crystallographic textures, the measurement of the sizes of crystallites [4]. During this thesis work, the device used to characterize the thin films synthesized is a D8 Advance diffractometer (Bruker) with Bragg-Brentano geometry in $\theta / 2\theta$ configuration with a copper anticathode ($K_{\alpha 1} = 1.5406 \text{ \AA}$). radiations, as a general rule the doublet K_{α} ($K_{\alpha 1}$ and $K_{\alpha 2}$) [5].

X-rays [6], like all electromagnetic waves, cause the electron cloud to move relative to the nucleus in atoms. These induced oscillations cause re-emission of electromagnetic waves of the same frequency : this phenomenon is called Rayleigh scattering (figure II-8). The wavelength of X-rays being of the order of magnitude of interatomic distances (a few Angstroms), the interference of the rays scattered by the atoms constituting the crystallized matter will be alternately constructive or destructive. Depending on the direction of space, we will therefore have a significant flow of X photons, or on the contrary very weak; these variations according to the directions form the phenomenon of X-ray diffraction. The directions in which the interferences are constructive, called "diffraction peaks", can be determined very simply by the following formula, called Bragg's law :

Where: d_{hkl} : inter-reticular distance of the planes (hkl) (A °)

θ : diffraction angle (degree) n : order of reflection = 1

λ : wavelength of photons emitted by the anticathode (A °)

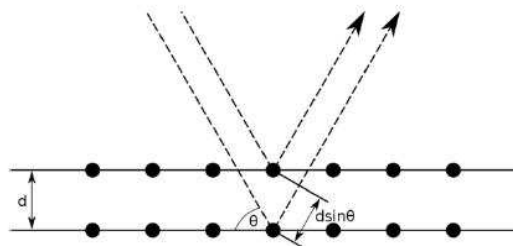


Figure II.1. Schematic representation of Bragg's diffraction law. The black spheres represent the atoms of a crystal structure.

In order to identify the phases constituting the samples studied, the diffractograms obtained are compared with the JCPDS files of the ICDD database. The position of the diffraction peaks is obtained in degrees (2θ) and related to the distance (d_{hkl}) between the planes (h, k, l) of the structure probed by means of Bragg's law.

Thus, it is possible to identify the crystal system (s) formed and the lattice parameters of the structure. Scherrer's (approximate) formula makes it possible to determine the size of crystallites:

$$t = \frac{k/\lambda}{(\beta) \cdot \cos\theta} \quad \text{Equation II-1}$$

with t the size of the crystallite (its diameter if it is considered to be spherical), λ the wavelength of the incident wave, θ half of the deviation of the wave (half of the position of the peak on the diffractogram) and β the width at mid-height of the peak corrected for the experimental width of the device.

The crystalline properties of samples were characterized by X-ray diffraction (XRD) using $\text{CuK}\alpha$ as a radiation ($\lambda = 1.5405 \text{ \AA}$) using a Bruker CCD-Apex instrument

II.5.2 Fourier transform infrared spectroscopy (FTIR)

The basic principle of Fourier Transformed InfraRed spectroscopy is based on the absorption of infrared radiation by the material analyzed. Under the effect of IR radiation, the material absorbs part of the light energy it receives. This absorption, which takes place when the energy supplied by the light beam is close to the vibrational energy of the molecule,

results in a vibration or a forced rotation of certain covalent bonds present in the material. The frequency of molecular vibration at which light energy is absorbed depends on the chemical environment, the nature of the bonds and the mass of the atoms involved, that is to say the chemical structure of the material. The goal of this spectroscopy is to analyze the chemical functions present in the material via the detection of vibrations characteristic of chemical bonds. This non-destructive technique is easy to implement . It allows analysis of both organic and inorganic materials. The associated experimental setups are numerous to allow the characterization of virtually any type of sample, regardless of their physical or surface state. We distinguish:

II.5.2.1 Transmission mounting

For layers deposited on a substrate transparent to infrared and for thin polymer films (ie low thickness $<10\ \mu\text{m}$). This setup can also analyze gels dispersed in a KBr pellet . In this arrangement, the absorption of the incident radiation is responsible for the reduction in the reflected or transmitted intensity. The analysis is carried out using a spectrometer mainly composed of a Michelson interferometer and an infrared (IR) radiation detector (ie pyroelectric). The Michelson interferometer consists of a beam splitter, a fixed mirror and a moving mirror. FIG. 9 describes the block diagram of a Fourier transform infrared spectrometer.

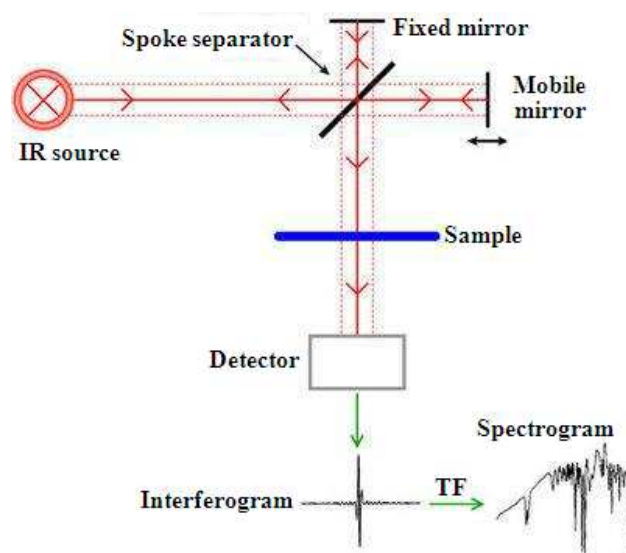


Figure II.2. Schematic diagram of the infrared spectrometer.

The IR source generates an infrared beam which goes to the Michelson interferometer. The latter allows the modulation of each wavelength of the beam at a different frequency. When the light beam arrives on the splitter, the reflected half arrives on the fixed mirror, the other half which passes through the splitter is directed on the mobile mirror. Destructive or constructive interferences between the two beams appear depending on the position of the moving mirror. The modulated beam coming from the two mirrors is absorbed by the sample then detected to be transformed into an electrical signal. This signal appears as an interferogram (signature of the intensity as a function of the position of the mirror: interferogram in the time domain) then converted into an infrared spectrum by a mathematical operation called the Fourier transform. The spectrum essentially provides two types of information:

II.5.2.2 Qualitative and quantitative information

This involves identifying chemical groups present in the material analyzed because the wavelengths absorbed by the sample are characteristic of these groups.

There are data tables which allow the absorption to be attributed to the different chemical groups present. Table 4 gives some examples of vibration bands characteristic of the main functions encountered in organic compounds.

Note, however, that the same group can give rise to several types of vibrations and therefore

- absorptions at different frequencies. Thus in the case of silicon bonded to 4 oxygen atoms of silica, the Si - O bond gives three absorption peaks due to: vibrations of valence or stretching ν (1080 cm^{-1}), vibration of deformation or bending δ (805 cm^{-1}), vibration of sway or rocking (450 cm^{-1}).

The identification of chemical groups is based on the deconvolution of the spectra obtained using specialized software (ie Fityk). This software makes it possible to decompose the lines of the spectrum into various known functions (Gaussian, exponential, etc.) in order to obtain a mathematical model.

Table II.1. Vibration frequencies of some functions encountered in organic compounds [7-10]

Compound	Characteristic vibrations	Vibration frequency (cm^{-1})
Saturated alkane	CH _x stretching	2950-2850
	CH _x strain	1500-1400
Unsaturated alcane	CH _x stretching	3050-3000
	C = C stretching	1600-1500
	Substituted aromatic (CH)	1900-1700
	Aromatic bending	800-750
Alcohol	OH stretching	3400 (wide)
	CO stretching	1050-1250
Ketone	OH deformation	1 area < 2 area < 3 area < Phenol
	C = O stretching	1690-1680
Aldehyde	HC = O	2800-2650
	C = O stretching	1710-1700
Acid	OH (with hydrogen bonding)	3200-2500 (wide)
	C = O stretching	1725-1700
	CO	1440-1395, 1320-1210
	OH deformation	950-900
Acid salt	COO ⁻ antisymmetric stretching	1615-1650

	COO ⁻ symmetrical stretching	1400-1300
Ester	C = O	1775-1720
	Aromatic	1250-1100
Amine	NH stretching	3400-3300 (1 ^{area} > 2 ^{area})
	NH deformation	1650-1550 (1 ^{area} > 2 ^{area} > Arom)
	CN stretching	1350-1250 (1 ^{area} > 2 ^{area} > Arom)
Amide	NH stretching	3350-3070 (1 ^{area} > 2 ^{area})
	C = O	1680-1630
	NH deformation	1650-1515 (1 ^{area} > 2 ^{area})
	CN stretching	1180-1040 (1 ^{area} < 2 ^{area})
Nitrile	C = N	2250
Isocyanate	N = C = O	2275
Sulfone	S = O	1100-1000
	CS stretching	740-690
Halide	SO ₂	1380-1300
	CF	1400-1000
	C-Cl	1175-650
	C- Br	590-510
	C-Cl	525-485

The intensity of the absorption bands depends mainly on the magnitude of the change in the dipole moment of the molecule associated with the vibration. Only vibrations involving a variation in the dipole moment of the molecule give rise to adsorption in the infrared. This involves determining the concentration of the chemical group responsible for absorption by the relationship that exists between the intensity of absorption, at the characteristic wavelength, and this concentration. The intensity is determined by measuring the area of the absorption peak to be able to carry out the quantitative analysis of the absorption bands, it is necessary to use the representation of the spectra in absorbance. According to Beer - Lambert's law , absorbance is defined by the relation:

$$A = Ln_{10}(I_0/I) = \epsilon cl \quad (II.2)$$

I_0 and I being respectively the intensities of the incident and transmitted beam.

A is proportional to the adsorption coefficient ϵ , to the concentration c of the chemical group and to the optical path l .

In practice, however, Beer -Lambert's law is, most often, subject to deviations for several reasons: the condition of monochromaticity, the diffuse (stray) light in the monochromator, the flatness and parallelism of the windows, etc.

The limit of detection of infrared spectrometry is difficult to define because the absorbance varies enormously from one vibration to another. Some molecules can be detected at concentrations of a few tens of ppm . (parts per million) while others are not detectable within a few percent.

II.5.2.3 Measuring device

The measurements are carried out using an FT-IR spectra was recorded from the range of 500-2500 cm^{-1} using a Bruker, Inc., Model alpha. The acquisition of the spectra is carried out with 40 scans per spectrum. The latter are analyzed after subtraction of the spectrum of the KBr pellets.



Figure II.3. FTIR device used

II.5.3 Scanning electron microscopy

The analysis of the surface morphology of the films and their fracture facies in cross section was carried out by means of secondary electron imaging in a scanning electron microscope (*SEM*) type (Zeiss model-SUPRA VP/500) which operates at 3 kV. This analysis technique is based on the detection of secondary electrons (SE) emerging from the surface

under the impact of primary electrons constituting the beam sweeping the surface of the area to be analyzed. In general, when a beam of primary electrons accelerated in a potential of the order of a few kV enters a sample, the electrons undergo a certain number of elastic and inelastic interactions with the constituent atoms of the sample. During an inelastic interaction, the primary electron interacts with the electrons of the material atom. This interaction leads to an energy transfer between the incident electrons and those of the target causing the slowing down of the incident electrons. Depending on the processes involved, the energy loss of the incident electron varies considerably, the electron being able to lose all of its energy or only part because the interaction takes place between comparable particles. When an electron is loosely bound (valence electron), it can acquire sufficient kinetic energy to be ejected. This interaction leads to a distribution of ejected electrons then called secondary electrons. Due to their low energy, secondary electrons are emitted from the surface layers close to the surface. The electrons that can be collected by the detector come from the first 3 to 30 nanometers of the sample (typically a few nm for metals and a little more for oxides). The emergent intensity varies greatly with the angle of incidence of the primary beam. It becomes maximum in grazing incidence and minimum perpendicular to the surface. The variation of the secondary emission with the angle of incidence offers the possibility of demonstrating by scanning electron microscopy a topographic contrast. It is also possible to demonstrate atomic mass contrast using a backscattered electron detector (BSE).

An X-photon energy dispersive analysis (EDSX) method was used to determine the chemical composition of films synthesized by magnetron sputtering. It is directly coupled with the morphological analyzes carried out. For EDSX, it is necessary to have a source of electrons with a sufficiently high energy in order to ionize the atoms constituting the material to be characterized. A hole is thus created and then filled by a succession of electronic transitions. This generates the emission of X photons of wavelength (or energy) specific to the difference energy of the two levels concerned by electronic transitions and, therefore, specific

to the nature of the emitting atoms. The characteristic spectrum of a given sample thus makes it possible to identify the constituent elements of the material and to make a semi-quantitative analysis, even quantitative if special precautions are taken and standard samples used.

It is important to note that the electron-matter interactions take place in an interaction volume called "interaction pear", which is a function of the material studied and increases with the acceleration voltage. Its thickness is approximately 1 μm (figure II-10). In our case, the thickness of the films is less than this value, so there is uncertainty in the quantification of the elements when elements of the film are also present in the substrate. This is why the measurements have generally been carried out for films deposited on silicon substrates simultaneously with the deposition on the other types of supports.

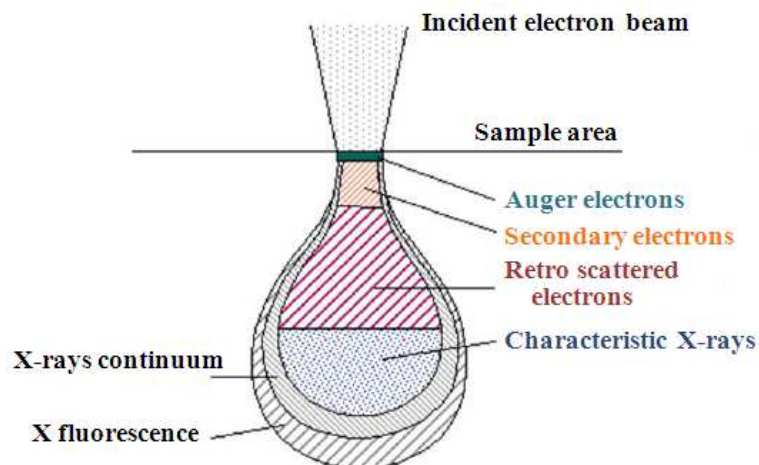


Figure II.4. Electron interaction pear in scanning electron microscopy inspired by[11]

The determination of the chemical composition is done through experimental spectrum modeling and uses ZAF corrective parameters based on the analysis conditions and the nature of the material studied without the use of standard samples. The acronym "ZAF" describes a procedure in which corrections for the effects of atomic number (Z), absorption (A) and fluorescence (F) are calculated separately from the appropriate physical models. It is the standard form of correction and is used with great success. Its main drawback remains that the absorption

correction is insufficient when the correction is large. It is therefore a semi-quantitative analysis. The established detection limit varies from 0.1 to a few atomic percent, depending on the nature of the atom being probed and the matrix in which it is found. In order to obtain the most accurate results, the composition measurements were repeated three to five times and then averaged.

II.5.4. X Photoelectron Spectroscopy (XPS)

The X-ray photoelectron spectroscopy technique (XPS: X-Ray Photoelectron Spectroscopy) is dedicated to extreme surface chemical analysis. It is particularly suitable for the chemical characterization of thin films because the probed depth is of the order of 10 nm. All elements are qualitatively and semi-quantitatively detectable using reference standards. It provides information on chemical bonds between the elements and their respective oxidation degrees. It will therefore be of great help to us in studying the degree of oxidation of tungsten in nanocomposite films. XPS is based on the photoelectric effect. A monoenergetic beam of X photons irradiates an area of the sample (figure II-21). These X photons are absorbed by matter. The energy transferred $h\nu$ serves, among other things, to excite and expel the core electrons of the atoms present. The bond energy E_B of a given level characteristic of the atom is expressed as a function of the incident energy, of the kinetic energy E_k and of the work function of the spectrometer such that $E_B = h\nu - E_k + \phi$. By measuring E_k , it is then possible to determine E_B is to go back to the electronic structure of the first layers from the surface and to the chemical environment of the elements. Unlike EELS which gives access to empty states of the conduction band, XPS is a means of accessing the electronic structure of occupied states of the heart.

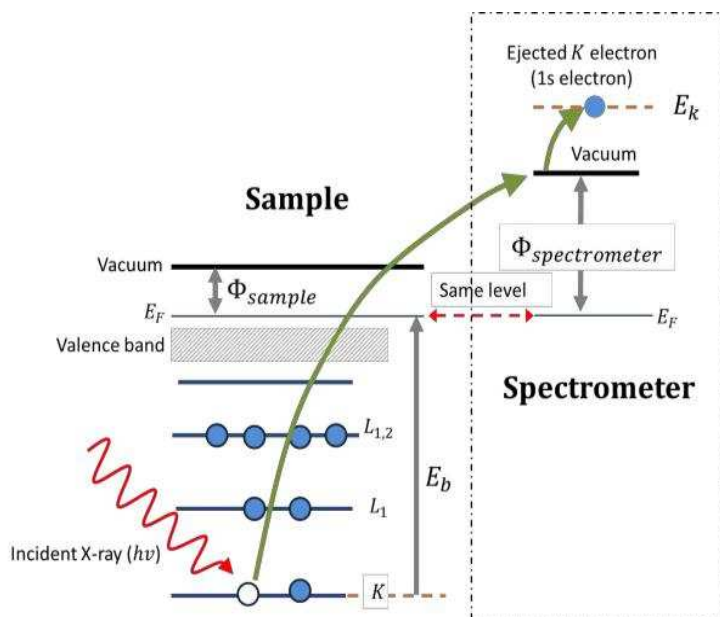


Figure II.5. Representation of the photoelectron emission mechanism by a photon with an energy $h\nu$ in the X-ray domain [12]

The XPS spectrum obtained is represented by a succession of peaks which correspond to a given energy E_B (for example the peak C 1s = excitation of the electrons of the 1s layer of carbon). It is thus possible to carry out an elementary analysis. For each element, each oxidation state can be differentiated from the others thanks to its own binding energy.

The X-ray photoelectron spectroscopy (XPS) analysis was carried out by VG-Microtech Multilab 3000 electron spectrometer. Monochromatized MgK_{α} (1253.6 eV) radiation was used.

II.6. Optical and electrical characterizations

II.6.1. UV-Visible spectrophotometry

Analysis of the films synthesized by spectrophotometry in the UV-Visible domain is necessary to demonstrate the transmittance properties of the films constituting the electrochromic system in the visible domain. It is then possible to compare the evolution of these as a function of the synthesis conditions of the films studied. It is also a suitable

technique for obtaining the absorption coefficient α of the material and measuring its optical gap. The ultraviolet UV-Vis absorption spectra were examined over the wavelength range 200-800 nm by Hitachi U-3000 Spectrophotometer.. The principle of the measurement is shown schematically in figure II-25. The device is calibrated in three steps. The first step is to establish the baseline by plotting the evolution of the transmittance for a sample whose transmittance value is 100%. It is in fact to characterize the transmittance of a calibrated slit corresponding to the location of the sample. Then, the transmittance of a glass substrate is measured as a function of the wavelength $T_s(\lambda)$. The measurement of the transmittance of the glass substrate coated with a film $T_t(\lambda)$ is then used to estimate the real transmittance of the film $T_f(\lambda)$ (figure II-26) taking into account that the imperfect transmittance of the glass is mainly due to reflections at the air-glass interfaces and that the number of air-glass interfaces goes from 2 to 1 between the measurement of the substrate alone and the measurement of the coated substrate:

$$T_f(\lambda) = \frac{T_t(\lambda)}{\sqrt{T_s(\lambda)}} \quad \text{Equation II- 3}$$

A second device was used to obtain an in-situ monitoring of the optical properties of the films by means of a coupling with an electrochemical cell. This coupling is discussed later.

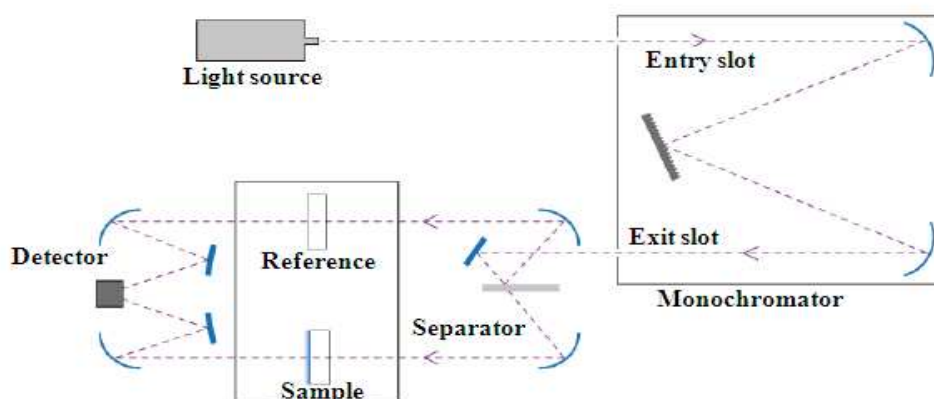


Figure II.6. Schematic of the dual beam and optical path configuration of the Varian Cary 500 spectrophotometer.

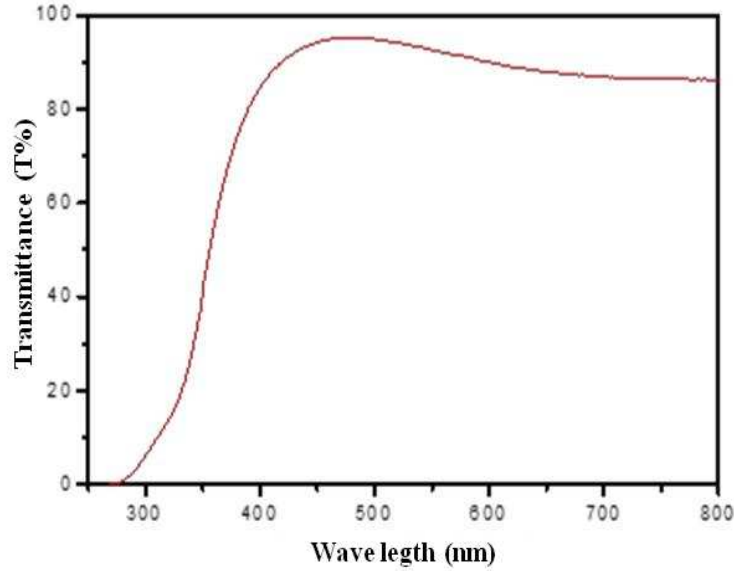


Figure II.7. Example of an optical transmittance curve of an example metal : Al film with a thickness of 110 nm [13]

From such a transmittance curve, it is possible to determine the absorption coefficient and the optical gap of the developed materials. These transmittance curves make it possible to determine numerous optical coefficients such as the refractive index n , the absorption coefficient α , the extinction coefficient k , over the entire window of measured wavelengths. These coefficients are calculated from the theoretical relationships between optical transmittance and absorption coefficient (α):

$$\alpha = \frac{1}{e} \ln\left(\frac{1}{T}\right) \text{ et } \alpha = \frac{4 \cdot \pi \cdot k}{\lambda} \quad \text{Equations II-. 4}$$

Where: e : film thickness (nm)

T : optical transmittance (between 0 and 1)

λ : wavelength (nm)

the optical band gap calculated by tauc relation $\alpha h\nu = B(h\nu - E_g)^y$, where E_g the optical band gap, h the planck's constant and ν the frequency of incident photons, B is a cst called the band tailing parameter, and y is the index, which can have defferent values (2, 3,

1/2 , 1/3) corresponding to indirect allowed and indirect forbidden transitions , direct allowed and direct forbidden transitions , respectively.the band gap of the present system was estimated by plotting $(\alpha h\nu)^2$ vs $h\nu$ as shown in inset of fig II8 and extrapolating the linear portion near the onset of absorption edge to the energy axis. For an indirect semiconductor, the absorption coefficient is related to the optical gap by the following expression[14] :

$$\alpha = (h \cdot \nu - E_g)^2 \quad \text{Equation II- 5}$$

E_g : optical gap (eV)

The optical gap is determined by the ordinate at the origin of the extrapolation of the increasing and linear part of the curve (figure II-27) according to the Tauc method[14] :

$$(\alpha \cdot h \cdot \nu)^{\frac{1}{2}} = f(h \cdot \nu) \quad \text{Equation II-6}$$

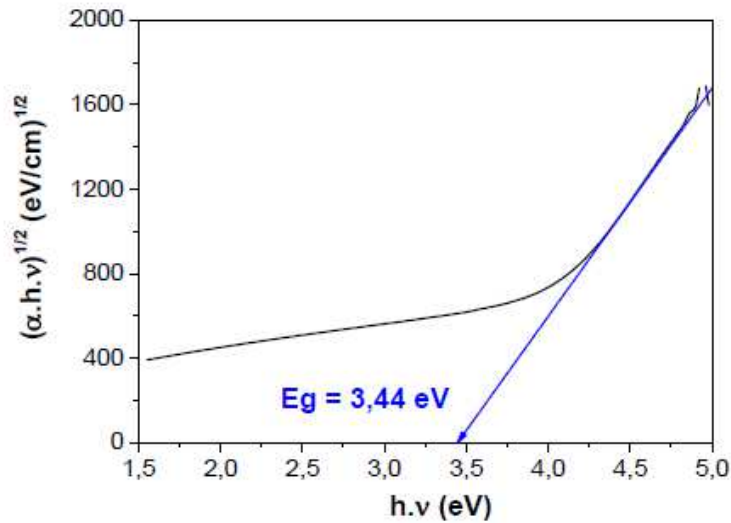


Figure II.8. Example of measurement of the indirect gap of a tungsten oxide film WO_3

II.6.2. Measurement of electrical resistivity by the 4-point method

The electrochromic effect being based on an ionic insertion coupled with an insertion of electrons, it is useful to measure the electrical resistance of the synthesized films. The

configuration adopted, known as the “four-point method”, is inspired by the method of Van der Pauw [15] which makes it possible to measure the resistivity of a thin film of known and assumed uniform thickness (figure II-28). On the other hand, the tips are aligned contrary to the method of Van der Pauw.

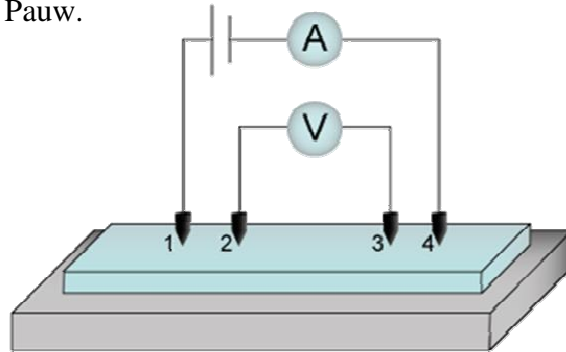


Figure II.9. Diagram showing the operation of the "4 points" method

Unlike the two-point method, the four-point method makes it possible to compensate the contact resistances between the current injection and voltage measurement points and thus to measure only the properties of the thin film. In general, when the thickness is negligible compared to the other dimensions, the resistance can be expressed in the form:

$$R = \frac{U}{I} = K \cdot \frac{\rho}{e} \quad \text{Equation II-7}$$

In this method, all four contacts should be placed symmetrically and aligned with the deposit (Figure II-9). The current injected between the two outer points is delivered by a Keithley 237 generator. It can vary from a few nano-amps to a few milli-amps depending on the resistive nature of the layer. The voltage is measured between the internal terminals by a Keithley 2700 voltmeter . The resistance measurement is averaged over 400 values. In order to consider the geometric peculiarity of thin films (surface / thickness ratio $\gg 1$) the following formula is used to determine, from the couple of values (I, V) measured, the resistivity ($\Omega \cdot \mu\text{m}$):

$$\rho = 4.532.e.\frac{V}{I}$$

Equation II- 8

where 4.532 is a specific form factor for measuring thin films , e : film thickness (cm), V : voltage measured between points 2 and 3 (V) and I : applied current between 1 and 4 (A)

Electronic conductivity is the inverse magnitude of resistivity ($\sigma = \frac{1}{\rho}$) and is expressed in (S.cm⁻¹).

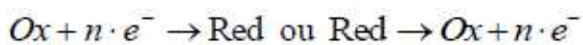
II.7. Electrochemical analysis techniques used

II.7.1. Oxidation-reduction reactions

During electrochemical reactions, two phenomena occur:

An exchange of electric charges through the electrode (film) -electrolyte (solution) interface An ionic movement of matter (cations) due to the influence of the field electrical established in the different electrodes.

These are governed by the following electrochemical oxidation-reduction reaction:



Equation II-9

Our study relates to the electrochromic system of oxide anion during intercalation of cations. This causes a reduction or an oxidation of the oxide , reactions corresponding respectively to the insertion or the deinsertion of cations. The redox reaction thus initiated in our analyzes is therefore as follows:

II.7.2. Electrochemical analysis technique

In this part, we will present the different electrochemical characterization products and methods, as well as the experimental set-up on which our work was done.

Electrochemical analyzes were carried out using a three-electrode experimental cell equipped with a working electrode, a platinum counter electrode, and RHE (reference electrode). All the electrochemical studies were carried in 1M HClO₄ aqueous solution as electrolyte at 25°C [1-2]. The experimental device used for electrochemical measurements is called a three-electrode assembly. It consists of an electrochemical cell containing a conductive liquid electrolyte in which three electrodes are immersed (figure II-31). The reference electrode is of the AgCl / Ag type of the Bioblock brand , (possibly fitted with a salt bridge filled with KNO₃ to avoid pollution of the electrolyte by chlorides). The counter-electrode is a Metrohm brand platinum plate electrode ($S \approx 1 \text{ cm}^2$) . Finally, the working electrode ($S \approx 2 \text{ cm}^2$) is the film to be tested that we synthesized on a (commercial) substrate made up of a thin film of electronically conductive ITO deposited on glass or a bilayer made of the same film coated with a solid electrolyte of the NaSICON type. The electrolytes used, an aqueous solution of 0.1M sodium sulfate Na₂SO₄ serving as a source of Na⁺ cations or an ionic liquid of the BePipTFSI type , are not stirred (non-stationary diffusion regime). The experiments are carried out at room temperature.

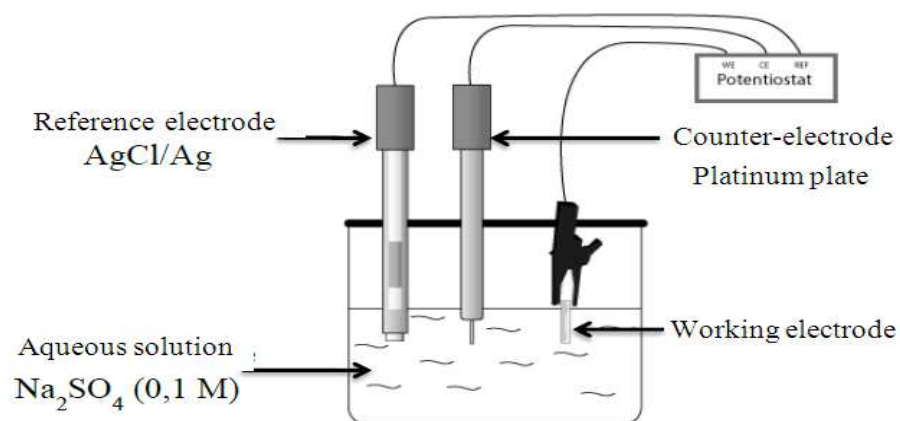
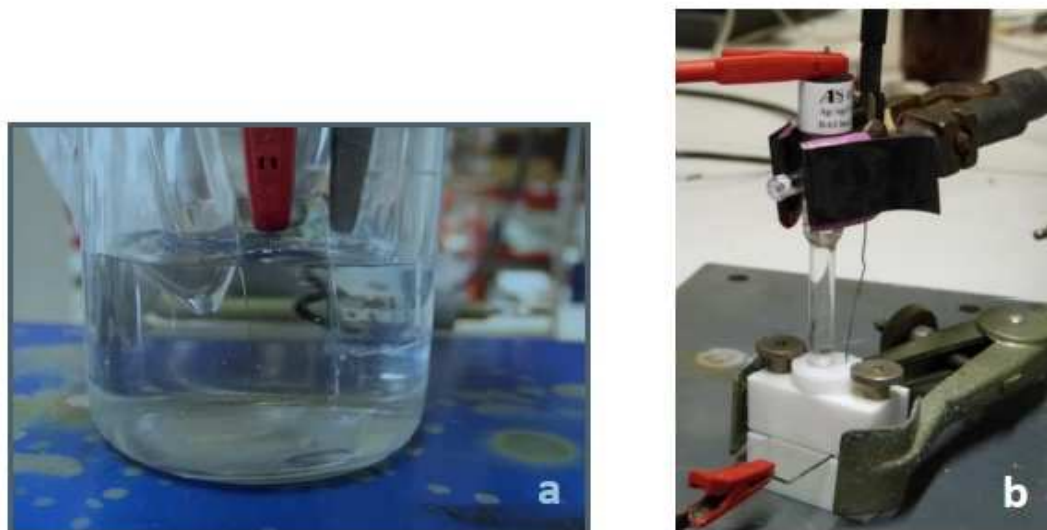


Figure II.10. Diagram of the 3-electrode cell used for electrochemical analyzes

Different configurations of electrochemical cells were used during this work. The cell which was used initially is said to be “closed” (figure II-32b). It has the advantage of being small and therefore of having a small volume of electrolyte solution but also of having a contact surface well defined by a seal of 1 cm in diameter. On the other hand, it makes it impossible to observe a change in color with the naked eye. It was thus decided to use an “open” cell (figure II-32a), using a beaker as container, to observe the possible coloring of the film. This second cell contains a larger volume of liquid solution, 30 cm^3 or more, and allows analyzes to be carried out on larger surfaces

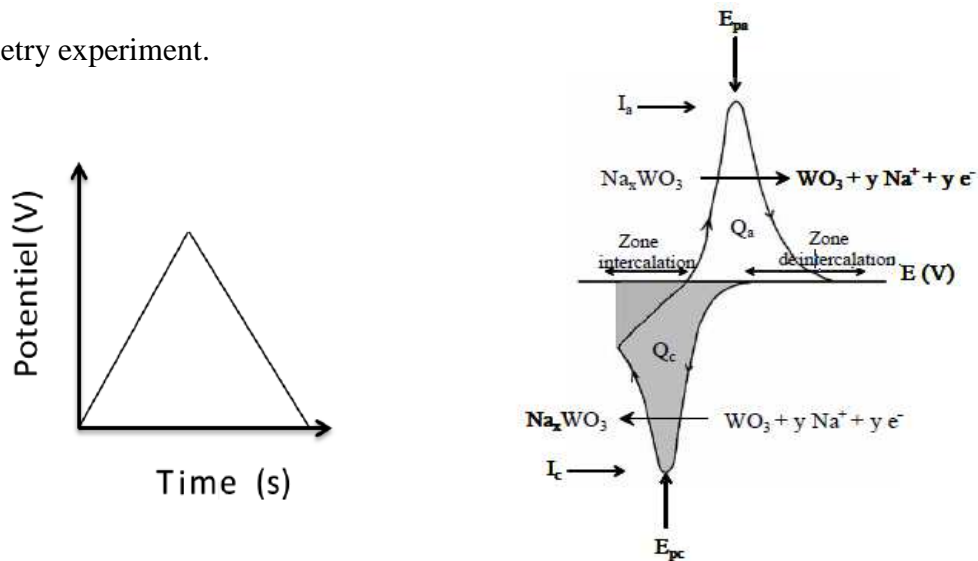


Figures II.11. Photographs of the “open” (a) and “closed” (b) cells

II.7.2.1 The cyclic voltammetry (CV)

Voltammetry techniques are based on the study of the relationship which is established between the electrode potential E and the current i which flows through an electrochemical cell when this potential is imposed. The measured current reflects the mechanism and rate of the different reactions associated with an electrode process, and allows a qualitative or quantitative determination of the associated characteristic parameters (thermodynamics and kinetics) when a theoretical model of the process is available. In cyclic voltammetry (CV), the imposed potential is a linear function of time at a constant rate (scanning speed), and in the same experiment, it is varied first in one direction (generally towards negative potentials), and then in the reverse direction. The scan makes it easy to observe the behavior of the system at different potentials and thus to identify the different electroactive species. Reversing the direction of the variation of the potential makes it possible to observe both the electrochemical behavior of the reactants and the products, and therefore the reversibility of the reactions. In addition, the scanning speed provides a means direct control of the kinetic regime of reactions (reversible, quasi-reversible, irreversible regime) and its variation makes

it possible to observe the reactions under different regimes and to diagnose their mechanistics. The cyclic voltammetry technique is generally applicable to all types of electrodes and electrolytes. Figure 3-2 shows the general shape of potential and current in a cyclic voltammetry experiment.



Description : The electrode potential is varied linearly at a constant scanning speed ν between two limit values E_{min} and E_{max} in several steps: (i) reduction of the potential from an initial value E_i to the minimum value E_{min} generally denoted E_λ , λ being the time at which E_{min} is reached, (ii) increase the potential of E_λ to a maximum value E_{max} , (iii) reduction of the potential of E_{max} to a value final E_f , (iv) repetition of the cycle if there's place.

Source : Bard A. J, Faulkner LR “Electrochemical Methods: Fundamental and Applications”, page 227

Figure II.12. Cyclic voltammetry: (a) shape of the electrode potential (b) Shape of the resulting voltammogram

The characteristics of interest of the curve i - E include the height of the current peaks cathode (i_{pc}) And anode (i_{pa}) And their ratio [16] , the values of potential E_{pc} And E_{pa} which the cathode and anode current peaks are observed and difference $\Delta E = E_{pa} - E_{pc}$

In the case of a reversible reaction of the form , $O + ne^- \rightleftharpoons R$ The values of are related to the thermodynamic and kinetic parameters of the electrochemical reactions by the equations

following (Parameters D_O , D_R And γ_O, γ_R Represent the diffusion coefficients and the species of the activity coefficients O and R respectively) :

- $i_{pc} = 0.4463 \left(\frac{F}{RT}\right)^{3/2} n^{3/2} A D_O^{1/2} C_o^* \nu^{1/2}$ (Equation II-10)

- $\frac{i_{pa}}{i_{pc}} \approx 1$ (Equation II-11)

- $E_p = E_{1/2} - 1.109 \frac{RT}{nF} \approx \frac{28.5}{n} \text{ mV à } 25^\circ\text{C}$ (Equation II-12)

$$E_{1/2} = E^0 + \frac{RT}{nF} \ln\left(\frac{\gamma_O}{\gamma_R}\right) + \frac{RT}{nF} \ln\left(\frac{D_R}{D_O}\right)^{\frac{1}{2}}$$

- $\Delta E_p \approx 2.3 \frac{RT}{nF} \approx \frac{59}{n} \text{ mV } 25^\circ\text{C}$ (Equation II-13)

i_p = current maximum in amps , n = number of electrons transferred in the redox event (usually 1) , A = electrode area in cm^2 , F = Faraday Constant in C mol^{-1} ,

D = diffusion coefficient in cm^2/s , C = concentration in mol/cm^3 , ν = scan rate in V/s

R = Gas constant in $\text{J K}^{-1}\text{mol}^{-1}$, T = temperature in K

The (Equation II-13) generally predicts that the peak current is proportional to the concentration of electroactive species involved, and the analysis of the variation of the concentration effect on the height of the peaks was used to laboratory as one of the techniques for identifying electrochemical reactions on voltammograms. Several other techniques were used to identify oxidized or reduced species, including methods by differential thermal analysis with the variation of the scanning speed, and the comparison of the results to those predicted by the thermodynamic considerations of the Pourbaix diagrams.

II.8. Thermal analysis

II.8.1 Thermogravimetric analysis

Thermogravimetric analysis (TGA) or thermogravimetry is used to study the physicochemical phenomena which result, under the effect of temperature, by a variation in mass. Thermogravimetry makes it possible to follow the variation in the mass of a material as a function of temperature or time in a controlled atmosphere (inert gas: nitrogen, and argon or oxidant: dioxygen). It is used to measure thermal stability, degradation characteristics, aging and to determine kinetic parameters.

A thermogravimetry device generally consists of a sealed enclosure making it possible to control the atmosphere of the sample containing an oven for managing the temperature, a microbalance and a thermocouple for measuring the temperature. A computer is used to control the assembly and to record the data (Figure II.8).

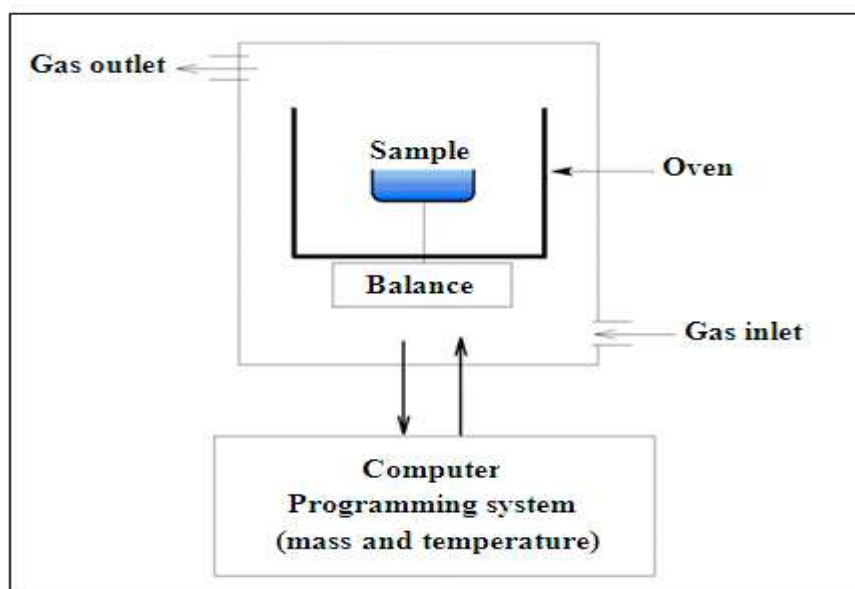


Figure II. 13. Diagram of the principle of thermogravimetric analysis

The thermogravimetric analysis measurements were conducted on Hitachi STA7200 Instrument under Nitrogen flow with a ramping rate of $10^{\circ}\text{C}\cdot\text{min}^{-1}$ for a temperature range from 25°C to 800°C . The device is equipped with a balance with an accuracy of $1\ \mu\text{g}$. The test sample is generally present for a mass of between 1 and 3 mg and which is introduced into an alumina boat.

II.9. Conclusion

The initial objective of this thesis work is to provide answers concerning the electrochemical behavior of polyaniline with three metals oxides (WO_3 , Al_2O_3 and OFI) to form nanocomposites as a priority.

In order to have a more in-depth, or at least more correct, study of the behavior of these composites, we have invested the time necessary for the structural and thermal characterization of the materials we have developed. We were able to benefit from the measurements carried out at the laboratory of chemistry-alicante-spain, but we also had access to many equipment available at the L.S.T.E laboratory- university of mustapha stambouli mascara, materials chemistry laboratory, faculty of exact and applied sciences-oran 1 ahmed ben bella university-oran- algeria. faculty of science and technology- university of mustapha stambouli mascara-mascara-algeria, hydraulique and chemistry laboratory of Mustapha stambouli -mascara-algeria, which was a real asset in being able to achieve our objectives as well as possible.

II.10. References

- [1] . Yamani K, Berenguer R, Benyoucef A, Morallón E (2019) Preparation of polypyrrole (PPy)-derived polymer/ZrO₂ nanocomposites: effects of nanoparticles interface and polymer structure. *Journal of Thermal Analysis and Calorimetry*. 135:2089-2100.
- [2] Kouidri FZ, Berenguer R, Benyoucef A, Morallon E (2019) Tailoring the properties of polyanilines/SiC nanocomposites by engineering monomer and chain substituents. *Journal of Molecular Structure*. 1188:121-128.
- [3] Bousalem S. Zeggai FZ. Baltach H, Benyoucef A (2020) Physical and electrochemical investigations on hybrid materials synthesized by polyaniline with various amounts of ZnO nanoparticle. *Chemical Physics Letters*. 741:137095.
- [4] Michikami, O.; Asahi, M. YBaCuO Epitaxial Film Formation by Magnetron Sputtering with Facing Targets I. Effects of Target and Substrate Positions. *Jpn. J. Appl. Phys.* **1991**, 30 (Part 1, No. 5), 939–944.
- [5] Broll, N. Caractérisation de solides cristallisés par diffraction X | Techniques de l'Ingénieur <http://www.techniques-ingenieur.fr/base-documentaire/mesures-analyses-th1/etudes-de-structure-et-caracterisation-42386210/caracterisation-de-solides-cristallises-par-diffraction-x-p1080/> (accessed Aug 11, 2016).
- [6] Graef, M. D.; McHenry, M. E. *Structure of Materials: An Introduction to Crystallography, Diffraction and Symmetry*; Cambridge University Press, 2007.
- [7] L. G. Bellamy. *The Infrared Spectra of Complex Molecules*. Chapman and Hall, **1975**.
- [8] G. Socrates. *Infrared Characteristic Group Frequencies*. John Wiley & Sons Ltd., **1980**.
- [9] B. Schrader. *Raman & Infrared Atlas of Organic Compounds*. VCH, **1989**.
- [10] A. H. KUPTSOV and G. N. ZHIZHIN. *Handbook of Fourier Transform Raman and Infrared Spectra of Polymers*. Elsevier, **1998**.

- [11] Brisset, F.; microanalyse, G. national de M. E. à B. et de. *Microscopie électronique à balayage et microanalyses*; EDP Sciences, 2012.
- [12] Watts, J. F.; Wolstenholme, J. *An Introduction to Surface Analysis by XPS and AES*; Wiley, 2003.
- [13] Jullien, M. Synthèse et Caractérisation de Films Minces D'oxydes Pour Le Développement D'un Système Electrochrome "Tout Céramique," Thèse d'Université, Vandoeuvre-les-Nancy, INPL, 2011.
- [14] Tauc, J.; Grigorovici, R.; Vancu, A. Optical Properties and Electronic Structure of Amorphous Germanium. *Phys. Status Solidi B* **1966**, *15* (2), 627–637
- [15] Van der Pauw. 1958 Van Der Pauw (Philips Res Rep) a Method of Measuring Specific Resistivity and Hall Effect of Discs of Arbitrary Shape
<https://fr.scribd.com/doc/44653007/1958-Van-Der-Pauw-Philips-Res-Rep-a-Method-of-Measuring-Specific-Resistivity-and-Hall-Effect-of-Discs-of-Arbitrary-Shape> (accessed Aug 13, 2016).
- [16] A. BAHLOUL ; Synthèse, caractérisation et utilisation de matériaux composites à base de POC + MnO₂ comme matériaux d'électrodes dans les piles Zn-MnO₂ ; Thèse de Doctorat, Université Ferhat Abbas-SETIF ; 2011

CHAPTER III

The influence of the addition of tungsten trioxide nanoparticle size on structure, thermal and electroactivity properties of hybrid materials reinforced PANI

III.1. Introduction

Metal oxides are a subject of attention because of their electronic, conductive, thermal stability, optical and magnetic properties adapted for a diversity of applications, such as SiO₂, TiO₂, Al₂O₃, V₂O₅, ZnO, SiC, ZrO₂, MnO₂, NiO and Fe₃O₄ have been extensively investigated as the electrode materials for semiconductives [1-11]. Among various nanoparticles, WO₃ is mostly studied among the many nanoparticles owing to its several advantages availability: strong adherence to substrate, good chemical stability and good chemical stability [12-14]. WO₃ has been successfully applied in electrocatalysis, photoanodes for solar energy, photoelectrocatalytic reactors, gas sensors and electrochromic devices. However, the wide band gap (2.5-2.8 eV) and low energy conduction band of WO₃ nanoparticle limit its application [15, 16]. One of the promising strategies to overcome the mentioned disadvantages is the formation of WO₃-based hybrid materials.

Herein, a new investigation has demonstrated that the PANI/ WO₃ nanocomposites synthesized by oxidation chemical or electrochemical of PANI inside WO₃ nanoparticle exhibiting two type (*p*- and *n*-) photoelectrochemical activity [5]. In addition, the incorporating of PANI into WO₃ gives rise to applications such as sensors [17], supercapacitor [18], humidity sensor [19], electrochromic energy storage [20], catalyst [21] and so on. Although PANI/ WO₃ have been assembled by adopting several techniques; nevertheless, the efficacy of these nanocomposites explored less in all the circumstances.

In this chapter, studies a simple and convenient method to fabricate PANI/WO₃ by oxidative polymerization. The hybrid materials properties, thermal stability and morphology and electrochemical behavior of synthesized samples were characterized using a number of various techniques.

III.2 Results and discussion

III.2.1. XPS spectroscopy

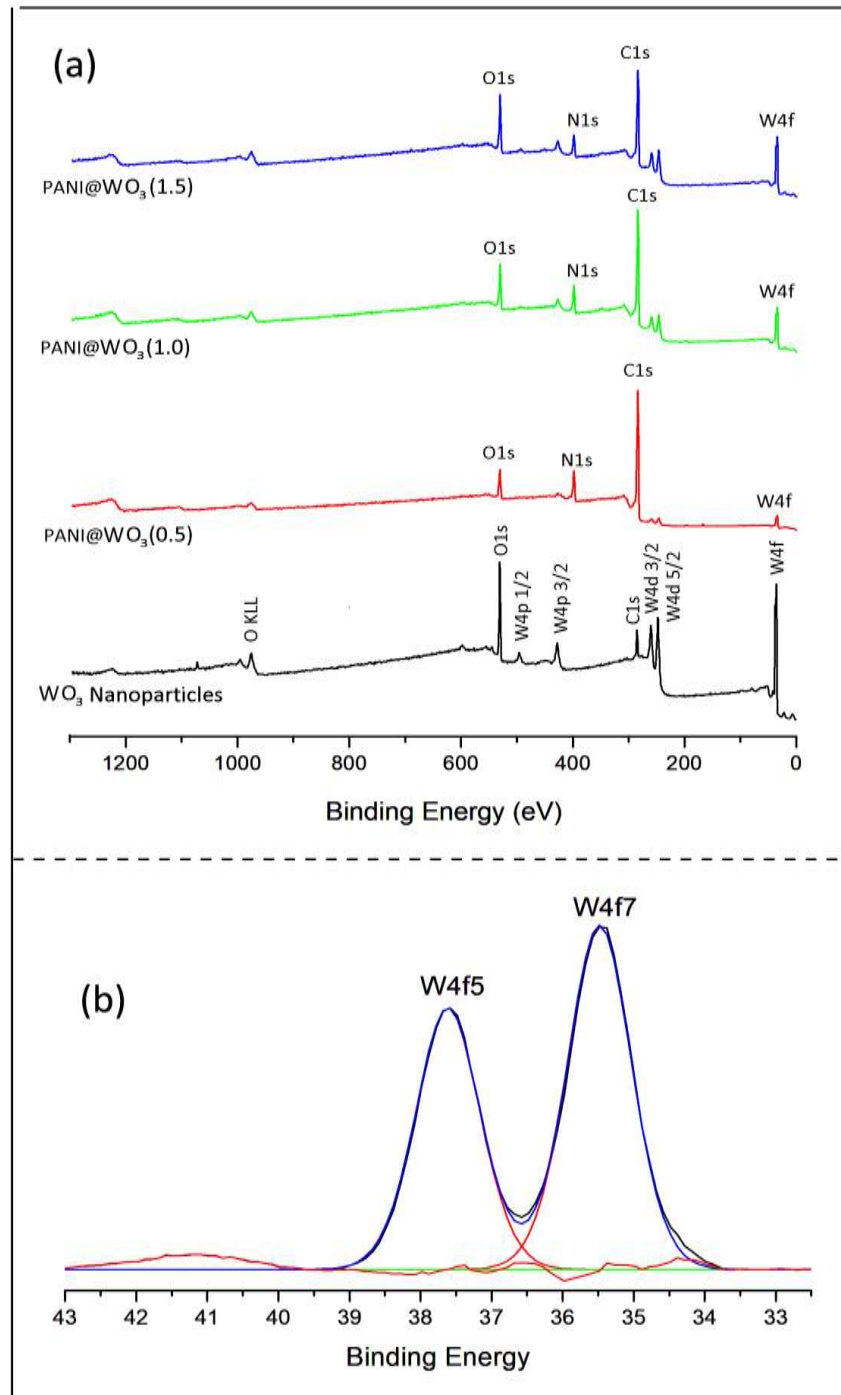


Figure III. 1. Survey (a) and high-resolution WO₃ nanoparticle; (b) X-ray photoelectron spectra of three PANI/ WO₃ samples.

The hybrid materials were examined by XPS. Figure III.1-a shows the full-scanning spectrum in the range from 0 at 1300 eV and the atomic composition of carbon (C), nitrogen (N), oxygen (O) and tungsten (W) in nanocomposites synthesized (Table 1). In WO₃ nanoparticles, the core level binding energies of the W spectrum (Fig. 1-b) can be divided into the clear two peaks at 35.45 eV and 37.60 eV which are ascribed to W4f7 and W4f5 species, respectively.

The C1s signal for PANI/WO₃ (0.5) can be resolved into four separate carbon bonding environments (Figure III.2). The low binding energy state at 284.59 eV (42.10%) with a FWHM (full width at half maximum) of 1.20 eV corresponds to C–C, C=C and C–H bonds. The second at 285.61 eV (23.66%) with a FWHM of 1.25 eV can be attributed to neutral C–N bonds that assigned to carbons bonded to neutral amine and imine nitrogens (Table 1). The third, at 286.77 eV (1.95%) with a FWHM of 1.85 eV is bonded to nitrogen (N3), the highest binding energy is expected at 288.68 eV (23.66%) with a FWHM of 2.04 eV is given to C=O bond. Similar C1s binding energy values are reported in the literature [6, 22]. In addition, the formation of PANI/WO₃ (1.0) further confirmed by C1s spectrum presenting at 284.57 eV (37.01% and FWHM is 1.20 eV), 285.59 eV (16.18% and FWHM is 1.12 eV), 286.51 (13.09% and FWHM is 1.72 eV) and 288.57 eV (3.52% and FWHM is 1.89 eV) attributed to C–C, C–N, C=N and C=O, respectively. The same time, the C1s survey scan of PANI/WO₃ (1.5) pose also four contributions of C–C (40.33% with FWHM 1.24 eV), C–N (22.23% and FWHM is 1.19 eV), C=N (10.40% with FWHM 1.71 eV) and C=O (1.81% with FWHM 1.81 eV) that corresponds to formation of PANI chains.

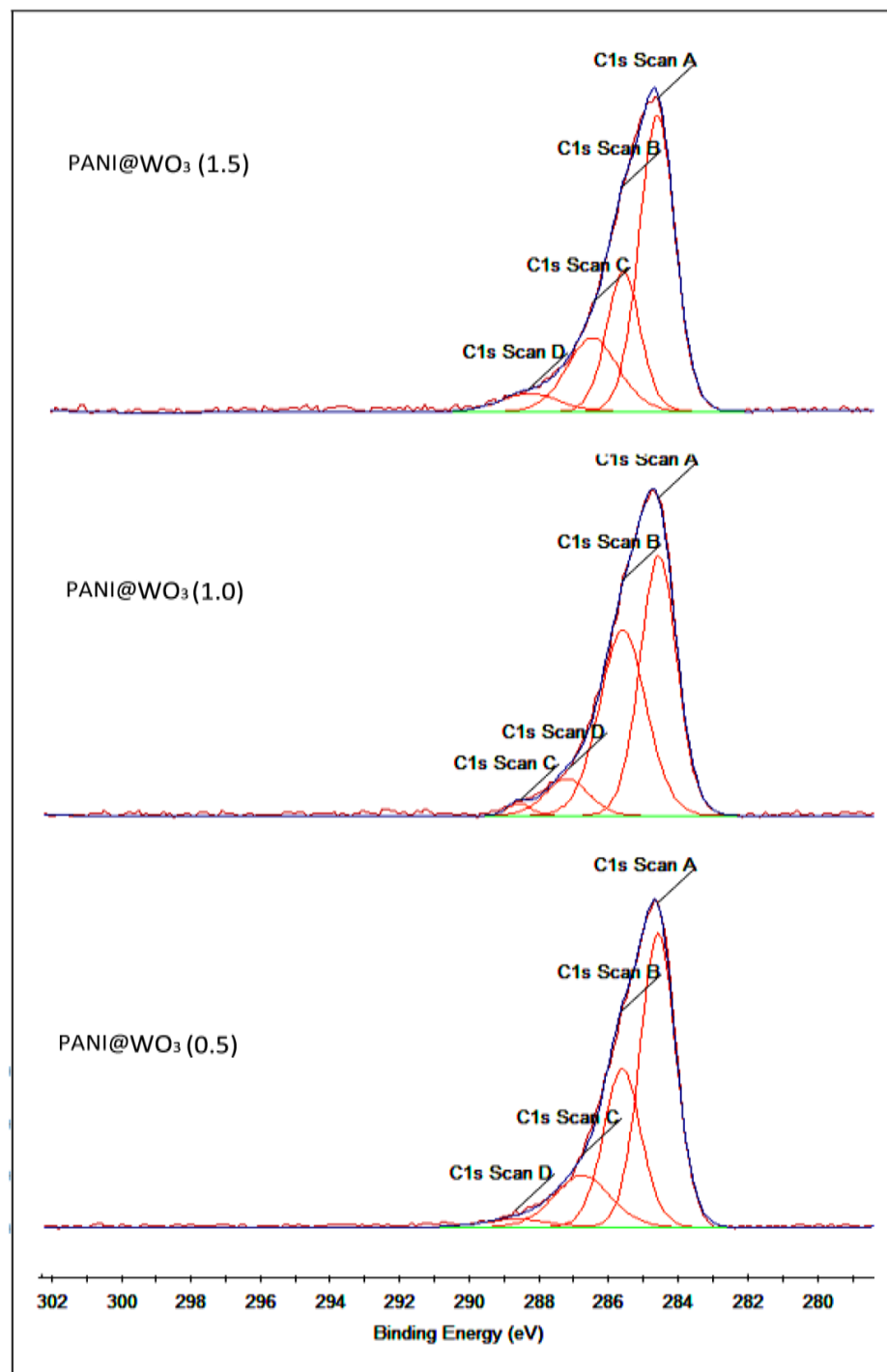


Figure III. 2. XPS spectra C1s of three PANI/ WO₃ nanocomposites synthesized.

Table III.1. XPS Binding Energy/eV results for nanocomposites: (A) WO₃ nanoparticles, (B) PANI/WO₃ (0.5), (C) PANI/WO₃ (1.0) and (D) PANI/WO₃ (1.5).

Elements	Samples & Binding Energy/eV				Remarks
	(A)	(B)	(C)	(D)	
W4f7	35.45	35.89	35.84	35.94	W ⁵⁺ state of Wolframic
W4f5	37.60	38.00	37.98	38.11	
C1s	284.60	284.59	284.57	284.51	C–C, C=C, C–H
	285.99	285.61	285.59	285.58	C–N
	//	286.77	286.51	286.46	C=N
	288.37	288.68	288.57	288.30	C=O
N1s	//	398.42	398.44	398.48	Imine =N-
	//	399.55	399.55	399.68	Amine -NH-, -NC-
	400.56	401.29	401.42	401.69	-N ⁺ H-, =N ⁺ -
O1s	530.24	530.98	530.77	530.80	W–O bond
	531.56	532.58	532.38	532.34	O=C
	//	534.51	533.31	533.60	C–O–H

Furthermore, the intensities value of C–C/C–N is useful under study as a measure of crosslinking degree in the nanocomposites PANI/ WO₃ (1.0) C–C/C–N proportion of 2.3 (Table III.1), which is the degree related with no crosslinking. Also, the crosslinking value of 1.8 for PANI/WO₃ (1.5) shows some significant value of cross linking, while the PANI/ WO₃ (0.5) degree of 1.1 appear the common proportion for highly crosslinked samples, whereas these are simply semi quantitative measures.

The fitting data for the N1s spectra of all nanocomposites synthesized are presented in Figure III. 3. its deconvolution leads three main components (Table 1). The component with the lowest binding energy, corresponds to imine (=N–) structure can be utilized to evaluate the density of flaws within the PANI, because this structure is believed to interrupt the conjugation chain. The second, higher energy state is due to the neutral and amine-like (–NH–) structure, whilst the highest binding energy state is due to the protonated amine units. (–NH⁺–) [23].

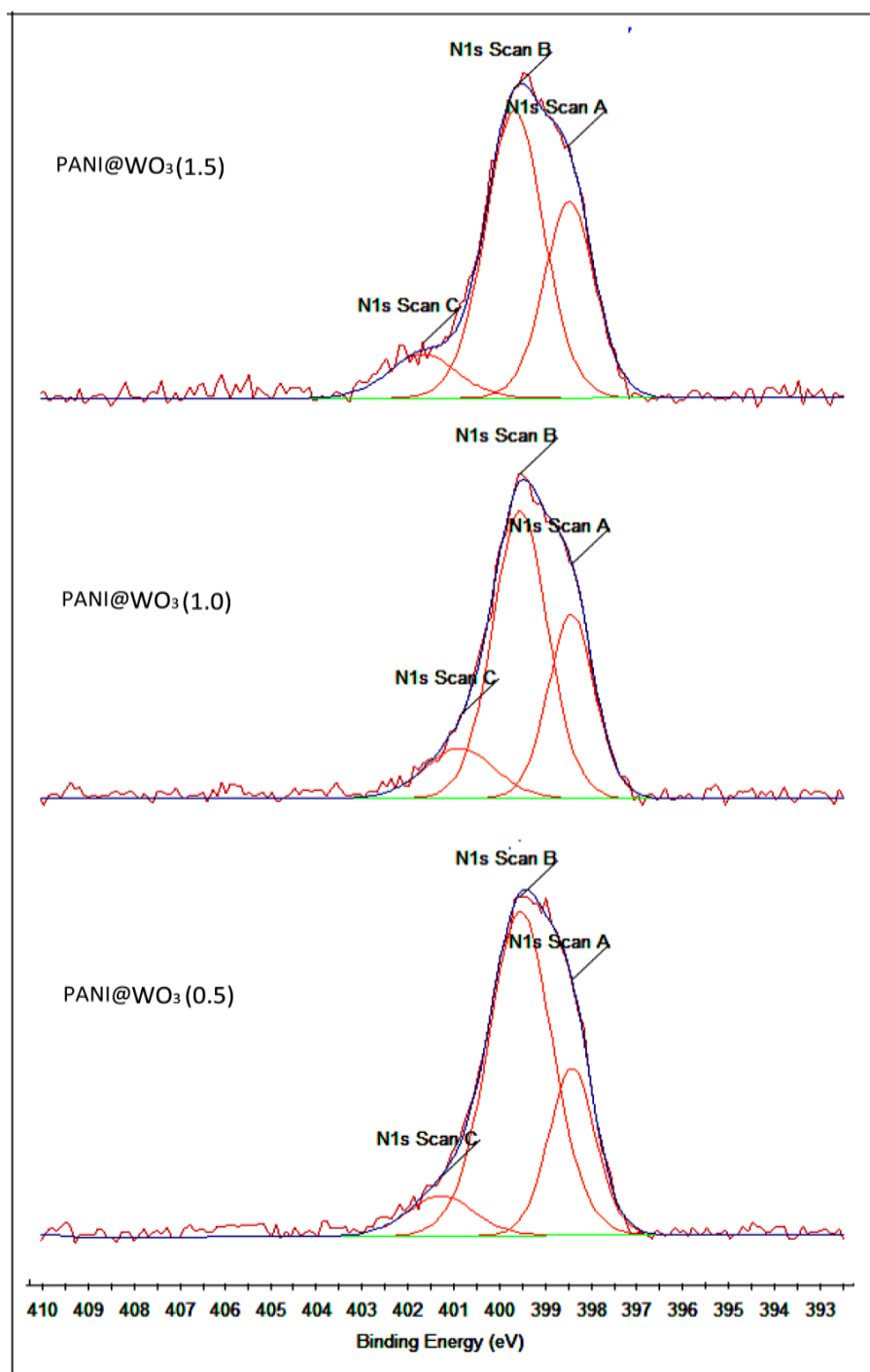


Figure III .3. XPS spectra N1s of three PANI/ WO₃ nanocomposites synthesized.

Table III.2. Doping degree and defect density in different PANI nanostructures

Sample	$[N^+/N]^b$ (doping degree)	$[= N - /N]^c$ (defect density)
PANI/WO ₃ (0.5)	0.08	0.24
PANI/WO ₃ (1.0)	0.12	0.31
PANI/WO ₃ (1.5)	0.09	0.33

The doping level was determined from the report of the area of the highest binding energy peak to the total area of the N1s peak, and the defect density from the ratio of the area of the lowest binding energy peak to the total area Table III.2. The doping level of PANI in PANI/WO₃ (0.5) is 0.08 and the density of flaws is only 0.24, while, the doping level of PANI/WO₃ (1.0) is 0.12 and the density of defects is up to 0.31. Finally, in the case of PANI/WO₃ (1.5) sample, the doping level and the density of defects is 0.09 and 0.33, respectively. The PANI/ WO₃ (0.5) has a lower defect density and higher doping degree, which presumably results in its faster charging discharging rate and higher capacitance. So, the different value of the N1s spectra suggests that these three samples have dissimilar distribution of N1 species, in other words, different doping states.

III.2.2 XRD studies

The diffraction peaks of crystalline WO₃ nanoparticle and nanocomposites can be seen in Figure III. 4, along different planes. The XRD patterns of pure PANI displayed lack of crystallinity. The peaks obtained at 2θ values 9.59°, 15.47°, 20.23° and 24.76° are in agreement with those reported by Sanches [24]. In addition, the peaks at 2θ values 23.15°, 23.62°, 24.39°, 26.62°, 28.65°, 28.92°, 33.27°, 33.60°, 34.20°, 35.62°, 41.45°, 41.90°, 42.50°, 47.20°, 49.96° and 55.89° correspond to (002), (200), (020), (120), (112), (112), (022), (202), (202), (122), (222),

(222), (320), (040), (440) and (620) reflections of WO₃ nanoparticle (JCPDS no. 431035). In a similar way, the diffraction peaks in three nanocomposites synthesized are slightly shifted to lower angle (see Table 2) due to the interaction between PANI chain and WO₃ [2-6, 25].

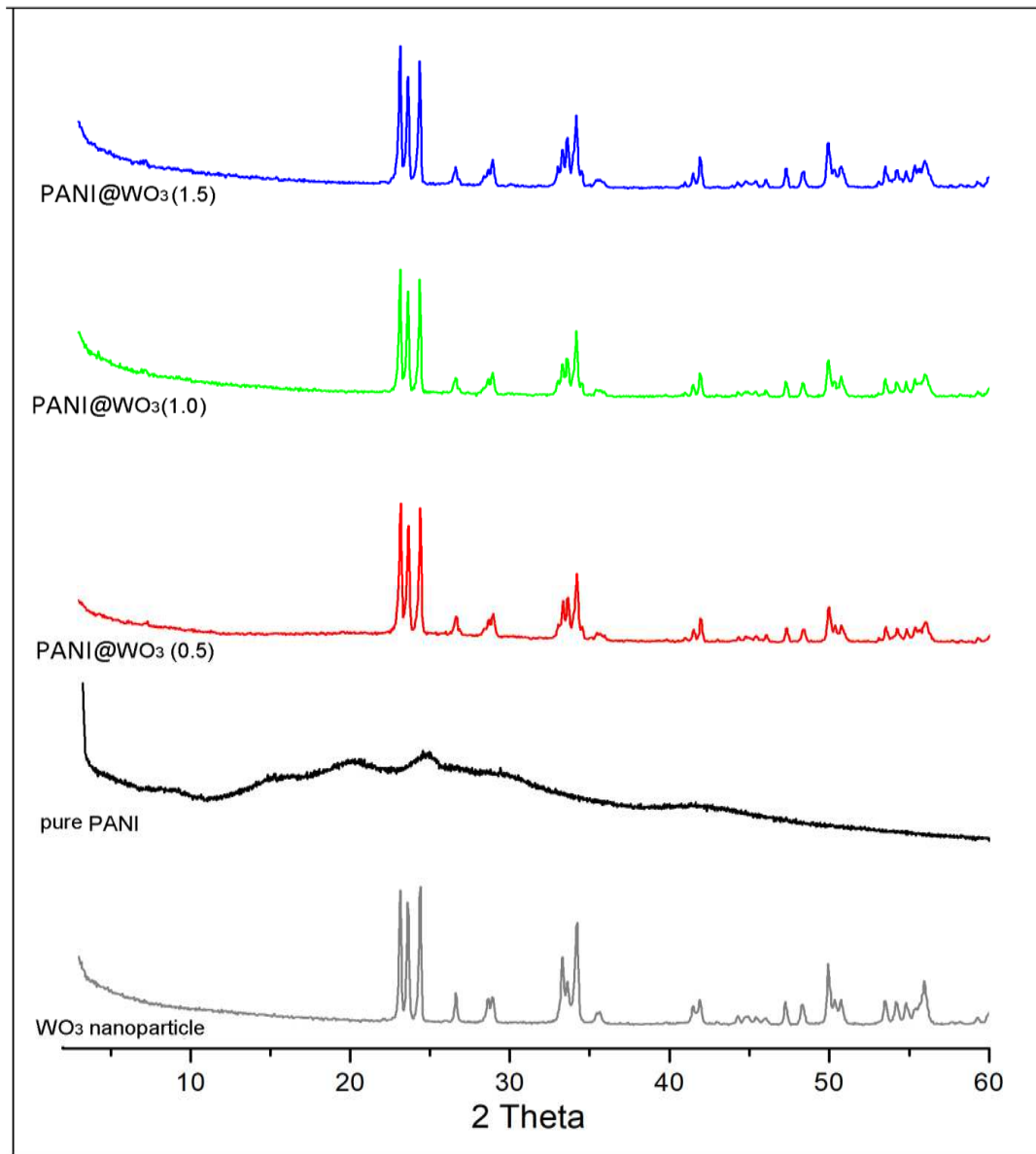


Figure III. 4. XRD patterns of pure PANI, WO₃ nanoparticle and three PANI/ WO₃ nanocomposites synthesized.

Table III.3. X-ray diffraction data with Bragg angle, *d*-spacing, FWHM and crystallite size of the main principal peak for WO₃ nanoparticles and nanocomposites.

Samples	Plane peaks	Braggs angle (2θ)	<i>d</i> -spacing (Å)	FWHM (2θ)	Size (nm)
WO ₃ nanoparticles	(002)	23.15	3.84	0.15	54.06
	(020)	23.62	3.76	0.17	47.74
	(200)	24.39	3.64	0.16	50.80
PANI/WO ₃ (0.5)	(002)	23.13	3.84	0.17	47.70
	(020)	23.61	3.76	0.20	40.58
	(200)	24.35	3.65	0.18	45.15
PANI/WO ₃ (1.0)	(002)	23.14	3.84	0.15	54.06
	(020)	23.64	3.76	0.18	45.09
	(200)	23.35	3.80	0.17	47.72
PANI/WO ₃ (1.5)	(002)	23.14	3.84	0.16	50.68
	(020)	23.61	3.76	0.19	42.71
	(200)	24.35	3.65	0.17	47.80

Finally, the value for the plane spacing (*d*-spacing) is determined from Bragg's law (eq. 1) [7, 8, 26].

$$d = \frac{\lambda}{2 \sin \theta} \quad (1)$$

where the average crystallite size (*D*) was determined from XRD data analysis is represented by θ based on the Debye-Scherrer law (eq. 2) [7,8,26].

$$D = \frac{k \cdot \lambda}{\beta \cdot \cos \theta} \quad (2)$$

with *D* : volume averaged crystallite size, *k* : Scherrer constant was considered as 0.9 in this context, β : size is line broadening at half of the maximum intensity (FWHM) in radian and λ : wavelength.

Besides, other XRD parameters such as *d*-spacing, Bragg angle, full width half maximum (FWHM) and crystalline size of the main principal peak for WO₃ nanoparticles with three PANI/WO₃ samples are presented in Table III.3. The crystallite size was found to be in the range from 40.58 to 54.06 nm.

III.2.3 FTIR spectroscopy

Figure III .5. shows FTIR absorption spectra of WO₃ nanoparticles, PANI, PANI/WO₃ (0.5), PANI/WO₃ (1.0) and PANI/WO₃ (1.5) registered in the range from 500 to 2500 cm⁻¹. The broad band appearing in the range 600-800 cm⁻¹ are describe of the various O–W–O stretching modes in the WO₃ crystal structure [27]. Likewise, the main absorption bands of the pure PANI, the band at 1637 cm⁻¹ correspond to C=N stretching vibrations for imine. The bands at 1586 and 1492 cm⁻¹ attributed to the C=C stretching of the quinoid ring and benzenoid ring, respectively. Those at 1309 and 1162 cm⁻¹ are assigned to the secondary aromatic amine C–N stretching vibrations. The peak at 824 cm⁻¹ is belong to the out-of-plane vibration of C–H on the 1,4-disubstituted ring. The peak at 1238 cm⁻¹ can be corresponding to various bending and stretching corresponds to C–C bond. These characteristic IR spectra of as-synthesized PANI are in excellent agreement with those obtained for PANI, suggesting the PANI formed [28].

Moreover, the all typical pure PANI absorption bands corresponds to C=N, C=C (quinoid ring and benzenoid ring), C–N, C–C and out-of-plane bending of C–H can be clearly seen in the three nanocomposite samples. Furthermore, It can be seen that the bands for C=N, C=C and C-N are all moved to lower wavenumbers due to strong interaction of WO₃ nanoparticle and PANI chain [5,8]. These results are agreed with those obtained by XPS study.

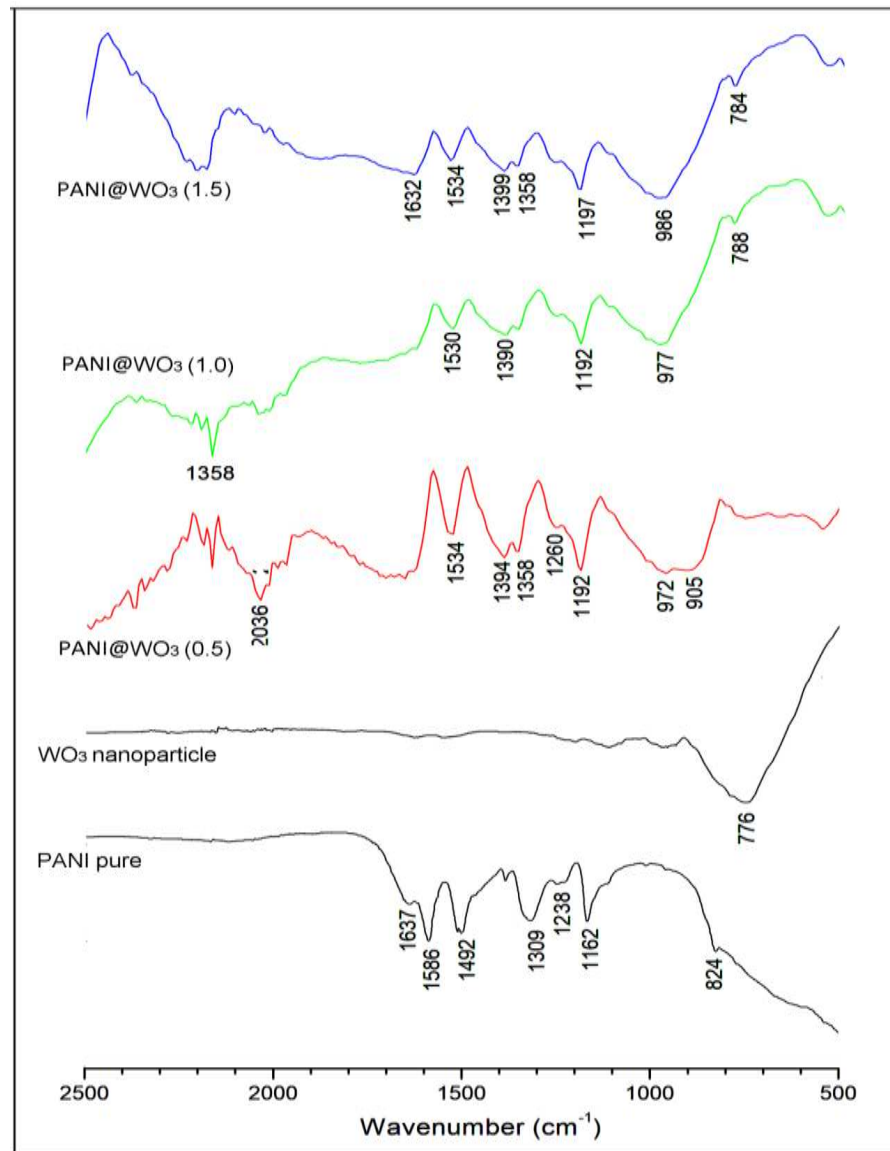


Figure III .5. FT-IR adsorption spectra of pure PANI, WO₃ nanoparticle and three PANI/ WO₃ nanocomposites synthesized.

III.2.4. Optical properties

For examine optic advantages of synthesized samples, UV–vis absorption spectrum was used out on materials. Figure III. 6. shows UV-vis spectra of hybrid materials synthesized solutions in DMSO, which were tested directly after dissolution. The pure PANI shows two absorption bands characteristic, where a acute peak at 334 nm and broad absorption peak at 567 nm appear, corresponds to $\pi-\pi^*$ transitions centered on the benzenoid and quinoid units,

respectively. Furthermore, the three nanocomposites show two characteristic absorption broad band peaks that belong to $\pi-\pi^*$ transition within the benzenoid units and $n-\pi^*$ indicates an aromatic ring transformation from a benzenoid to a more quinoid, respectively (Table 3) [29].

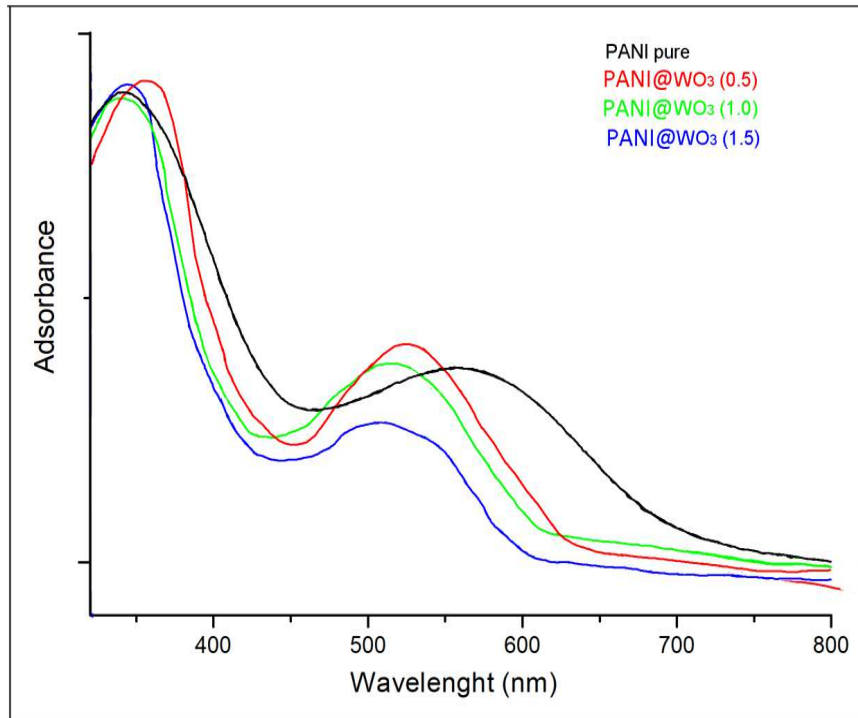


Figure III. 6. UV-vis spectra of pure PANI and three PANI/ WO₃ samples dispersed in DMSO

Table III.4. UV-vis absorption spectra properties (λ_1 , λ_2 and λ_{onset}) optical band gap energy (E_g) of PANI/WO₃ nanocomposites.

Samples	λ_1 (nm)	λ_2 (nm)	λ_{onset} (nm)	E_g (eV)
Pure PANI	342	560	741	1.67
PANI/WO ₃ (0.5)	351	525	659	1.88
PANI/WO ₃ (1.0)	343	520	648	1.91
PANI/WO ₃ (1.5)	345	517	624	1.98

It has been observed that the acute of UV–vis spectra of three samples are analogous to those of pure PANI and some moving in the bands is observed can be caused by the interaction between the aromatic polyaniline chains and WO₃ nanoparticle. Likewise, the content of WO₃

was increased in the polyaniline matrix, there shows slightly red shifted. So, the optical band gap is found depending upon the composition of hybrid materials [30].

The optical band gap of the samples was calculated from stronger relative intensity of absorption peak in the long wavelength in the Einstein formula (eq. 3) [31], the results are

abstracted in Table III.4.

$$E_g = \frac{h.c}{\lambda_{onset}} \quad (3)$$

where E_g : band gap energy ; $h = 4.14 \times 10^{-15}$ eVs ; $c = 2.99 \times 10^8$ ms⁻¹ ; λ_{onset} : wavelength at maximum absorbance.

The optical band gap of the pure PANI, PANI/ WO₃ (0.5), PANI/ WO₃ (1.0) and PANI/ WO₃ (1.5) is 1.67 eV, 1.88 eV, 1.91 eV and 1.98 eV, respectively. So, the optical characteristics of samples are mainly determined by the highest occupied molecular orbital (HOMO) and the lowest unoccupied molecular orbital (LUMO). Generally, the band gap will increase with increasing the WO₃ content into PANI matrix is belong to the destabilization of the HOMO than of the LUMO through nanoparticle replacement. In addition, augmentation in the values of optical energy gap of samples may be interpreted in terms of polymer changing structures due to types of bonds formed between the WO₃ and PANI chains [32].

III.2.5. TGA analysis

The TGA were useful to describe the thermal behavior of the samples nanocomposite, as shown in Figure III. 7. A minor mass loss (~0.98 %) was detected when heating the WO₃ up to ca. 900°C. This result showed a very good thermal stability of nanoparticle. However, the pure PANI shows three degradation steps [5-7], where the first mass loss step of 5.63% due to the volatilization of water molecules at 140°C, and the second one of 47.69% related to

degradation of the polymers chain between 140-450°C. The final step of weight loss at around may be due to the final carbonization of material at 450-700°C (12.97% mass loss). Also, three-step weight loss was observed of nanocomposites synthesized. The first weight loss (1.58-4.33%) below 130°C is due to evaporation of adsorbed water and the second heating step begin around 160°C to 580°C was due to the thermochemical decomposition of the organic materials (6.34-19.22%). Finally, the third weight loss step between 580-900°C assigned to the thermal degradation of nanocomposite molecules (9.29-16.05%). So, addition of WO₃ nanoparticles to the PANI shows a significant effect on the thermal stability for hybrid materials. Furthermore, this overall confirms that the PANI amount formation onto the nanoparticle significantly increases in the order PANI/ WO₃ (1.5) < PANI/ WO₃ (1.0) < PANI/ WO₃ (0.5). Besides, these results were in good approval with those obtained through analysis of XPS analysis.

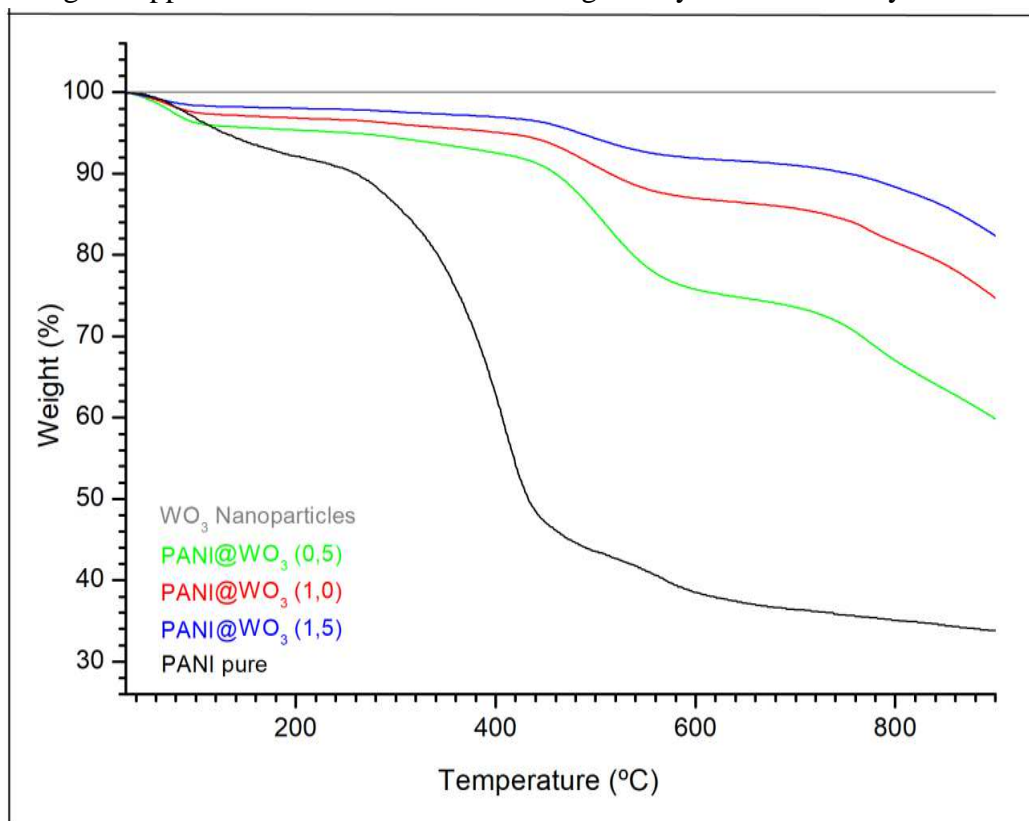


Figure III. 7. Thermogravimetric analysis of pure PANI, WO₃ nanoparticle and three PANI/WO₃ nanocomposites obtained in N₂ atmosphere at 10 °C.min⁻¹

Morphology of PANI/ WO₃ nanocomposites

Figure III. 8. represents the Scanning Electron Microscopy (SEM) images of all PANI/ WO₃ nanocomposites. The structure and morphology view of the PANI/ WO₃ (0.5) observed that nanoparticles are surrounded by PANI matrix and hence it appears as a dense top layer (almost invisible pores), which covers nearly the section of the nanoparticles. Likewise, in the PANI/ WO₃ (1.0), the structure observed by SEM shows a clear evolution of morphology according to the PANI chain. On the contrary, for PANI/ WO₃ (1.5), there appears to be little change in the thickness of the nanocomposite was observed.

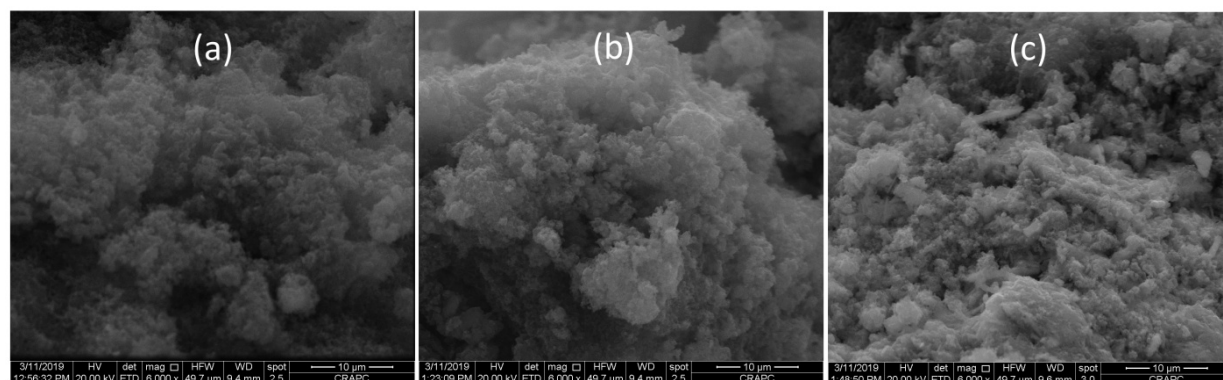


Figure III. 8. SEM image of nanocomposites prepared for (a) PANI/ WO₃ (0.5) ; (b) PANI/ WO₃ (1.0) ; (c) PANI/ WO₃ (1.5).

III.2.6. Electrochemical Analysis

Among the electrochemical analysis methods, the cyclic voltammetry (CV) became a significant and broadly applied electroanalytical method in numerous field of chemistry. It is vastly used to examine a diversity of redox processes. The CV was used to study the electrochemical stability of the pure PANI and PANI/WO₃ samples prepared (Figure III. 9). The pure PANI shows two typical redox peaks, the first redox peak appearing between

0.46/0.29V is the oxidation leucoemeraldine to leucoemeraldine radical cation with the peak-to-peak potential separation (ΔE_p) was 170 mV, whereas that the second redox peak is the emeraldine radical cation to emeraldine and the third redox peak at 0.89/0.81V is the transformation of the pernigraniline radical cation to pernigraniline with $\Delta E_p = 80$ mV (Table 4). Furthermore, the CV of the two PANI/WO₃ (0.5 and 1.0) samples present also the two redox pair characteristics of PANI, but the redox processes promotes a slight displacement in the E_{pa} and E_{pc} of both peaks as compared with pure polymer (Table III. 4). This behavior can be attributed to the intercalation of the PANI with WO₃, whereas that the difference in the CV curves shows that there is variation in the chain structure. Moreover, a poor definition of redox peaks of PANI/WO₃ (1.5) nanocomposite was observed, this behavior was interpreted as a strong interaction between the polymeric matrix and the incorporated nanoparticles.

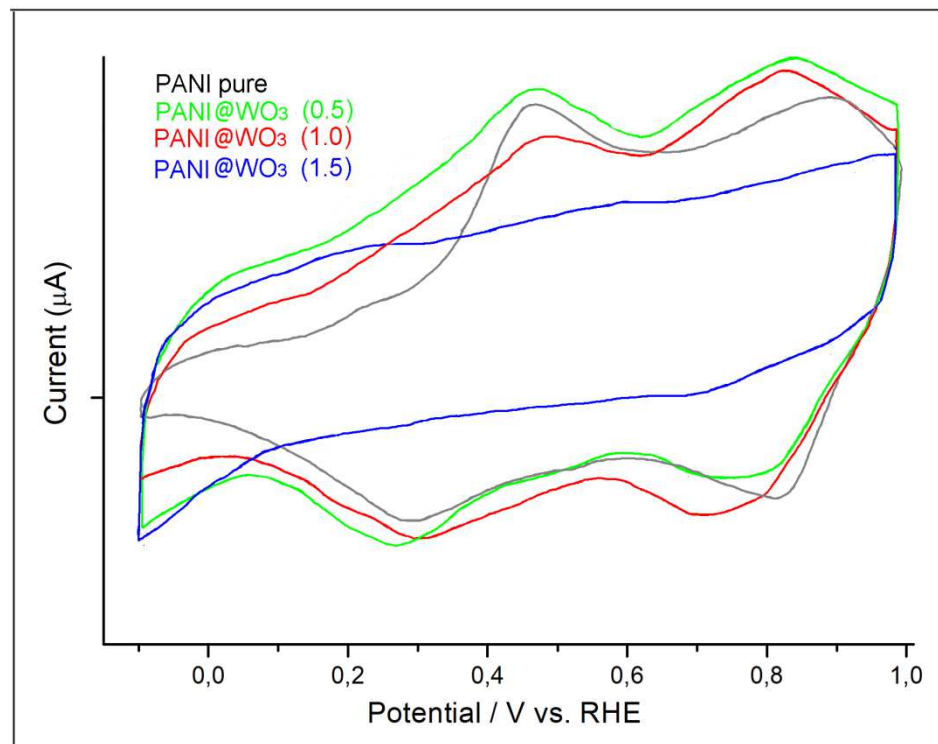


Figure III. 9. Stabilized cyclic voltammograms recorded for a graphite carbon electrode covered by pure PANI

Table III.5. Electrochemical parameters obtained from CVs of pure PANI and PANI/WO₃ nanocomposites on glassy carbon electrode in 1M HClO₄ solution at scan rate 50 mV.s⁻¹.

Samples	Potential / V					
	A_1/C_1	$E_{1/2}$	ΔE_p	A_2/C_2	$E_{1/2}$	ΔE_p
Pure PANI	0.46/0.29	0.375	0.17	0.89/0.81	0.85	0.08
PANI/WO ₃ (0.5)	0.48/0.24	0.36	0.24	0.84/0.77	0.805	0.07
PANI/WO ₃ (1.0)	0.49/0.31	0.40	0.18	0.82/0.71	0.765	0.11
PANI/WO ₃ (1.5)	//	//	//	//	//	//

Abbreviations: A : potential of anodic peak; C : potential of cathodic peak; ΔE_p : the peak-to-peak potential separation; $E_{1/2}$: half-wave potential.

III.3. Conclusions

Novel nanocomposites formed from WO₃ nanoparticles and the conducting form of PANI was successfully obtained by chemical oxidative method in the presence of ammonium persulfate as an oxidant. The synthesis of PANI/WO₃ nanocomposites were confirmed by means of XPS, FTIR, XRD, SEM and UV-vis spectroscopies.

The FTIR technique confirmed the presence of PANI with WO₃ nanoparticle and provided clear evidence regarding the development of new hybrid materials. Moreover, the XPS analysis indicated the details of comprising elements contributing to the synthesis of PANI/WO₃ samples. In addition, the XRD patterns studies confirmed the increase of crystalline portion in the nanocomposites upon that addition of WO₃ nanoparticle for PANI matrix. Observation of the samples by SEM showed dispersion homogeneity of the PANI chain at nanoparticle. The optical band gap of materials found to increase with the content of WO₃. Furthermore, the TGA results demonstrated a change in the thermal performance of the PANI by the presence of WO₃ nanoparticles. Further, the electrochemical properties were

investigated with cyclic voltammetry, the PANI/WO₃ (0.5) and PANI/WO₃ (1.0) samples have excellent electroactivity properties suggesting their potential application in the electrode

III.4. References

- [1] Benykhlef S, Bekhoukh A, Berenguer R, Benyoucef A, Morallon E (2016) PANI-derived polymer/Al₂O₃ nanocomposites: Synthesis, characterization and electrochemical studies. *Colloid and Polymer Science*. 294:1877-1885
- [2] Bekhoukh A, Zehhaf A, Benyoucef A, Bousalem S, Belbachir M (2017) Nanoparticles Mass Effect of ZnO on the Properties of Poly(4-Chloroaniline)/Zinc Oxide Nanocomposites. *Journal of Inorganic and Organometallic Polymers and Materials*. 27:13-20.
- [3] Chouli F, Radja I, Morallon E, Benyoucef A (2017) A Novel Conducting Nanocomposite Obtained by p-Anisidine and Aniline With Titanium(IV) Oxide Nanoparticles: Synthesis, Characterization, and Electrochemical Properties. *Polymer Composites*. 38:254-260.
- [4] Benyakhou S, Belmokhtar A, Zehhaf A, Benyoucef A (2017) Development of novel hybrid materials based on poly(2-Aminophenyl disulfide)/Silica Gel : preparation, characterization and electrochemical studies. *Journal of Molecular Structure* 1150:580-585.
- [5] Daikh S, Zeggai FZ, Bellil A, Benyoucef A (2018) Chemical polymerization, characterization and electrochemical studies of PANI/ZnO doped with hydrochloric acid and/or zinc chloride: Differences between the synthesized nanocomposites. *Journal of Physics and Chemistry of Solids*. 121:78-84.
- [6] Yamani K, Berenguer R, Benyoucef A, Morallón E (2019) Preparation of polypyrrole (PPy)-derived polymer/ZrO₂ nanocomposites: effects of nanoparticles interface and polymer structure. *Journal of Thermal Analysis and Calorimetry*. 135:2089-2100.
- [7] Kouidri FZ, Berenguer R, Benyoucef A, Morallon E (2019) Tailoring the properties of polyanilines/SiC nanocomposites by engineering monomer and chain substituents. *Journal of Molecular Structure*. 1188:121-128.

- [8] Bousalem S, Zeggai FZ, Baltach H, Benyoucef A (2020) Physical and electrochemical investigations on hybrid materials synthesized by polyaniline with various amounts of ZnO nanoparticle. *Chemical Physics Letters*. 741:137095.
- [9] Ouis D, Zeggai FZ, Belmokhtar A, Benyoucef A, Meddah B, Bachari K (2020) Role of p-Benzoquinone on Chemically Synthesized Nanocomposites by Polyaniline with V₂O₅ Nanoparticle. *Journal of Inorganic and Organometallic Polymers and Materials*. doi.org/10.1007/s10904-020-01508-7.
- [10] Dirican M, Yanilmaz M, Asiri AM, Zhang X (2020) Polyaniline/MnO₂/porous carbon nanofiber electrodes for supercapacitors. *Journal of Electroanalytical Chemistry*. 861:113995
- [11] Fayemi OE, Adekunle AS, Swamy BEK, Ebenso EE (2018) Electrochemical sensor for the detection of dopamine in real samples using polyaniline/NiO, ZnO, and Fe₃O₄ nanocomposites on glassy carbon electrode. *Journal of Electroanalytical Chemistry*. 818:236-249.
- [12] Wei H, Yan X, Wu S, Luo Z, Wei S, Guo Z (2012) Electropolymerized Polyaniline Stabilized Tungsten Oxide Nanocomposite Films: Electrochromic Behavior and Electrochemical Energy Storage. *J. Phys. Chem. C*. 116:25052-25064.
- [13] Zhang J, Wang XL, Xia XH, Gu CD, Zhao ZJ, Tu JP (2010) Enhanced electrochromic performance of macroporous WO₃ films formed by anodic oxidation of DC-sputtered tungsten layers. *Electrochimica Acta*. 55:6953-6958.
- [14] Balaji S, Djaoued Y, Albert AS, Brüning R, Beaudoinc N, Robichaud J (2011) Porous orthorhombic tungsten oxide thin films: synthesis, characterization, and application in electrochromic and photochromic devices. *Journal of Materials Chemistry*. 21:3940-3948.
- [15] Hosseini MG, Sefidi PY, Mert AM, Kinayyigit S (2020) Investigation of solar-induced photoelectrochemical water splitting and photocatalytic dye removal activities of camphor

sulfonic acid doped polyaniline-WO₃-MWCNT ternary nanocomposite. *Journal of Materials Science & Technology*. 38:7-18.

[16] Zhang R, Ning F, Xu S, Zhou L, Shao M, Wei M (2018) Oxygen vacancy engineering of WO₃ toward largely enhanced photoelectrochemical water splitting. *Electrochimica Acta*. 274:217-223.

[17] Wang SH, Shen CY, Su JM, Chang SW (2015) A room temperature nitric oxide gas sensor based on a copper-ion-doped polyaniline/tungsten oxide nanocomposite, *Sensors*. 15:7084-7095.

[18] Yuksel R, Durucan C, E.Unalan H (2016) Ternary nanocomposite SWNT/WO₃/PANI thin film electrodes for supercapacitors, *Journal of Alloys and Compounds*. 658:183-189.

[19] Kumar R, Yadav BC (2016) Fabrication of Polyaniline (PANI)-Tungsten oxide (WO₃) Composite for Humidity Sensing Application. *Journal of Inorganic and Organometallic Polymers and Materials*. 26:1421-1427.

[20] Eren E, Alver C, Karaca GY, Uygunb E, Oksuz AU (2018) Enhanced electrochromic performance of WO₃ hybrids using polymer plasma hybridization process, *Synthetic Metals* 235:115-124.

[21] Asim N, Syuhami MF, Badiei M, Yarmo MA (2014) WO₃ Modification by Synthesis of Nanocomposites, *APCBEE Procedia*. 9:175-180.

[22] Qaiser AA, Hyland MM, Patterson DA (2012) Effects of various polymerization techniques on PANI deposition at the surface of cellulose ester microporous membranes: XPS and electrical conductivity studies. *Synthetic Metals*. 162:958-967

[23] Lia M, Zhou S (2018) α -Fe₂O₃/polyaniline nanocomposites as an effective catalyst for improving the electrochemical performance of microbial fuel cell. *Chemical Engineering Journal*. 339:539-546.

- [24] Sanches EA, da Silva JMS, Ferreira JMO, Soares JC, dos Santos AL, Trovati G, Fernandes EGR, Mascarenhas YP (2014) Nanostructured Polyaniline Emeraldine-base form (EB-PANI): a structural investigation for different neutralization times. *Journal of Molecular Structure*. 1074:732-737.
- [25] Tzou K, Gregory RV (1993) A method to prepare soluble polyaniline salt solutions-in situ doping of PANI base with organic dopants in polar solvents. *Synthetic Metals*. 53:365-377.
- [26] Khayet M, García-Payo MC (2009) X-Ray diffraction study of polyethersulfone polymer, flat sheet and hollow fibers prepared from the same under different gas-gaps, *Desalination*. 245:494-500.
- [27] Ingham B, Chong SV, Tallon JL (2005) Layered tungsten oxide-based Organic-Inorganic hybrid materials: an Infrared and Raman study,” *Journal of Physical Chemistry B*. 109:4936-4940.
- [28] Manuel J, Salguero T, Ramasamy RP (2019) Synthesis and characterization of polyaniline nanofibers as cathode active material for sodium-ion battery. *Journal of Applied Electrochemistry*. 49:529-537.
- [29] Khanna PK, Singh N, Charan S, Visawanath AK (2005) Synthesis of Ag/polyaniline nanocomposite via an in situ photo-redox mechanism. *Materials Chemistry and Physics*. 92:214-219.
- [30] Irimpan L, Nampoorei VPN, Radhakrishnan P (2008) Spectral and nonlinear optical characteristics of nanocomposites of ZnO-CdS, *Journal of Applied Physics*. 103:094914-094918.

[31] Segets D, Gradl J, Taylor RK, Vassilev V, Peukert W (2009) Analysis of optical absorbance spectra for the determination of ZnO nanoparticle size distribution, solubility, and surface energy. *ACS Nano*. 3:1703-1710.

[32] Ebrahim S, Kashyout AH, Soliman M (2009) Ac and Dc conductivities of polyaniline/poly vinyl formal blend films. *Current Applied Physics*. 9:448-454.

CHAPTER IV
PANI/Al₂O₃
Aluminium oxide

IV.1. Introduction

A wide variety of nanoparticles have been studied with the aim of improving polymers for their applications, alumina Al₂O₃ or aluminium oxide is an amphoteric oxide that exists in nature as the minerals corundum Al₂O₃; diasporite (Al₂O₃.H₂O); gibbsite (Al₂O₃.3H₂O) and most commonly as boehmite, which is an impure form of gibbsite [1], among the different metal oxide NPs, alumina NPs have a range of useful properties, including good thermal conductivity, high strength and stiffness, mechanical strength, inertness to most oxides and alkalis, high adsorption capacity, wear resistance, oxidation, thermal stability and electrical insulation and so on, in addition, it is inexpensive, non-toxic and highly abrasive [2-4], due to physicochemical properties many studies propose Al₂O₃ NPs with great potential to fit targeted application in the field of the pigment porous ceramic membranes, catalysts or catalyst carriers ultrafiltration membranes, electrical insulation, high voltage insulators, fiber tubes, ballistic armor, abrasion resistant tube and thermometry sensors.

Polyaniline (PANI) has been recognized to be the most important conducting polymers, although it has exhibited great potential for commercial application due to its unique electrical, optical and photoelectrical properties as well as its ease of preparation and excellent environmental stability [5-9], its mechanical properties don't meet the requirement of a number of applications because PANI is neither soluble in common solvent nor thermally processable. Therefore, researchers have attempted to prepare PANI blends or composites of improved processability and mechanical properties while maintaining the inherent electroactive properties of the polymer [1].

So the potential use of such material as reinforcing component may result in increasing its commercial value besides giving a purpose for this by-product, in this paper, synthesis of

conducting polymer nanocomposite based on alumina and PANI is reported , the influence of prepared nanosized Al₂O₃ content on the morphology, thermal stability , electric and dielectric properties of resulting nanocomposites are also investigated .

Table IV.1. the conditions and yeild of our synthesis

<i>Products</i>	<i>Conditions</i>	<i>Dopant</i>	<i>yeild</i>	<i>Time</i>	<i>Temperature</i> (°C)	<i>Mole fraction</i>
Polymer/Al ₂ O ₃		HCl	86,92%,	24 h	5 For The first 3 ^h From the reaction	monomer: oxydant 1 :1

IV.2 Results and discussion

IV.2.1. X-ray photoelectron spectroscopy (XPS)

The nanocomposites were examined by XPS. Figure IV.1 shows the full scanning spectrum in the range from 0 at 1300 eV and the atomic composition of carbon (C), nitrogen (N), oxygen (O) and aluminum (Al) in nanocomposites synthetized (Table IV.1).

Table IV.2. Summary of the XPS binding energy values (eV) obtained for nanocomposites: (A) Al₂O₃ nanoparticles, (B) PANI/Al₂O₃ (2%) and (C) PANI/Al₂O₃ (4%).

Elements	Samples & Binding Energy/eV			Remarks
	(A)	(B)	(C)	
Al2p	74	//	//	Al-O
Al2s	117	//	//	Al metal
C1s	//	284.61	284.55	C-C, C=C, C-H
	//	285.63	285.64	C-N
	//	287.07	287.05	C=N
	//	289.05	288.90	C=O
N1s	//	398.20	398.26	Imine =N-
	//	399.46	399.53	Amine -NH-, -NC-
	//	//	401.00	-N ⁺ H-, =N ⁺ -
O1s	527.65	531.26	531.47	Al ₂ O ₃
	528.98	532.72	533.60	Hydroxides
	530.09	534.38	534.88	Carbonates

In Al₂O₃ nanoparticles, the core level binding energies of the Al₂O₃ spectrum shows into the clear two peaks at 74 eV and 117 eV which are ascribed to Al2p and Al2s species, respectively.

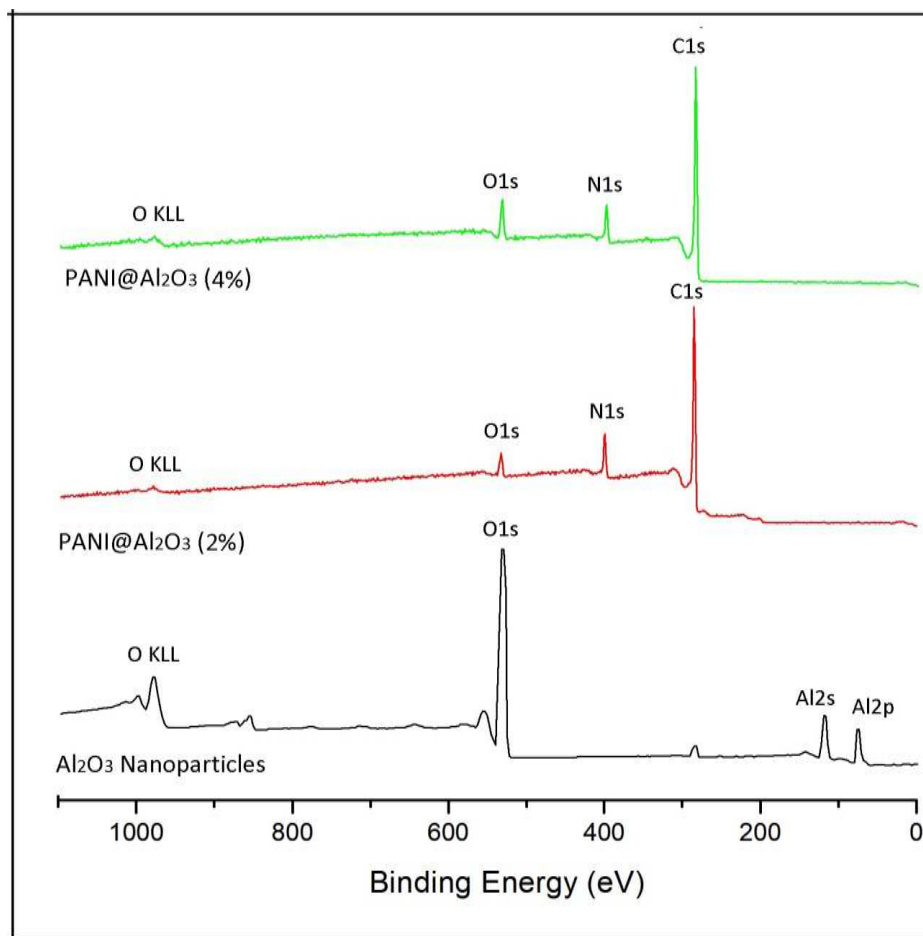


Figure IV. 1. XPS spectra (survey scan) of Al₂O₃ and PANI/Al₂O₃ samples.

The C1s signal for PANI/Al₂O₃ (2%) can be resolved into four bonding environments (Figure IV. 2).

The lowest binding energy state at 284.61 eV (40.31%) with a FWHM (full width at half maximum) of 1.50 eV corresponds to C–C, C=C and C–H bonds. The second at 285.63 eV (31.16%) with a FWHM of 1.67 eV can be assigned to neutral C–N bonds, that corresponding to the carbons bonded to neutral amine and imine nitrogens (Table IV. 1). The third, at 287.07 eV (9.61%) with a FWHM of 1.92 eV is bound to the cation radical nitrogen, while the highest energy state at 289.05 eV (3.64%) with a FWHM of 1.92 eV is given to C=O bond. Similar

C1s binding energy values are reported in the literature [12, 13]. In addition, the formation of PANI/Al₂O₃ (4%) further confirmed by C1s spectrum presenting at 284.55 eV (38.86% and FWHM is 1.64 eV), 285.64 eV (31.18% and FWHM is 1.69 eV), 287.05 (78.74% and FWHM is 1.67 eV) and 288.90 eV (24.01% and FWHM is 1.75 eV) attributed to C–C, C–N, C=N and C=O, respectively; that corresponds to formation of PANI chains.

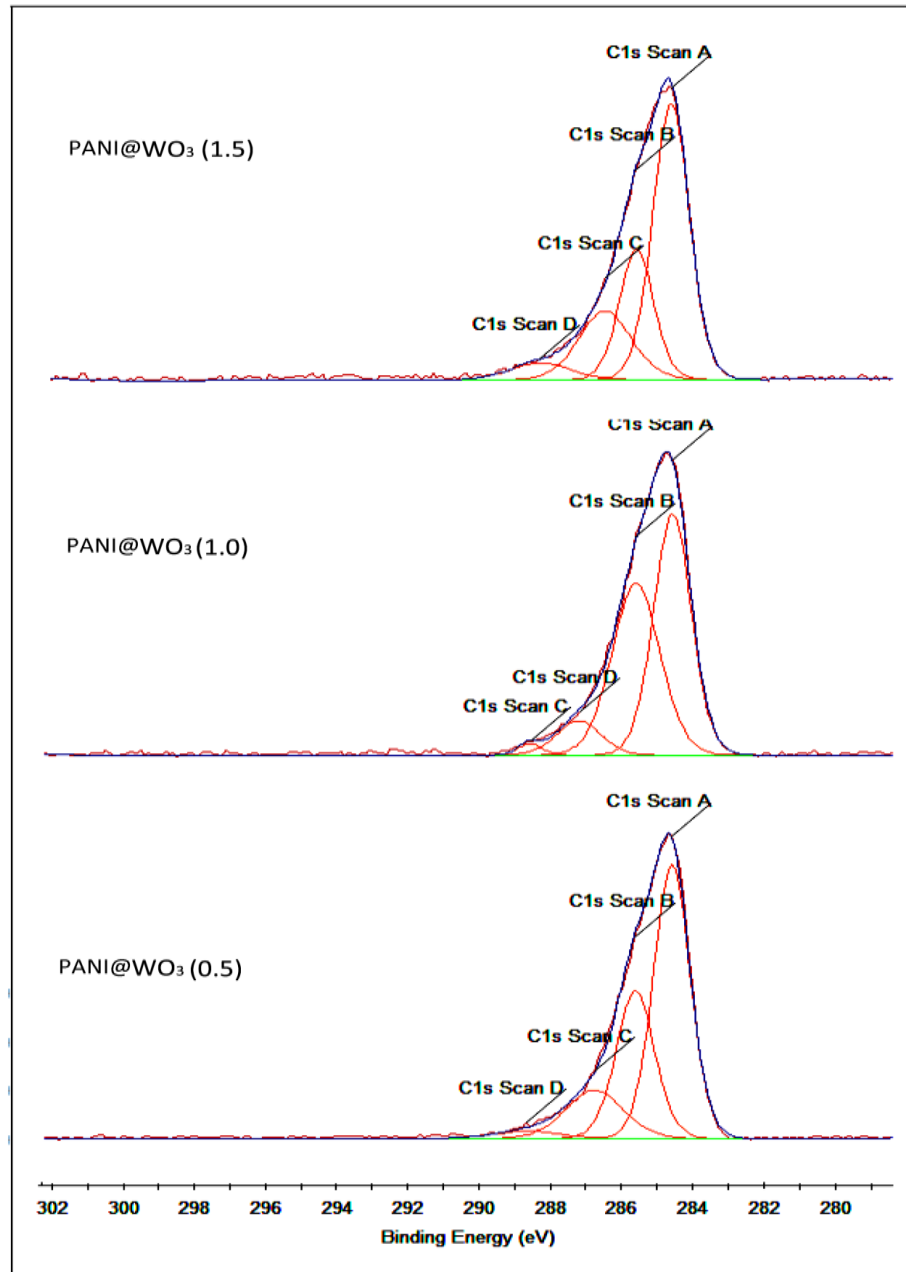


Figure IV. 2. XPS spectra C1s of three PANI/Al₂O₃ nanocomposites synthesized.

Furthermore, the intensity report C–C/C–N is helpful in study the existence of crosslinking in the nanocomposites under studied as a measurement of cross linking grade PANI/Al₂O₃ (4%) demonstrated the highest C–C/C–N ratio of 2.3 (Table 1), which is the degree related with no crosslinking. Also, the crosslinking value of 1.8 for PANI/Al₂O₃ (6%) shows some important level of crosslinking, while the PANI/Al₂O₃ (2%) degree of 1.1 explains the common ratio for highly crosslinked nanomaterials, although these are merely semi quantitative measures.

The fitting data for the N1s spectra of all nanocomposites synthesized are presented in Figure IV. 3.

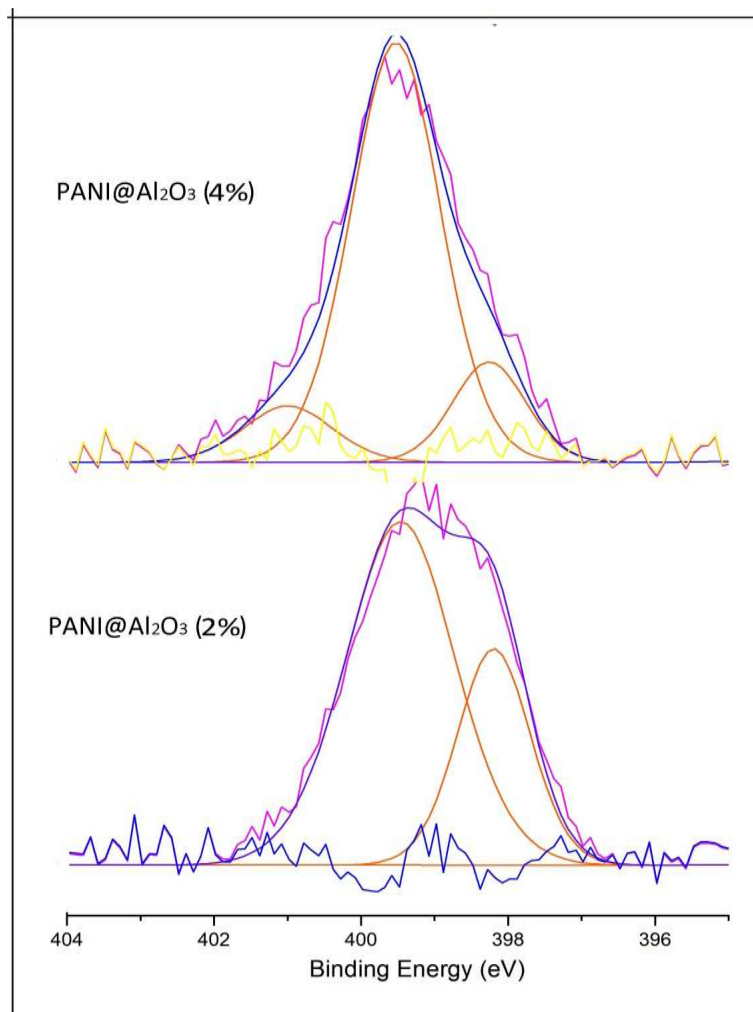


Figure IV. 3. XPS spectra N1s of three PANI/Al₂O₃ nanocomposites synthesized.

its deconvolution leads three main components (Table IV. 1). The lowest binding energy peak which is concerning to the imine like structure (=N-) can be utilized to evaluate the degree of defects within the PANI, because the structure is considered to interrupt the electron jumping on the polymer chains. The second, higher energy state is owing to the neutral and amine-like structure (-NH-), while the highest energy state is due to the protonated amine units. (-NH⁺-) [12]. The doping level was calculated from the ratio of the area of the highest binding energy peak to the total area of the N1s peak, and the defect density from the ratio of the area of the lowest binding energy peak to the total area. The doping level of PANI in PANI/Al₂O₃ (2%) is 0.57 and the degree of defects is only 0.24, while, the doping level of PANI/Al₂O₃ (4%) is 0.75 and the density of defects is up to 0.10. The PANI/Al₂O₃ (4%) has a higher doping degree and lower defect density, which probably results in its higher capacitance and faster charging discharging rate. So, the different value of the N1s spectra suggests that these three samples have dissimilar distribution of N1 species, in other words, different doping states.

Table IV.3. Doping degree and defect density in different PANI nanostructures

Sample	$[N^+/N]^b$ (doping degree)	$[=N-/N]^c$ (defect density)
PANI/WO ₃ (0.5)	0.57	0.24
PANI/WO ₃ (1.0)	0.75	0.10

IV.2.2. X-ray diffraction

Figure IV. 4. shown the diffraction peaks of crystalline Al₂O₃ and nanocomposites, along different planes. XRD patterns of pure PANI exhibit loss of crystallinity. The peaks located at 2θ values 9.59°, 15.47°, 20.23° and 24.76° are in agreement with those reported by Sanches

[13]. In addition, the peaks at 2θ values 25.54° , 35.10° , 37.73° , 43.34° , 52.51° , 57.50° , 61.33° , 66.44° and 68.18° correspond to (012), (104), (110), (113), (024), (116), (018), (214) and (300) reflections of Al₂O₃ nanoparticle (JCPDS no. 001-1243). In a similar way, the diffraction peaks in three samples synthesized are slightly shifted to lower angle (see Table IV. 2) due to the interaction between PANI chain and Al₂O₃ [10,14-18].

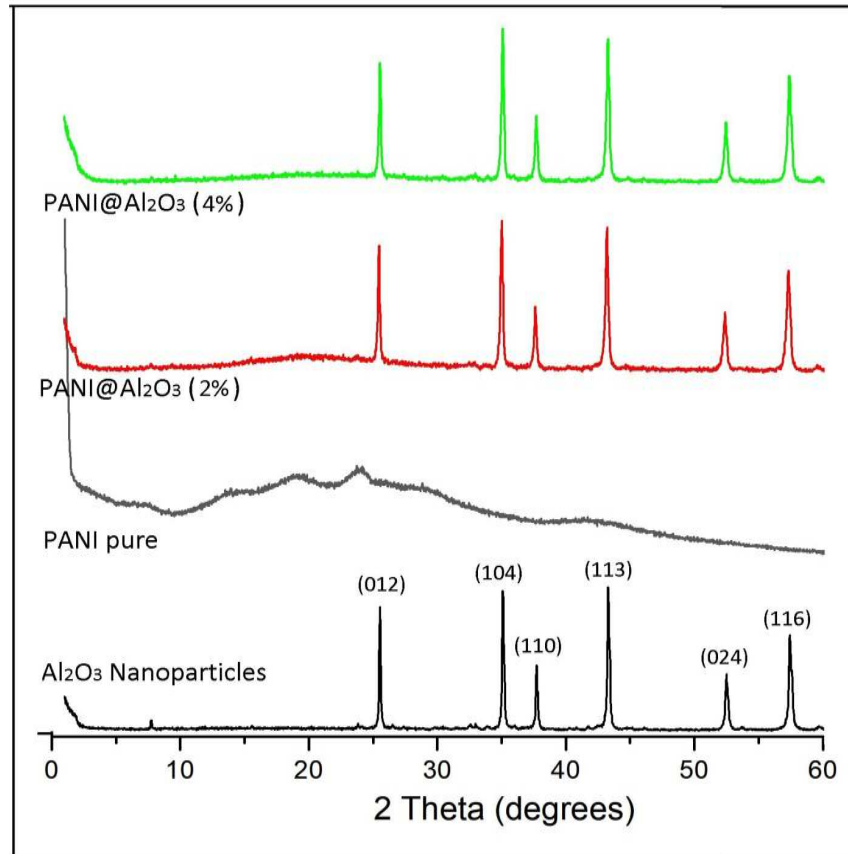


Figure IV. 4. XRD patterns of pure PANI, Al₂O₃ nanoparticle and PANI/Al₂O₃ nanocomposites synthesized.

Finally, the interplanar distances (d-space) were determined through Bragg formula (eq. 1) [19-21].

$$d = \frac{\lambda}{2 \sin \theta} \quad (1)$$

where the diffraction angle is represented by θ . The crystalline size (D) was calculated through Scherrer formula (eq. 2) [19-21].

$$D = \frac{k \cdot \lambda}{\beta \cdot \cos \theta} \quad (2)$$

The k is Scherrer constant, was considered as 0.9 in this work. β is the line broadening value at half of the maximum intensity (FWHM), which is expressed as $\Delta 2\theta$ in radians.

Besides, other XRD parameters such as Bragg angle, d-spacing, full width half maximum (FWHM) and crystallite size of the main principal peak for Al₂O₃ nanoparticles and three PANI/Al₂O₃ samples are presented in Table IV.2. The crystallite size was found to be in the range from 39.66 to 49.36 nm.

Table IV.4. XRD data and calculated particle sizes for Al₂O₃ nanoparticles and nanocomposites

Compounds	Plane peaks	Braggs angle 2θ	d -spacing Å	F.W.H.M 2θ	Size nm
Al ₂ O ₃ nanoparticles	(104)	35.10	3.08	0.17	48.99
	(110)	37.73	2.38	0.17	49.36
PANI/Al ₂ O ₃ (2%)	(104)	35.08	2.55	0.21	39.66
	(110)	37.71	2.38	0.21	39.96
PANI/Al ₂ O ₃ (4%)	(104)	35.16	2.55	0.20	41.66
	(110)	37.77	2.38	0.21	39.96

IV. 2.3. FT-IR spectroscopy

Figure IV.5. shows the FTIR absorption spectra of Al₂O₃ nanoparticles, pure PANI, PANI/Al₂O₃ (2%) and PANI/Al₂O₃ (4%) recorded in the range from 500 to 2000 cm⁻¹. The two characteristic peaks at 553 cm⁻¹ and 635 cm⁻¹ due to Al–O stretching vibrations in the Al₂O₃

crystal lattice [22]. Also, the main absorption bands of the pure PANI, the peak at 1637 cm⁻¹ correspond to C=N stretching mode for imine. The bands at 1586 and 1492 cm⁻¹ be attributed to the C=C stretching of the quinoid/benzenoid ring, respectively. The bands at 1309 and 1162 cm⁻¹ are ascribed to C-N stretching of the secondary aromatic amine. This at 824 cm⁻¹ is belonging to the out-of-plane bending of C-H on the para-disubstituted ring. These typical bands of as-synthesized PANI are in good accord with those registered for PANI, confirming the formation of PANI chains [23].

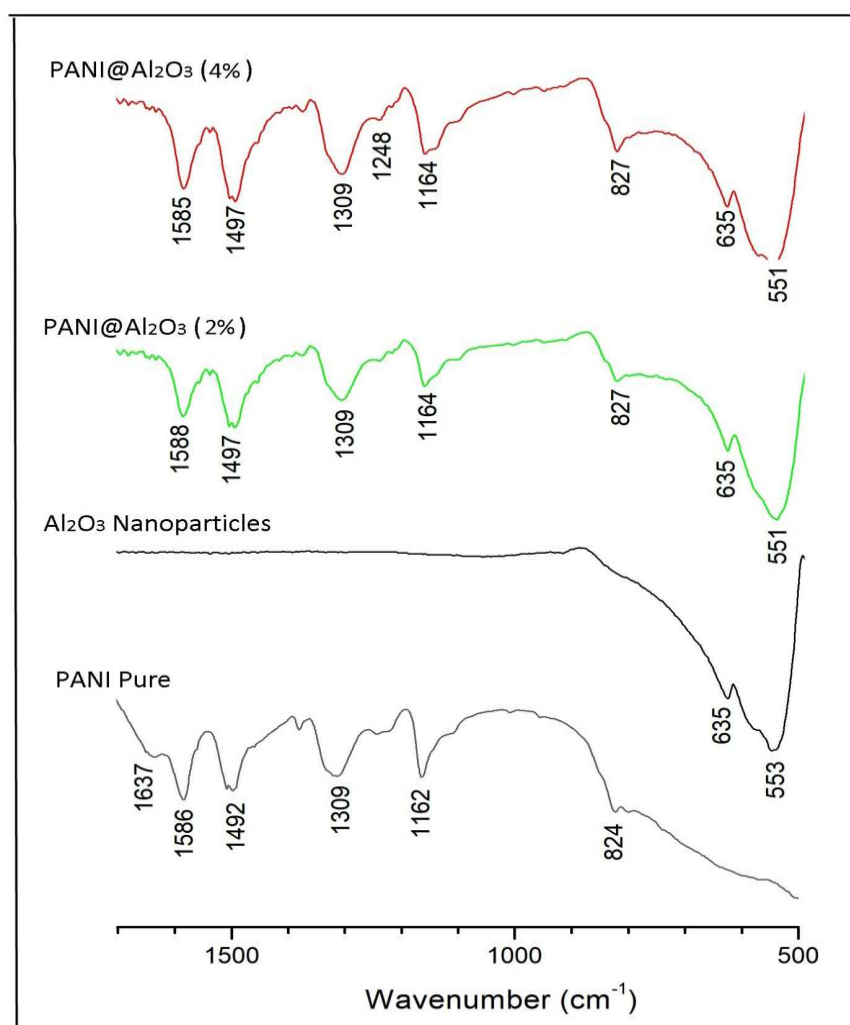


Figure IV. 5. FTIR spectra of pure PANI, Al₂O₃ nanoparticle and three PANI/Al₂O₃ nanocomposites synthesized.

Moreover, the all typical pure PANI absorption bands corresponds to C=N, C=C (quinoid/benzenoid ring), C-N, C-C and out-of-plane bending of C-H can be clearly seen in the three nanocomposite samples. Furthermore, the characteristic stretching frequencies are shifted towards the lower frequency side in the composite when compared to pure pani ,The above peaks confirm the formation of the nanocomposite and also suggest an electrostatic kind of interaction between the polymeric chain and Al₂O₃ nanoparticle

IV.2.4. Optical characterization

Figure IV.6. shows the UV-vis spectra of nanocomposites prepared solutions in DMSO, which were tested directly after dissolution. The first peak at 335 nm is related to the $\pi-\pi^*$ transition of the benzenoid rings, and the second, at 625 nm is related to π -polaron transitions. Moreover, the three hybrid materials show two characteristic absorption broad band peaks that associated to $\pi-\pi^*$ transition and $n-\pi^*$ transition of benzenoid ring and of benzenoid to quinoid, respectively (Table IV.3) [24]. It has been found that the form of UV spectra of all samples are similar with some moving of nanocomposites bands. Further, It can be seen that the peaks red shift as Al₂O₃ content increases in PANI matrix. So, the optical properties of nanocomposites strongly depend on composition of PANI/Al₂O₃ sample [25].

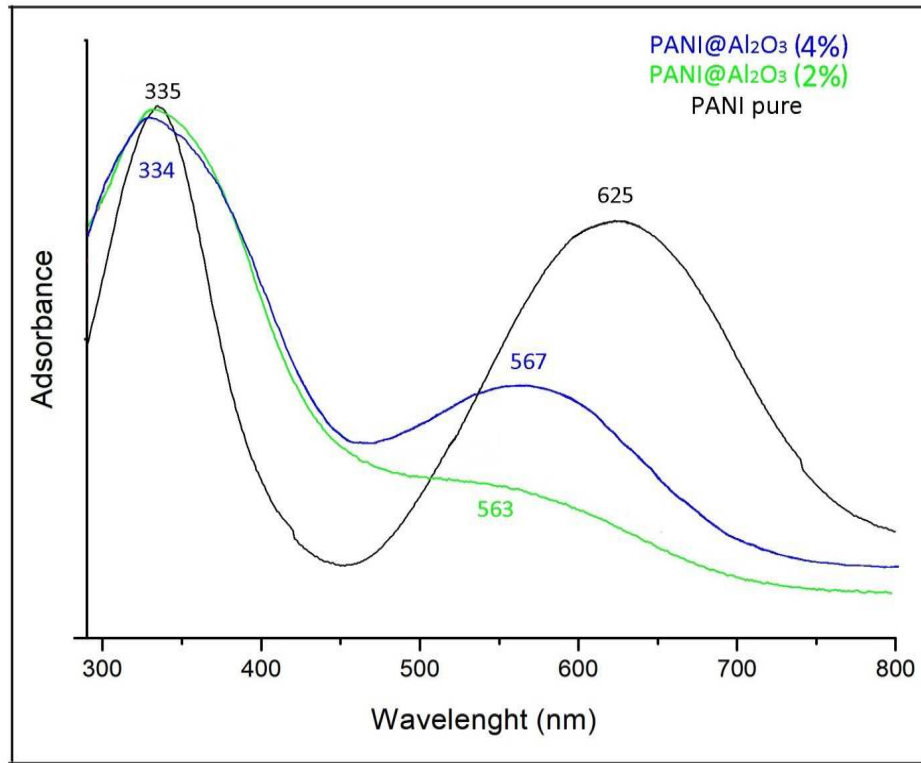


Figure IV. 6. UV-vis spectrum

The gap energy of nanomaterials was calculated by plotting (A^2) versus (hv) in the Tauc formula (eq. 3) [26], the results are summarized in Table IV.3.

Table IV. 5. Characteristics of UV-Vis absorption spectra of PANI/Al₂O₃ nanocomposites.

Compounds	λ_1 / nm	λ_2 / nm	E_g / eV
Pure PANI	335	625	3.22
PANI/Al ₂ O ₃ (2%)	334	563	2.95
PANI/Al ₂ O ₃ (4%)	334	678	2.88

$$A = (hv - E_g)^{1/2} \quad (3)$$

where hv is the photon energy, h is Planck's constant, E_g is the optical energy gap, A is the constant, for direct transitions $n = 1/2$. We plot a graph between $(\alpha hv)^2$ versus hv (Figure

IV.6), the extrapolation of the straight line to $(\alpha h\nu)^2 = 0$ axis gives E_g (where the absorption is reduced near zero).

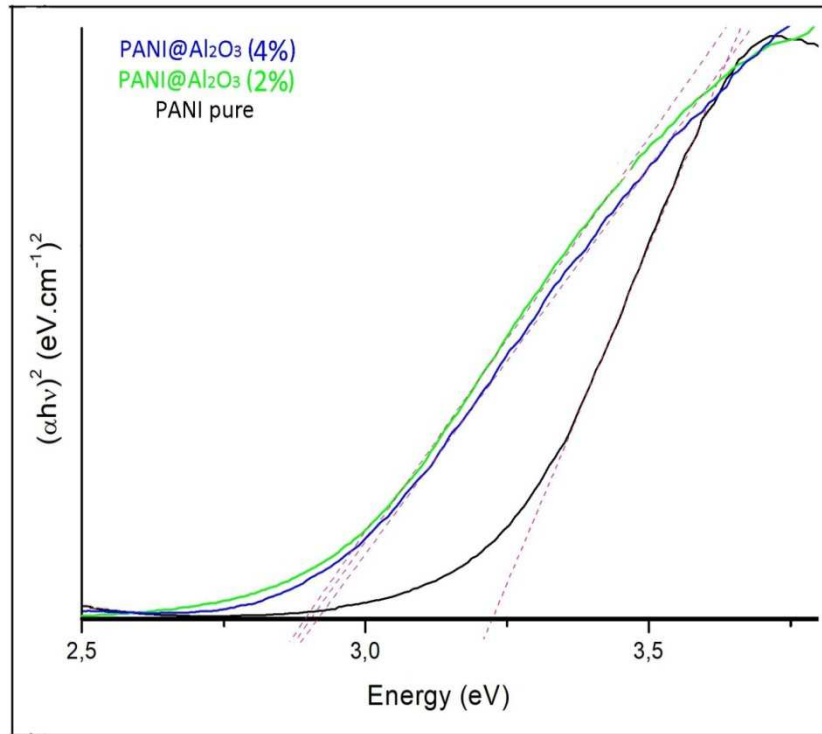


Figure IV.7. Tauc plots (b) corresponding to pure PANI and PANI/Al₂O₃ nanocomposites dissolved in DMSO.

The optical band gap of the pure PANI, PANI/Al₂O₃ (2%) and PANI/Al₂O₃ (4%) is 3.22 eV, 2.95 eV and 2.88 eV, respectively. Thus, the optical properties of samples are defined by the highest occupied molecular orbital (HOMO) and the lowest unoccupied molecular orbital (LUMO) energy levels. Generally, the augmentation of band gap by an increase in content of Al₂O₃ nanoparticles in the PANI matrix is associated to the destabilization of HOMO-LUMO through nanoparticle replacement. In addition, augmentation in the energy gap values of samples may be clarified in terms of the modified in the structure of polymer due to the creation of some kinds of bonding between the Al₂O₃ nanoparticles and polymer matrix [27].

IV.2.5. Thermogravimetric analysis (TGA)

The TGA of the samples were characterized (Figure IV. 8). It can be seen that as the Al₂O₃ nanoparticles content increased, the thermal stabilities of the nanocomposites improved. For all of the samples, the weights of the materials decreased rapidly from 250°C to 450°C, which may be due to the thermochemical decomposition of the organic materials. It also, the weight loss onset around 550-900°C indicates the structural decomposition of materials. In particular PANI/Al₂O₃ (4%) which seems more stable than the other nanocomposites, where the first mass loss step of 2.03% due to the volatilization of water molecules at 160°C, and the second one of 12.86% related to degradation of the PANI chain between 160-550°C. The third and final step is the carbonization of nanocomposite, which occurs within the temperature of 550-900°C (8.28% mass loss). In addition, a minor mass loss (~0.64 %) was observed when heating the nanoparticle up to ca. 900°C. This highlights the high thermal stability of this nanoparticle. This phenomenon may be related to the interactions between the PANI and Al₂O₃, which improve the thermal stability of the hybrid materials. Furthermore, this overall confirms that the PANI amount formation onto the nanoparticle significantly increases in the order PANI/Al₂O₃ (2%) < PANI/Al₂O₃ (4%). Besides, these results were in good agreement with those obtained through analysis of the XPS analysis.

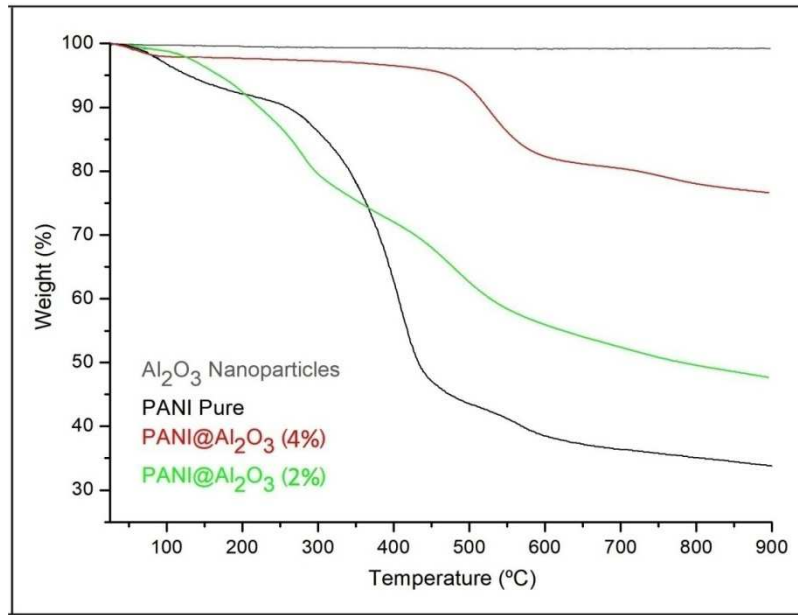


Figure IV .8. TGA of pure PANI, Al₂O₃ nanoparticle and PANI/Al₂O₃ nanocomposites.

IV.2.6. Surface morphologies

Figure IV.9. represents the SEM images of all PANI/Al₂O₃ nanocomposites. From the surface morphology of PANI/Al₂O₃ (4%) (IV. 9 (b)), it can be seen that the surfaces were more uniform, which indicates that the PANI and Al₂O₃ nanoparticles have high interactions with good compatibility. Compared with PANI/Al₂O₃ (2%) sample, the SEM showed small change in the thickness of the nanocomposite occurred, with an inhomogeneous distribution of nanoparticles.

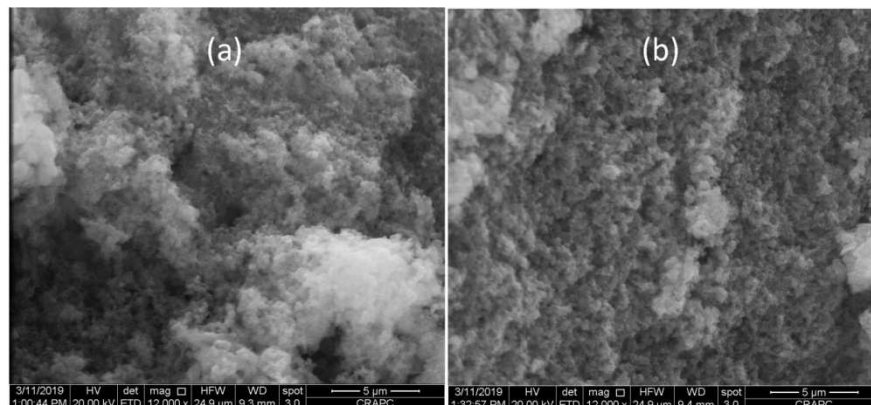


Figure IV. 9. SEM images of nanocomposites prepared for (a) PANI/Al₂O₃ (2%) ; (b)

PANI/Al₂O₃ (4%)

IV.2.7. Electrochemical Analysis

Among the electrochemical analysis methods, the cyclic voltammetry (CV) has become an important and widely used electroanalytical technique in many areas of chemistry. It is widely applied to investigate a variety of redox processes. The CV was used to study the electrochemical stability of the pure PANI and PANI/Al₂O₃ samples prepared (IV. 10).

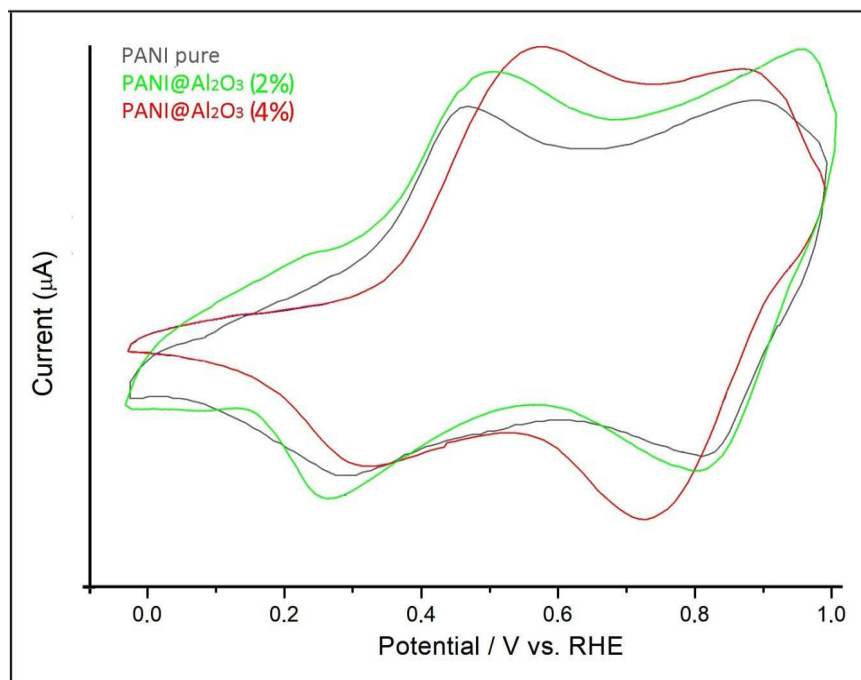


Figure IV. 10. Stabilized CV recorded at 50 mV.s⁻¹ in a 1 M HClO₄ solution for a GC electrode covered by pure PANI and PANI/Al₂O₃ nanocomposites.

The pure PANI shows two typical redox peaks, the first redox peak appearing between 0.46/0.28V is the oxidation leucoemeraldine to leucoemeraldine radical cation with the peak-to-peak potential separation (ΔE_p) was 180 mV, whereas that the second redox peak is the emeraldine radical cation to emeraldine and the third redox peak at 0.89/0.81V is the transformation of the pernigraniline radical cation to pernigraniline with $\Delta E_p = 80$ mV (Table IV.4). Furthermore, the CV of the all PANI/Al₂O₃ samples present also the two redox pair

characteristics of PANI, but the redox processes promotes a slight displacement in the E_{pa} and E_{pc} of both peaks as compared with pure polymer (Table 4).

Table IV.6. Parameters of the peaks of electrochemical saturation of pure PANI and PANI/Al₂O₃ nanocomposites in 1M HClO₄ solution on the GC electrode according to the CV data.

Electrodes	Electrochemical parameters (mV)					
	x_1/y_1	$E_{1/2}$	ΔE_p	x_2/y_2	$E_{1/2}$	ΔE_p
Pure PANI	460/280	370	180	890/810	850	80
PANI/Al ₂ O ₃ (2%)	480/290	385	190	940/830	885	110
PANI/Al ₂ O ₃ (4%)	570/310	440	260	870/730	800	140

where, x : Anodic peak ; y : Cathodic peak ; $E_{1/2}$: halfwave potential ; ΔE_p : peak to peak potential separation.

This behavior can be attributed to the intercalation of the PANI with Al₂O₃, whereas that the difference in the CV curves shows that there is variation in the chain structure. Further, all hybrid materials shows two electrochemical redox processes and the PANI deposited at Al₂O₃ appeared to keep electroactivity and the electrochemical properties.

IV.3. Conclusions

Nanocomposites are synthesized by aniline monomer with different contents of Al₂O₃ nanoparticles using a chemical oxidative polymerization method by ammonium persulfate as an oxidant. As synthesized samples were characterized by XPS, FTIR, SEM, XRD and UV-vis. which confirms the formation of hybrid materials, also gives the confirmation about an interaction between PANI and Al₂O₃ nanoparticles. TGA result show that thermal stability of PANI/Al₂O₃ (4%) is higher than their (6%) and (2%) samples, respectively. Importantly, this work represents an efficacious way of setting the optical properties of the synthesized nanocomposites, obtained by adjusted the amounts of Al₂O₃ during polymerization, the

analysis of the band gap shows the lowest value of optical band gap of 2.88 eV for PANI/Al₂O₃ (4%) compared to PANI/Al₂O₃ (2%) with 2.95 eV and 2.91. Further, the electrochemical properties were investigated with cyclic voltammetry, the all samples synthesized have excellent cycle stability suggesting their potential application in the electrode material for electrochemical field.

IV.4. References

- [1] S. Benykhlef, A. Bekhoukh, R. Berenguer, A. Benyoucef, E. Morallon. PANI-derived polymer/Al₂O₃ nanocomposites: Synthesis, characterization and electrochemical studies. *Colloid and Polymer Science*. 294 (2016) 1877-1885
- [2] S. Eslah, M. Nouri. Synthesis and Characterization of Tungsten Trioxide/Polyaniline/Polyacrylonitrile Composite Nanofibers for Application as a Counter Electrode of DSSCs. *Russian Journal of Electrochemistry*. 55 (2019) 291-304.
- [3] E.A. Özerol, A.Ç. Bozdoğan, B.F. Şenkal, M.Okutan. The effect on the impedance characteristics of the metal oxides (Al₂O₃ and ZnO) doping into polyaniline. *Materials Science in Semiconductor Processing*. 56 (2016) 357-361.
- [4] T. Campbell, R.K. Kalia, A. Nakano, P. Vashishta. Dynamics of Oxidation of Aluminum Nanoclusters using Variable Charge Molecular-Dynamics Simulations on Parallel Computers. *Physical Review Letters*. 82 (1999) 4866-4869.
- [5] E. Ozkazanc, H. Ozkazanc. Multifunctional polyaniline/chloroplatinic acid composite material: Characterization and potential applications. *Polymer Engineering and Science*. 59 (2019) 66-73.
- [6] L. Hao, X. Zhou, J. Liu. Release of ZrO₂ nanoparticles from ZrO₂/Polymer nanocomposite in wastewater treatment processes. *Journal of Environmental Sciences*. 91 (2020) 85-91.
- [7] P.G. Romero. Hybrid Organic-Inorganic Materials-In Search of Synergic Activity. *Advanced Materials*. 13 (2001) 163-174.
- [8] F. Fusalba, D. Bélanger. Electrochemical characterization of polyaniline-molybdenum trisulfide electrode in non-aqueous media. *Electrochimica Acta*. 45 (2000) 3877-3883.

- [9] M. Hasan, M.O. Ansari, M.H. Cho, M. Lee. Ammonia sensing and DC electrical conductivity studies of p-toluene sulfonic acid doped cetyltrimethylammonium bromide assisted V₂O₅/polyaniline composite nanofibers. *Journal of Industrial and Engineering Chemistry*, 2015, 22: 147-152.
- [10] K. Yamani, R. Berenguer, A. Benyoucef, E. Morallón. Preparation of polypyrrole (PPy)-derived polymer/ZrO₂ nanocomposites: effects of nanoparticles interface and polymer structure. *Journal of Thermal Analysis and Calorimetry*. 135 (2019) 2089-2100.
- [11] A.A. Qaiser, M.M. Hyland, D.A. Patterson. Effects of various polymerization techniques on PANI deposition at the surface of cellulose ester microporous membranes: XPS and electrical conductivity studies. *Synthetic Metals*. 162 (2012) 958-967
- [12] M. Lia, S. Zhou. α -Fe₂O₃/polyaniline nanocomposites as an effective catalyst for improving the electrochemical performance of microbial fuel cell. *Chemical Engineering Journal*. 339 (2018) 539-546.
- [13] E.A. Sanches, J.M.S. da Silva, J.M.O. Ferreira, J.C. Soares, A.L. dos Santos, G. Trovati, E.G.R. Fernandes, Y.P. Mascarenhas. Nanostructured Polyaniline Emeraldine-base form (EB-PANI): a structural investigation for different neutralization times. *Journal of Molecular Structure*. 1074 (2014) 732-737.
- [14] A. Bekhoukh, A. Zehhaf, A. Benyoucef, S. Bousalem, M. Belbachir. Nanoparticles Mass Effect of ZnO on the Properties of Poly(4-Chloroaniline)/Zinc Oxide Nanocomposites. *Journal of Inorganic and Organometallic Polymers and Materials*. 27 (2017) 13-20.
- [15] F. Chouli, I. Radja, E. Morallon, A. Benyoucef. A Novel Conducting Nanocomposite Obtained by p-Anisidine and Aniline With Titanium(IV) Oxide Nanoparticles: Synthesis, Characterization, and Electrochemical Properties. *Polymer Composites*. 38 (2017) 254-260.

- [16] S. Benyakhou, A. Belmokhtar, A. Zehhaf, A. Benyoucef. Development of novel hybrid materials based on poly(2-Aminophenyl disulfide)/Silica Gel : preparation, characterization and electrochemical studies. *Journal of Molecular Structure* 1150 (2017) 580-585.
- [17] S. Daikh, F.Z. Zeggai, A. Bellil, A. Benyoucef. Chemical polymerization, characterization and electrochemical studies of PANI/ZnO doped with hydrochloric acid and/or zinc chloride: Differences between the synthesized nanocomposites. *Journal of Physics and Chemistry of Solids*. 121 (2018) 78-84.
- [18] K. Tzou, R.V. Gregory. A method to prepare soluble polyaniline salt solutions-in situ doping of PANI base with organic dopants in polar solvents. *Synthetic Metals*. 53 (1993) 365-377.
- [19] F.Z. Kouidri, R. Berenguer, A. Benyoucef, E. Morallon. Tailoring the properties of polyanilines/SiC nanocomposites by engineering monomer and chain substituents. *Journal of Molecular Structure*. 1188 (2019) 121-128.
- [20] S. Bousalem, F.Z. Zeggai, H. Baltach, A. Benyoucef. Physical and electrochemical investigations on hybrid materials synthesized by polyaniline with various amounts of ZnO nanoparticle. *Chemical Physics Letters*. 741 (2020) 137095.
- [21] M. Khayet, M.C. García-Payo, X-Ray diffraction study of polyethersulfone polymer, flat sheet and hollow fibers prepared from the same under different gas-gaps, *Desalination* 245 (2009) 494-500.
- [22] P. Tarte. Infrared Spectra of Inorganic Aluminates and Characteristic Vibrational Frequencies of AlO₄ Tetrahedra and AlO₆ Octahedra. *Spectrochim. Acta*. 23 (1967) 2127-2143.

- [23] J. Manuel, T. Salguero, R.P. Ramasamy. Synthesis and characterization of polyaniline nanofibers as cathode active material for sodium-ion battery. *Journal of Applied Electrochemistry*. 49 (2019) 529-537.
- [24] P.K. Khanna, N. Singh, S. Charan, A.K. Visawanath. Synthesis of Ag/polyaniline nanocomposite via an in situ photo-redox mechanism. *Materials Chemistry and Physics*, 92 (2005) 214-219
- [25] L. Irimpan, V.P.N. Nampoori, P. Radhakrishnan, Spectral and nonlinear optical characteristics of nanocomposites of ZnO-CdS, *Journal of Applied Physics*. 103 (2008) 094914-094918.
- [26] D. Segets, J. Gradl, R.K. Taylor, V. Vassilev, W. Peukert, Analysis of optical absorbance spectra for the determination of ZnO nanoparticle size distribution, solubility, and surface energy. *ACS Nano*, 3 (2009) 1703-1710.
- [27] S. Ebrahim, A.H. Kashyout, M. Soliman. Ac and Dc conductivities of polyaniline/poly vinyl formal blend films. *Current Applied Physics*. 9 (2009) 448-454.

CHAPTER V

PANI/OPUNTIA Ficus indicat

V.1 Introduction

Opuntia ficus indica (prickly pear) is a tree native to arid and semi-arid regions of Mexico. it is a succulent plant capable of storing a large quantity of water and presents no danger to human health. , in Algeria this plant Is available in very quantities, this culture has several interests in different areas: forage and market gardening, the cosmetics industry , food , medicine and also in the field of adsorption chemistry . the opuntia ficus indica (OFI) is amixture of acidic and neutral polysacharide consisting primarily of 24.6-42 % of arabinose , 21-40.1% of glactose , 8-12.7% glacturonic acid , 7-13.1% of rhamnose and 22-22.2% of axylose [1]. Figure.V.1



Figure.V.1 OFI cladodes

These hybrid materials can be used in numerous field including ion exchange materials: conducting materials , photocatalysis , adsorption etc

Table IV.1. the conditions and yeild of our synthesis

<i>Products</i>	<i>Conditions</i>	<i>Dopant</i>	<i>yeild</i>	<i>Time</i>	<i>Temperature</i> (°C)	<i>Mole fraction</i>
Polymer/Al ₂ O ₃		HCl	79,43%	24 h	5 For The first 3 ^h From the reaction	monomer: oxydant 1 :1

V.2 Results and discussion

V.2.1. FTIR

FTIR spectrum is utilized to analyses the functioned groups , nature of bonding and the chemical structure of compounds , it is also utilized as the probe technique to determine the oxidation state of Pani fig. 02 displays the FT-IR spectra of Pani , OFI-A , and Pani/OFI-A composite.

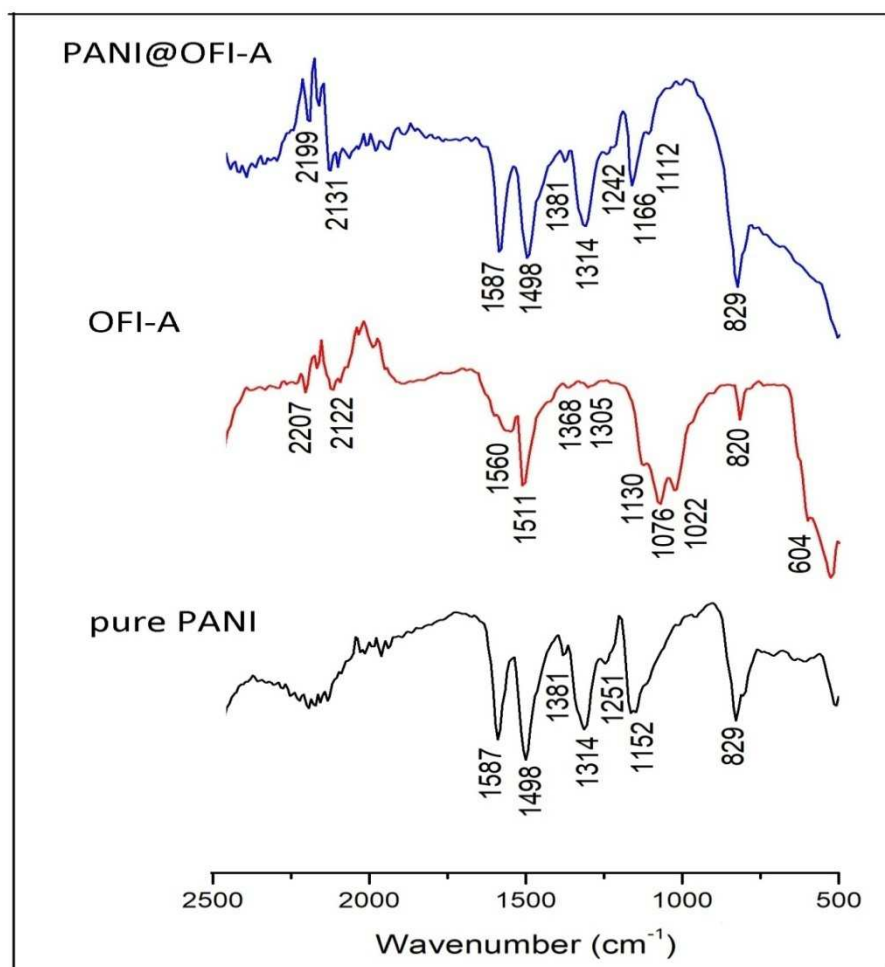


Figure V. 2. FTIR spectra of pure PANI, OFI and three PANI/OFI nanocomposites synthesized.

For the PANI gained by a simple oxidation reaction, the bands at 1637cm^{-1} correspond to C=N stretching vibrations for imine. The bands at 1587 and 1498cm^{-1} attributed to the C=C stretching of the quinoid ring and benzenoid ring, respectively. Those at 1314 and 1152cm^{-1} are assigned to the secondary aromatic amine C-N stretching vibrations. The peak at 829cm^{-1} is belong to the out-of-plane vibration of C-H on the 1,4-disubstituted ring. The peak at 1251cm^{-1} can be identical to various bending and stretching corresponds to C-C bond. These characteristic IR spectra of as-synthesized Pani are in excellent agreement with those obtained for Pani, proposing the Pani formed [2]. Likewise, the FT-IR spectra of OFI-A appear in the group $500\text{-}2500\text{cm}^{-1}$, the bands around $2100\text{-}2300\text{cm}^{-1}$ may be owing

to asymmetric stretching vibration of CH_2 and the symmetric stretching vibration of $-\text{CH}_3$, respectively, of aliphatic acids [3]. The stretching vibration band at 1560cm^{-1} is owing to asymmetric stretching of the carboxylic COO^- double band of deprotonated carboxylate functional groups [4], at 1511 cm^{-1} is of phenolic $-\text{OH}$ stretching, the peaks observed at 1368cm^{-1} which reflect stretching vibration of symmetrical or asymmetrical ionic carboxylic groups ($-\text{COOH}$ of pectine) [4], the band at 1076cm^{-1} could be owing to the vibration of $-\text{C}-\text{O}-\text{C}$ and OH of polysaccharides [5], the peaks at $1130-1022\text{ cm}^{-1}$ are owing to the $\text{C}-\text{O}$ stretching vibration of ketones, aldehydes and lactones or carboxyl groups [6].

Moreover, the intensity of the vibration bands after the formation of the composite became smaller in the FTIR spectra of PANI/OFI-A.

V.2.2 XRD analysis

XRD analysis was utilized to inspect the structure of Pani and Pani/OFI-A composite and investigated the effect of the OFI-A on the Pani structure. Figure. 03 displays the typical XRD patterns of Pani and Pani/OFI-A composite, broad diffraction peaks exist between 10° and 30° owing to the parallel and perpendicular of the polymer Pani chain, the Pani peak diffracted at an angle of $2\theta = 5.01^\circ$ and $2\theta = 21.24^\circ$ with a d-spacing 1.76Å and 0.41Å , respectively. The XRD pattern which shows low crystallinity of the conductive polymer due to the repetition of benzoide and quinoide rings in Pani chains [7], Pani crystal size, d , is in the range of $6.84-11.7\text{ nm}$ which was counted by Scherer's equation, in the existing of OFI-A, crystal size of composite stay in the range of $6.62-8.02\text{ nm}$ according to fig 03 in the given range registered for the broad peak, two featured sharp peaks at $2\theta = 4.57^\circ$ and $2\theta = 18.21^\circ$ with planes of (121) and (113), respectively, are shifted to lower angle owing to the interaction between Pani chain and OFI-A [8-13]

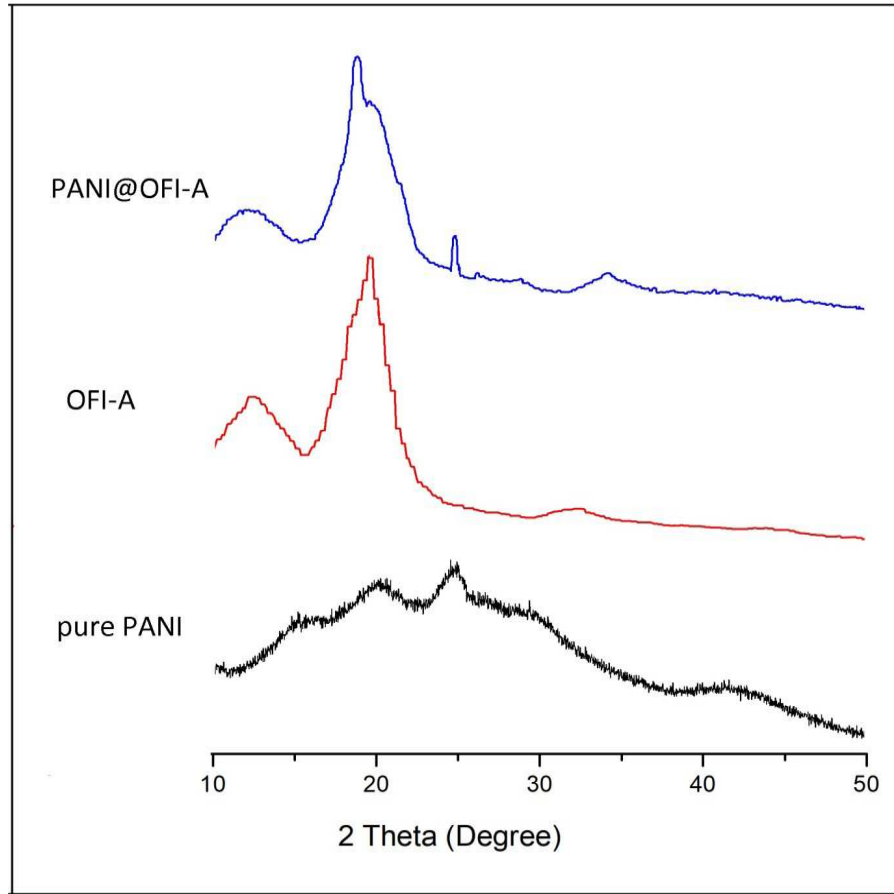


Figure V. 3. XRD patterns of pure PANI, OFI and PANI/OFI composites synthesized.

Finally, the value for the plane spacing (d -spacing) is calculated from Bragg's law (eq. 1) [14-16].

$$d = \frac{\lambda}{2 \sin \theta} \quad (1)$$

where the average crystallite size (D) was determined from XRD data analysis is represented by θ based on the Debye-Scherrer law (eq. 2) [14-16].

$$D = \frac{k \cdot \lambda}{\beta \cdot \cos \theta} \quad (2)$$

with D : volume averaged crystallite size, k : Scherrer constant was considered as 0.9 in this context, β : size is line broadening at half of the maximum intensity (FWHM) in radian and λ : wavelength.

Besides, other XRD parameters such as d -spacing, Bragg angle, full width half maximum (FWHM) and crystalline size of the main principal peak for OFI-A particles with Pani /OFI-A composite are shown in Table.01. The results assure previous results test which describe the effect of OFI-A in PANI/OFI-A composite as we shown In fig.03 the OFI-A have an effect on the crystal identity of PANI while they can developing in properties of this conductive polymer

Table V.1. X-ray diffraction data with Bragg angle, d -spacing, FWHM and crystallite size of the main principal peak for PANI, OFI-A and OFI-A samples.

Samples	Plane peaks	Braggs angle (2θ)	d -spacing (Å)	FWHM (2θ)	Size (nm)
PANI	(121)	5.01	1.76	3.65	6.84
	(113)	21.24	0.41	2.17	11.70
OFI-A	(121)	4.78	1.84	3.77	6.62
	(113)	19.97	0.44	3.16	8.02
PANI/OFI-A	(121)	4.57	1.93	3.98	6.27
	(113)	18.21	0.48	3.37	7.50

V.2.3. SEM analysis

The morphology of the composites we are examined by scanning electron microscopy SEM analysis of the surfaces of the composites. figure. 04a presents micrographs of OFI-A , while figure. 04b presents the morphology of the conductive polymer Pani , as can be seen in figure. 04c the combination of the two materials Pani with OFI-A . to optimally improve the conductivity of the composites it is significant for the particles to form a percolation network within the polymer matrix .fig. 04c the SEM image of Pani/OFI-A composites seems like a similar morphology of Pani in fig.04b, it indicates that the OFI-A nanocrystals are impregnated within the Pani which means that the pani is coated on the crystals during in situ polymerization.

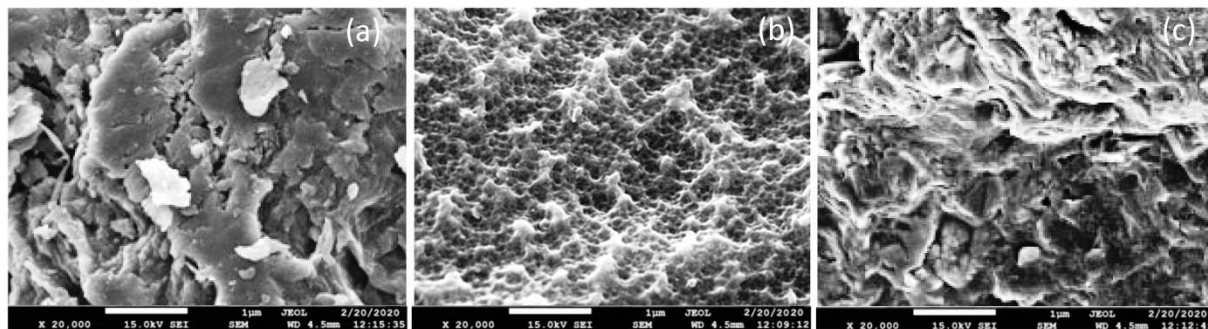


Figure V.4. SEM images of the materials prepared for (a) OFI ; (b) PANI; (c) PANI/OFI

4 points method :

Conductivity values are measured by the four points method , the conductivity measurement are obtained after having the resistivity with the the method of four points in line[17] , using lucas lab equipement , the samples are dried under vacuum for 24hours ; of pellets (0.013m of diameter) are prepared using a FT-IR mold by applying pressure of $7,4.10^8$ pa . measuring the conductivity of a conductive composite by applying ohm's law requires injecting a current into the sample . as can be seen in table n°2 , the electrical conductivity of Pani/OFI-A composite has found $6,24.10^{-5}$ S.cm⁻¹. previous studies observe that the conductivity of semiconductor materials is between 10^{-7} - 10^2 and the conductivity of the most doped conductive polymers are located approximately in this region [18]. The addition of OFI-A particles in the conductive polymer matrix pani causes an increase in electric conductivity compared to pure PANI 4.84 S.cm⁻¹. these results illustrate that OFI-A is a good conductive materials .polymers such as pani have a conjugated system facilitate the transport of electrons. So , the increasing in the conductivity of the composite shows that the presence of OFI-A particles has reforced the transport of electrons in the path of the molecular chains of polymers .

Table V. 2. The electrical conductivity values of PANI, OFI-A and OFI-A samples.

Samples	PANI	OFI-A	PANI/OFI-A
Conductivity/S.cm ⁻¹ (10 ⁻⁵)	4.84	9.25	6.24

Table V.2: the values of the electrical conductivity of composite and the pure materials pani and OFI-A, respectively.

V.2.4. TGA analysis

Thermal stability of Pani/OFI-A composite and pure materials Pani OFI-A are examined using TGA measurements , as we shown in figure V.5 , TGA curve of OFI-A presents that about 10% weight loss occurring in the temperature range of 10C° - 140C° which can be attributed to expulsion of water molecules , major weight loss (60%-70%) was observed in the temperature range of 140 °C-700 °C concerning the decomposition of protein chain within the OFI-A . the decomposition temperatures obtained from thermograms of pure Pani shows three stage mass loss behavior , the first step at 140C° lost about 5,63% of mass is mainly due to release of water , and the second one of 47,69% related to removal of the dopants between 140-450C° range , the mass loss occurring between the range of 450 °C-700 °C around 13% corresponds to decomposition or thermal degradation of the polymers chain . the thermal stability was decreased after combination with Pani.

In addition, the decomposition temperature was observed from thermogram of Pani/OFI-A composite shows also 3 step mass loss behavior, the first step at 140 °C, the weight losses during this step is about 6% owing to desorption of physically absorbed water, the evaporation of residual solvents such as methanol, while the second step is a decomposition step and has the great mass loss of about 51% attributed to removal of dopants, the final step of mass loss estimated at 15% between 370 °C-700 °C due to decomposition of the polymers chains in the composite, the weight loss at all stage is for composite compared to

that of pure PANI, the difference in mass loss between composite PANI/OFI-A and pure PANI may be owing to the difference in their chemical and geometrical nature.

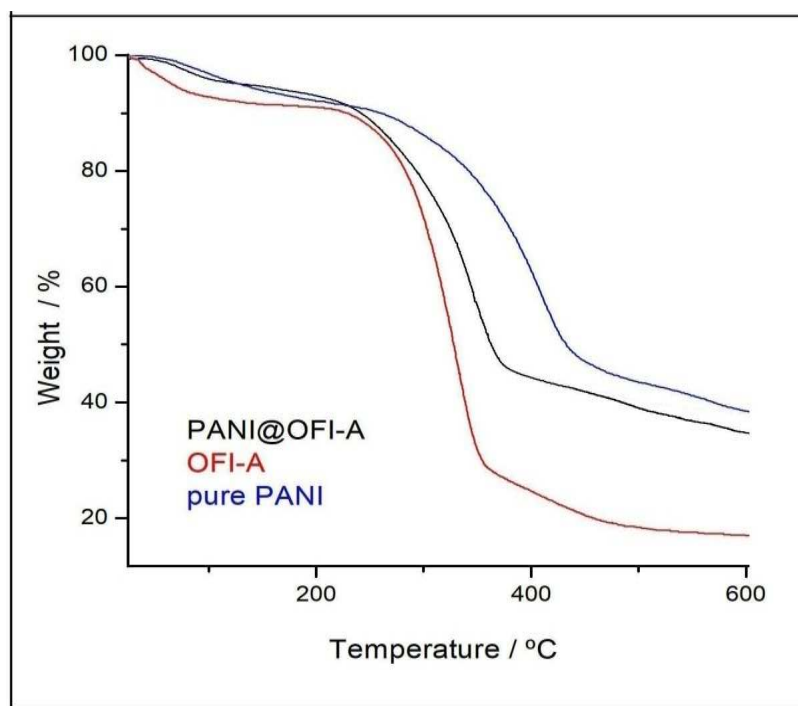


Figure V.5. TGA of pure PANI, OFI and PANI/OFI nanocomposites.

V.3. Conclusion

The composites polyaniline / OFI-A have been prepared by in situ chemical oxidative polymerization , the results of spectroscopic such as (XRD,SEM,FT-IR,TGA, electrical conductivity) indicate that Pani/OFI-A composite is succesfully prepared in this research , the thermal stability of pani is known to be effected by several factors such as the structure of the polymer backbone and oxidation state [19-22]. in the literature the existing of interaction between Pani chains and OFI-A surface is reported to weaken the polyaniline interchain interaction, thus lowering the thermal stability of the composite [21, 23-28] . this can explain the lower thermal stability of our composite with respect of Pani ref. on the other hand, the composite pani/OFI-A have shown good electrochemical properties, the electrical

conductivity was increased as compared to that pure pani from $4,84 \text{ S.cm}^{-1}$ to $6,24.10^{-5} \text{ S.cm}^{-1}$. overall, the pani/OFI-A composite has excellent electroactivity properties

V.4. References

- [1] . Trachtenberg S, Mayer AM. Composition and properties of Opuntia ficus-indica mucilage. *Phytochemistry* 1981;20:2665–8.
- [2] Manuel J, Salguero T, Ramasamy RP (2019) Synthesis and characterization of polyaniline nanofibers as cathode active material for sodium-ion battery. *Journal of Applied Electrochemistry*. 49:529-537.
- [3] Li FT, Yang H, Zhao Y, Xu R. Novel modified pectin for heavy metal adsorption. *Chin Chem Lett* 2007;18:325–8.
- [4] Farinella NV, Matos GD, Arruda MAZ. Grape bagasse as a potential biosorbent of metals in effluent treatments. *Bioresour Technol* 2007;98:1940–6.
- [5] Ibarra JV, Moliner R. Coal characterization using pyrolysis-FTIR. *J Anal Appl Pyrol* 1991;20:171–84
- [6] Chandrasekhar S, Pramada PN. Rice husk ash as an adsorbent for Methylene Blue-effect of ashing temperature. *Adsorption* 2006;12:27–43
- [7] L. Shi, X. Wang, L. Lu, X. Yang, X. Wu, Preparation of TiO₂/ polyaniline composite from a lyotropic liquid crystalline solution, *Synthetic Metals* 159 (2009) 2525–2529.
- [8] Bekhoukh A, Zehhaf A, Benyoucef A, Bousalem S, Belbachir M (2017) Nanoparticules Mass Effect of ZnO on the Properties of Poly(4-Chloroaniline)/Zinc Oxide Composites. *Journal of Inorganic and Organometallic Polymers and Materials*. 27:13-20.
- [9] Chouli F, Radja I, Morallon E, Benyoucef A (2017) A Novel Conducting Composite Obtained by p-Anisidine and Aniline With Titanium(IV) Oxide Particles: Synthesis, Characterization, and Electrochemical Properties. *Polymer Composites*. 38:254-260.

- [10] Benyakhou S, Belmokhtar A, Zehhaf A, Benyoucef A (2017) Development of novel hybrid materials based on poly(2-Aminophenyl disulfide)/Silica Gel : preparation, characterization and electrochemical studies. *Journal of Molecular Structure* 1150:580-585.
- [11] Daikh S, Zeggai FZ, Bellil A, Benyoucef A (2018) Chemical polymerization, characterization and electrochemical studies of PANI/ZnO doped with hydrochloric acid and/or zinc chloride: Differences between the synthesized composites. *Journal of Physics and Chemistry of Solids*. 121:78-84.
- [12] Yamani K, Berenguer R, Benyoucef A, Morallón E (2019) Preparation of polypyrrole (PPy)-derived polymer/ZrO₂ composites: effects of particles interface and polymer structure. *Journal of Thermal Analysis and Calorimetry*. 135:2089-2100.
- [13] Tzou K, Gregory RV (1993) A method to prepare soluble polyaniline salt solutions- in situ doping of PANI base with organic dopants in polar solvents. *Synthetic Metals*. 53:365-377.
- [14] Kouidri FZ, Berenguer R, Benyoucef A, Morallon E (2019) Tailoring the properties of polyanilines/SiC composites by engineering monomer and chain substituents. *Journal of Molecular Structure*. 1188:121-128.
- [15] Bousalem S, Zeggai FZ, Baltach H, Benyoucef A (2020) Physical and electrochemical investigations on hybrid materials synthesized by polyaniline with various amounts of ZnO nanoparticle. *Chemical Physics Letters*. 741:137095.
- [16] Khayet M, García-Payo MC (2009) X-Ray diffraction study of polyethersulfone polymer, flat sheet and hollow fibers prepared from the same under different gas-gaps, *Desalination*. 245:494-500
- [17] X.F. Yang, G.C. Wang, R.Y. Wang, X.W. Li. *ElectrochimicaActa*. 55 (2010) 5414-5419.
- [18] . B. Sari, M. Talu (1998) Electrochemical Polymerization and Analysis of Some Aniline Derivatives. *Turkish Journal of Chemistry*. 22:301-307.

- [19] Ansari, R.; Keivani, M.B. Polyaniline Conducting Electroactive Polymers Thermal and Environmental Stability Studies. *E-Journal Chem.* 2006, 3, 202–217
- [20] Alves, W.F.; Venancio, E.C.; Leite, F.L.; Kanda, D.H.F.; Malmonge, L.F.; Malmonge, J.A.; Mattoso, L.H.C. Thermo-analyses of polyaniline and its derivatives. *Thermochim. Acta* 2010, 502, 43–46.
- [21] Chandrakanthi, N.; Careem, M.A. Thermal stability of polyaniline. *Polym. Bull.* 2000, 44, 101–108.
- [22] Lu, X.; Tan, C.Y.; Xu, J.; He, C. Thermal degradation of electrical conductivity of polyacrylic acid doped polyaniline: Effect of molecular weight of the dopants. *Synth. Met.* 2003, 138, 429–440.
- [23] Li, X.; Wang, G.; Li, X.; Lu, D. Surface properties of polyaniline/nano-TiO₂ composites. *Appl. Surf. Sci.* 2004, 229, 395–401.
- [24] Lee, I.S.; Lee, J.Y.; Sung, J.H.; Choi, H.J. Synthesis and electrorheological characteristics of polyaniline-titanium dioxide hybrid suspension. *Synth. Met.* 2005, 152, 173–176.
- [25] Ansari, M.O.; Mohammad, F. Sensors and Actuators B : Chemical Thermal stability , electrical conductivity and ammonia sensing studies on p -toluenesulfonic acid doped polyaniline : titanium dioxide (p TSA/Pani:TiO₂) composites. *Sensors Actuators B. Chem.* 2011, 157, 122–129.
- [26] Alves, W.F.; Venancio, E.C.; Leite, F.L.; Kanda, D.H.F.; Malmonge, L.F.; Malmonge, J.A.; Mattoso, L.H.C. Thermo-analyses of polyaniline and its derivatives. *Thermochim. Acta* 2010, 502, 43–46.
- [27] Nabid, M.R.; Golbabaee, M.; Moghaddam, A.B. Polyaniline/TiO₂ Composite : Enzymatic Synthesis and Electrochemical Properties. *Int. J. Electrochem. Sci.* 2008, 3, 1117–1126.

- [28] Li, X.; Chen, W.; Bian, C.; He, J.; Xu, N.; Xue, G. Surface modification of TiO₂ particles by polyaniline. *Appl. Surf. Sci.* 2003, 217, 16–22.

This thesis work focused on the synthesis by simple chemical oxidation and the characterization of the properties of metal and inorganic elements: tungsten oxide WO_3 and alumina Al_2O_3 and opuntia ficus indica OFI crystalline with the aim of better understanding the link between the conditions of development, composition and properties of thin films in order to promote their future application.

The first chapter of the bibliographic nature highlighted the knowledge useful for this study concerning the structural, optical, electrical and electronic structure of tungsten oxide WO_3 and alumina and opuntia ficus indica in crystalline form. In particular, the main models proposed to explain the physical and chemical properties of the particles WO_3 and Al_2O_3 and OFI during the insertion of cations or from oxygen substoichiometry as well as the electronic structure diagram of molecular orbitals were presented.

In Chapter 2 the different profiling techniques used in this work as well as the associated experimental devices have been revealed. For the purposes of our study, the basic principle of each technique was called and described the corresponding devices. In each case, examples and related factors were identified. Performance and limits were also noted. Finally, the characteristics of these techniques have been distinguished to show their areas of excellence and their respective borders on the one hand, and on the other to show their complementarity when they exist.

In chapter 3 Hybrid materials based on WO_3 , modified with polyaniline have been obtained. Samples have been synthesized by chemical polymerization of aniline monomer with WO_3 nanoparticles, the ammonium persulfate have been used as oxidizers, The resulting samples were fully characterized by XPS, XRD, FTIR, SEM and UV-vis spectroscopies which have shown that polymerizations have been carried out. Importantly, this work represents an efficacious way of setting the optical properties of the synthesized nanocomposites, we have

been confirmed the successful synthesis of the three PANI/ WO_3 samples. TGA shows an improved thermal stability by the presence of WO_3 in nanocomposites compared to PANI. Interestingly, the analysis of the band gap shows lowest value of optical band gap of 1.88 eV for PANI/ WO_3 (0.5) compared to PANI/ WO_3 (1.0) and PANI/ WO_3 (1.5) with 1.91eV and 1.98eV, respectively. In chapter 4 with the same manner by adjusted the amounts of Al_2O_3 during polymerization, the analysis shows also that the lowest evaluate of optical band gap is 2.88 eV for PANI/ Al_2O_3 (4%) compared to PANI/ Al_2O_3 (2%) with 2.95 eV. The XRD exhibit that the nanoparticles give the crystallin shape to our nanocomposites. The surfaces morphology informations was given by SEM that display a homogeneity of the nanocomposites synthesized. Good electroactivity response where achieve two pairs oxidation/reduction with improved thermal stability for the synthesized hybrid materials have been observed.

chapter 5 presents the conductivity and thermal stability characterisation of polyaniline Pani with nopal opuntia ficus indica OFI-A, the composite was synthesized via a chemical oxidation method of the aniline with nopal powder in acid. The composition morphology and structure of the composite Pani/OFI-A were characterized via Fourier transform infrared spectroscopy FTIR, X-ray diffraction XRD, scanning electron microscopy SEM, this characterizations assured the successful synthesis of the nanocomposite. The composite shows a good conductivity (6.24 S.cm^{-1}) than to pure polyaniline (4.84 S.cm^{-1}). Nevertheless, Thermogravimetry analysis TGA displays a decreasing in the thermal stability by the existence of nopal in the composite compared to pure polyaniline. The present chapter is focuses on the study of the synthesis of polyaniline with nopal opuntia ficus indica (Pani/OFI-A) owing to their chemical interest, particularly those having the most promising expected adsorption benefit with good conductivity.

finally, Polyaniline in various forms has been widely explored as an electrode material for supercapacitors due to its high theoretical charge storage capacity, facile-cost-effective synthesis, good mechanical strength and ultrafast charge transport. However, commercialization of such pristine forms is very much restricted by low solubilities, rapid agglomeration during device design accompanied by poor electrochemical life and fast environmental decomposition. The blending with nano-carbon materials, metal oxides and other competent materials, may result in high quality materials– “nanocomposites” with superior features is ideally fit for future generation energy storage devices. The present chapter deals with detailed discussions on designing, the fabrication of such binary and ternary nanocomposites, correlating their morphology with electrochemical behavior, so as to optimize their supercapacitive performances. Such an attempt would help to outline the present status and future aspects of these materials which will be of first-hand assistance especially to the beginners to this field of research.

We can see in our work the successful of the three nanocomposite synthesizing and the quantite propotional to start your work depend on your field of application . besides, we are looking forward to progress a new nanocomposites with great adsorption capacity

Abstract

Structuring composite materials, at the nanometer scale, that is to say synthesize nanocomposite materials, is an interesting way to optimize their properties. This is the context of this PhD dealing with the synthesis of nanocomposites constituted of polyaniline with metallic and inorganic nanoparticles (tungsten oxide, alumina, opuntia ficus indica), the nanocomposite was synthesized via in-situ oxidation method of the aniline with the nanoparticles. The main objective of this paper is to demonstrate that it is possible to synthesize a hybrid material with good conductivity and good thermal stability. FTIR, UV-Vis, XPS, SEM, and XRD confirmed the successful synthesis of the three nanocomposites. TGA shows an improved thermal stability by the presence of WO_3 and alumina in nanocomposites compared to PANI. The analysis of the band gap shows a good conductivity (6.24 S/cm) of the PANI/opuntia ficus indica nanocomposites than to pure polyaniline (4.84 S/cm). Interestingly, they show the lowest value of optical band gap of 1.88 eV for PANI/ WO_3 (0.5) compared to PANI/ WO_3 (1.0) and PANI/ WO_3 (1.5) with 1.91 eV and 1.98 eV, respectively. In addition, the electroactivity properties were investigated by cyclic voltammetry to explore the benefits of these types of hybrid materials in electrochemical applications.

Keywords: nanocomposite, polyaniline, tungsten oxide, alumina, opuntia ficus indica

ملخص :

تعد هيكلية المواد المركبة على نطاق النانومتر ، أي توليف المواد المركبة النانوية ، طريقة مثيرة للاهتمام لتحسين خصائصها ، وهذا هو سياق هذه الرسالة الدكتوراه التي تتناول تخليق المركبات النانوية المكونة من البوليانيلين مع المواد الغير عضوية (اكسيد التنغستن ، الالومينا ، اوراق شجرة البربري) تم تصنيع المركبات النانوية من خلال طريقة الاكسدة في الموقع للانيلين مع المواد النانوية ، الهدف الرئيسي من هذه الدراسة هو اثبات انه من الممكن تجميع مادة هجينة تجمع الموصلية الجيدة مع الاستقرار الحراري الجيد ، الاجهزة المستعملة (جهاز فورييه للاشعة الحمراء ، مطيافية الاشعة فوق البنفسجية ، مطيافية الاشعة السينية بالالكترون الضوئي ، مجهر المسح الالكتروني ، حيود الاشعة السينية) اكدت التوليف الناجح للمركبات النانوية الثلاثة . يظهر التحليل الحراري الوزني استقرارا حراريا محسنا من خلال وجود اكسيد التنغستن و الالومينا في المركبات النانوية مقارنة بالبوليانيلين ، و يظهر تحليل فجوة النطاق الموصلية الجيدة تقدر ب 6.24س/سم لمركب بوليانيلين/بربري مقارنة بالبوليانيلين النقي 4.84س/سم . ومن المثير للاهتمام انها تظهر ادنى قيمة لفجوة النطاق البصري البالغة 1.88 اليكترون فولت لمركب بوليانيلين/اكسيد التنغستن .بالاضافة لذلك ، تم فحص خواص النشاط الكهربى بواسطة مقياس الجهد الدوري لاستكشاف فوائد هذه الانواع من المواد الهجينة في التطبيقات الكهروكيميائية .

الكلمات الرئيسية : المركبات النانوية، البوليانيلين ، اكسيد التنغستن ، الالومينا ، اوراق شجرة البربري

Resumé

La structuration des matériaux composites, à l'échelle nanométrique, c'est-à-dire synthétiser des matériaux nanocomposites, est une manière intéressante d'optimiser leurs propriétés. C'est le contexte de cette thèse traitant de la synthèse de nanocomposites constitués de polyaniline avec des nanoparticules métalliques et inorganiques (oxyde de tungstéine, alumine, opuntia ficus indica), le nanocomposite a été synthétisé via la méthode d'oxydation in-situ de l'aniline avec les nanoparticules, L'objectif principal de cette étude est de démontrer qu'il est possible de synthétiser une collection de matériaux hybrides avec une bonne conductivité et une bonne stabilité thermique, FTIR, UV-Vis, XPS, SEM et XRD ont confirmé la synthèse réussie des trois nanocomposites. La TGA montre une stabilité thermique améliorée par la présence de WO₃ et d'alumine dans les nanocomposites par rapport à PANI, l'analyse de la bande interdite montre une bonne conductivité (6,24 S / cm) des nanocomposites PANI @ opuntia ficus indica par rapport à la polyaniline pure (4,84 S /cm) . Fait intéressant, ils montrent la valeur la plus basse de la bande interdite optique de 1,88eV pour PANI @ WO₃ (0,5) par rapport à PANI @ WO₃ (1,0) et PANI @ WO₃ (1,5) avec 1,91eV et 1,98eV, respectivement. En outre, les propriétés d'électroactivité ont été étudiées par voltamétrie cyclique pour explorer les avantages de ces types de matériaux hybrides dans les applications électrochimiques.

Les mots clés : nanocomposites , polyaniline , oxyde de tungstéine, alumine, opuntia ficus indica